論文 / 著書情報
Article / Book Information

題目(和文)	
Title(English)	Study on Pressure Control of Industrial Compressible Fluid for Gas Supply System
著者(和文)	PENGJiehong
Author(English)	Jiehong Peng
出典(和文)	学位:博士（工学）, 学位授与機関:東京工業大学, 報告番号:甲第10345号, 授与年月日:2016年9月20日, 学位の種別:課程博士, 審査員:只野 耕太郎,吉田 和弘,髙山 俊男,松村 茂樹,吉岡 勇人
Citation(English)	Degree:, Conferring organization: Tokyo Institute of Technology, Report number:甲第10345号, Conferred date:2016/9/20, Degree Type:Course doctor, Examiner:,,,,
学位種別(和文)	博士論文
Type(English)	Doctoral Thesis

Study on Pressure Control of Industrial Compressible Fluid for Gas Supply System

Supervisor:

Associate professor Kotaro Tadano

Professor Kazuhiro Yoshida

Department of Mechano-Micro Engineering

Tokyo Institute of Technology

Jiehong Peng

August 2016

Contents

Nomenclature:

Universal

C_D:	discharge coefficient	[/]
C_p:	constant pressure specific heat capacity	[J/(kg·K)]
C_v:	constant volume specific heat capacity	[J/(kg·K)]
G:	mass flow rate	[kg/s]
P_D:	downstream pressure	[MPa]
P_U:	upstream pressure	[MPa]
P_a:	atmosphere pressure	[kPaG]
Q:	volumetric flow rate	[L/min]
Q_{porous}:	quantity of flow in the porous material	[L/min]
R:	gas constant	[J/(kg·K)]
S_e:	effective area of restriction	[mm^2]
S_h:	heat transfer area	[m^2]
c:	damping coefficient	[(N·s) /m]
h:	thermal conductivity	[W/(K·m)]
q:	heat transfer on wall	[J]
t:	time	[s]
μ:	dynamic viscosity	[Pa·S]
ΔP:	pressure difference	[kPa]
θ:	average temperature of flow	[K]
θ_a:	temperature of atmosphere	[K]
κ:	specific heat ratio	[/]
ρ:	density	[kg/m^3]

Chapter 1

P_1:	pressure of upstream pipeline	[kPaG]
P_2:	pressure of downstream pipeline	[kPaG]
P_c:	pressure in control chamber	[kPaG]
P_d:	pressure in diaphragm chamber	[kPaG]
Q_2:	downstream flow rate	[m^3/h]
R_f:	flow resistance	[(Pa·h)/m^3]
V_2:	volume of downstream	[m^3]
V_d:	volume of diaphragm chamber	[mL]

Chapter 2

A_2:	amplitudes of P_2	[kPaG]
A_d:	amplitudes of P_d	[kPaG]
K_d:	gain of the pressure response P_d	[dB]
K_{p1}:	flow rate constant of porous material	[L/(min·kPa)]
L:	length of pipe	[m]
P_1:	pressure of upstream pipeline	[kPaG]
P_2:	pressure of downstream pipeline	[kPaG]
P_d:	pressure in chamber	[kPaG]
V:	volume of chamber	[m^3]
d:	diameter of the orifice	[mm]
m:	mass of the air in the chamber	[kg]
r:	radius of pipe	[m]
ϕ_2:	phase of P_2	[°]
ϕ_d:	phase of P_d	[°]

$\Delta\phi_d$:	phase difference	[°]
θ_1:	flow temperature	[K]

Chapter 3

A_c:	amplitudes of P_c	[kPaG]
A_d:	amplitudes of P_d	[kPaG]
A_i:	amplitudes of P_i	[kPaG]
G_1:	mass flow rate through orifice 2	[kg/s]
G_2:	mass flow rate through outlet of the valve	[kg/s]
G_N:	mass flow rate through the nozzle-flapper	[kg/s]
G_d:	mass flow rate through the test restrictions	[kg/s]
K_c:	gain of the pressure response P_c	[dB]
K_d:	gain of the pressure response P_d	[dB]
K_{p2}:	flow rate constant of porous material	[L/(min·kPa)]
P_1:	pressure of upstream pipeline	[kPaG]
P_2:	pressure of downstream pipeline	[kPaG]
P_c:	pressure in control chamber	[kPaG]
P_d:	pressure in diaphragm chamber	[kPaG]
P_i:	input pressure	[kPaG]
P_o:	downstream pressure	[kPaG]
P_{set}:	setting pressure of the valve	[kPaG]
S_d:	effective area of the diaphragm	[m^2]
S_{e2}:	effective area of orifice 2	[mm^2]
S_{e3}:	effective area of the outlet	[mm^2]
S_{ex}:	effective area of the nozzle-flapper	[mm^2]

V_c:	sum volume of the ITC, control chamber, and pipe	[m^3]
V_d:	volume of diaphragm chamber	[m^3]
V_o:	downstream volume	[m^3]
d_N:	diameter of the nozzle	[mm]
k_1:	spring constant of the adjustment spring	[N/mm]
k_2:	spring constant of the counter spring	[N/mm]
m:	mass of the air in the chamber	[kg]
m_v:	total mass of the moving part	[kg]
x:	displacement between the nozzle and flapper	[m]
ϕ_c:	phase of P_c	[°]
ϕ_d:	phase of P_d	[°]
ϕ_i:	phase of P_i	[°]
$\Delta\phi_c$:	phase difference of P_c	[°]
$\Delta\phi_d$:	phase difference of P_d	[°]

Chapter 4

A_d:	effective area of the diaphragm	[m^2]
D_1:	diameter of the diaphragm	[m]
D_2:	diameter of the diaphragm metal disc	[m]
D_e:	equivalent diameter of the diaphragm	[m]
G_1:	mass flow rate through orifice	[kg/s]
G_2:	mass flow rate through on-off valve	[kg/s]
G_A:	mass flow rate of main pilot valve A	[kg/s]
G_B:	mass flow rate of sub pilot valve A	[kg/s]
G_a:	mass flow rate through the bleed hole	[kg/s]

G_d:	mass flow rate through the damping hole	[kg/s]
G_i:	mass flow rate into the working room	[kg/s]
G_o:	mass flow rate out the working room	[kg/s]
M_1^*:	fitting coefficient	[mm^{-2}]
M_1:	fitting coefficient	[L/(min·mm^4)]
M_2^*:	fitting coefficient	[mm^{-1}]
M_2:	fitting coefficient	[L/(min·mm^3)]
M_3^*:	fitting coefficient	[/]
M_3:	fitting coefficient	[L/(min·mm^2)]
M_4^*:	fitting coefficient	[mm]
M_4:	fitting coefficient	[L/(min·mm)]
N_1^*:	fitting coefficient	[mm^{-1}]
N_1:	fitting coefficient	[L/(min·mm^3)]
N_2^*:	fitting coefficient	[/]
N_2:	fitting coefficient	[L/(min·mm^2)]
N_3^*:	fitting coefficient	[mm]
N_3:	fitting coefficient	[L/(min·mm)]
P_2:	pressure of downstream pipeline	[kPaG]
P_{2setA}:	setting pressure of main pilot valve A	[PaG]
P_{2setB}:	setting pressure of sub pilot valve B	[PaG]
P_d:	pressure in damping room	[kPaG]
P_v:	pressure in air room	[kPaG]
P_w:	pressure in working room	[kPaG]
Q_A:	quantity of flow in main pilot valve A	[L/min]

Q_B:	quantity of flow in sub pilot valve B	[L/min]
S_{ea}:	effective area of bleed hole	[mm^2]
S_{ed}:	effective area of damping hole	[mm^2]
S_{ei}:	effective area of nozzle-flapper	[mm^2]
S_{eiA}:	effective area of nozzle-flapper in main pilot valve A	[mm^2]
S_{eiB}:	effective area of nozzle-flapper in sub pilot valve B	[mm^2]
S_{eo}:	effective area of outlet	[mm^2]
V_{a0}:	initial volume of the air room	[m^3]
V_a:	volume of the air room	[m^3]
V_{d0}:	initial volume of the damping room	[m^3]
V_d:	volume of the damping room	[m^3]
V_{w0}:	initial volume of the working room	[m^3]
V_w:	volume of the working room	[m^3]
k:	spring constant	[N/m]
m_A:	mass of air in the air room	[kg]
m_W:	mass of air in the working room	[kg]
m_d:	mass of diaphragm	[kg]
m_e:	equivalent mass of the motion parts	[kg]
m_s:	mass of spring	[kg]
m_v:	mass of valve stem	[kg]
x_0:	initial length of the spring	[m]
x:	displacement of valve motion	[m]
ΔV:	change volume	[m^3]

Chapter 5

A:	cross-sectional area of the pipe	[m^2]
A_P:	maximum amplitude of gas column vibration	[PaG]
G_1:	mass flow rate through upstream orifice	[kg/s]
G_2:	mass flow rate through nozzle-flapper	[kg/s]
P_1:	upstream pressure in pipe experiment	[kPaG]
P_2:	pressure in chamber	[kPaG]
P_{2ref}:	pressure balance point	[kPaG]
P_b:	pressure at back of pipe	[PaG]
P_f:	pressure in front of pipe	[PaG]
Q_m:	measurement flow rate	[L/min]
Q_{real}:	actual flow rate	[L/min]
S:	sound pressure coefficient	[$K^{-1/2}$/m]
S_{e1}:	effective area of upstream orifice	[mm^2]
S_{ex}:	effective area of nozzle-flapper	[mm^2]
T_p:	time constant	[s]
T_{pA}:	time constant of air	[s]
T_{pH}:	time constant of hydrogen	[s]
T_{pM}:	time constant of methane	[s]
T_{pP}:	time constant of propane	[s]
T_t:	period of gas column vibration	[s]
V_2:	volume of the chamber	[m^3]
V:	unit volume of air	[m^3]
a^*:	converted flow rate gain	[/]
a:	flow rate gain	[kg/(s·Pa)]

c:	sound speed	[m/s]
d:	diameter of the orifice	[mm]
m:	unit mass of air	[kg]
u:	flow velocity	[m/s]
μ^*:	relative viscosity	[/]
θ_1:	flow temperature	[K]

Chapter 1 Introduction

1.1 Industrial Compressible fluid

After the industrial revolution, compressible fluid is widely used in the pneumatic control field and the energy source field. Relative to the high Mach number in aerospace, the Mach number of the industrial compressible flow is generally no more than 1 Ma, and the maximum flow velocity of the chocked flow reaches to 1 Ma. In addition, the industrial compressible fluid is often an internal flow in the gas equipment such as tank, valve, and pipe. In this chapter, four common industrial compressible fluid are introduced as follows.

1.1.1 Air

Air as a compressible fluid medium in the pneumatic system has been widely applied in mechanical products, automobile, semiconductor, CNC machine, and so on. Pneumatic systems have numerous advantages, such as high effectiveness, high durability and reliability, and environmental friendliness. Therefore, the industrial scale of pneumatic equipment, that are constituted of air cylinders, solenoid valve, actuators, air compressor, and the like, is considerably large. For example, the shipment of the pneumatic equipment in Japan is more than 300 billion JPY in the year of 2014 (data from Japan Fluid Power Association). In addition, the current demand of the pneumatic equipment is rapidly increasing in China year by year [1].

1.1.2 Methane and propane

Methane, commonly known as natural gas whose combustion products are only water and carbon dioxide, is a cleaner fuel than coal. Nowadays, many cities use methane as a sustainable fuel in their city energy supply systems because it can be easily distributed by pipeline infrastructure [2]. According to the data from the U.S. Energy Information Administration (EIA), the total natural gas consumption in the U.S. is more than 27000 billion cubic feet in 2015. The consumption of natural gas also continues to grow year by year in Japan, it is particularly growing very fast in China in recent years as shown in Figure 1.1. On the other hand, propane known as LP gas, which can be liquefied, is usually employed in the areas that lack the necessary infrastructure, such as gas pipe-lines, because of its high energy density.

What is worth mentioning is that natural gas vehicle (NGV) is very popular in many countries such as China, Iran, India, et al, because it can run with lower emissions of carbon and less wasted than gasoline.

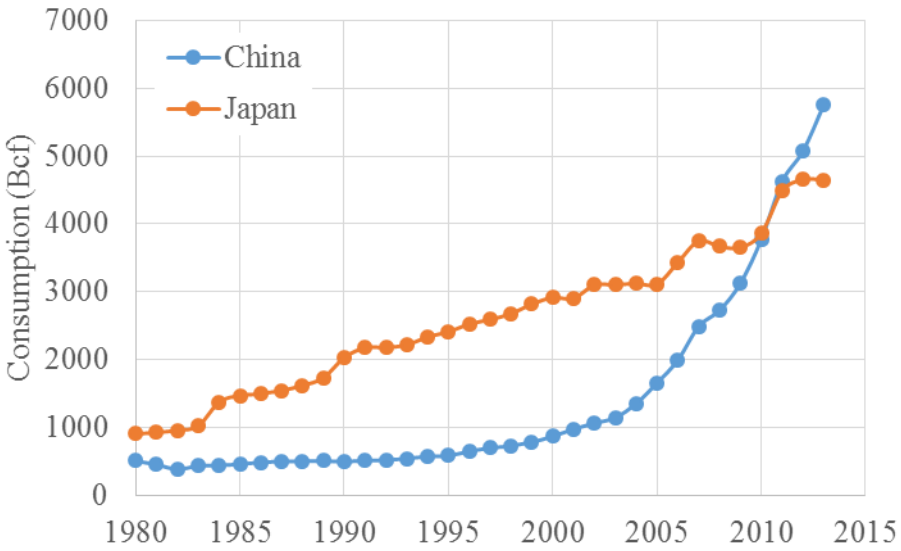

Fig.1.1 Natural gas consumption by years (EIA)

1.1.3 Hydrogen

Although methane and propane are cleaner than coal, when they are burning, the process still emits greenhouse gases. With the deterioration of the global greenhouse effect, hydrogen has been proposed as an environmentally friendly fuel that produces only water as a combustion product [3][4]. Certainly, hydrogen is also a very efficient fuel source than gasoline and other traditional energy sources. However, some disadvantages also limit the application of hydrogen up to now. For example, for the production of hydrogen, a cheap and renewable source, a proper storage, a safe handing fuel cell, and a refilling station need to be secured [5]. The most compelling application is the hydrogen fuel cell vehicle [6], and NEDO basic technology development program for safe hydrogen utilization was launched in 2003 for research on the earlier hydrogen stations and fuel cell vehicles in Japan [7].

1.2 Pressure control technology of four gases

Pressure control technology is indispensable for utilizing various gases. Gas equipment such as the air actuator or gas stoves have to work under an appropriate pressure. And since the flammable gases are easily to cause an explosion [8], a fine design in pressure control of gas equipment (e.g. self-actuated regulator system) is availed to the system for anti-explosion. Due to the different property and application purpose of these four gases above, the pressure control equipment and method also have a considerable difference.

1.2.1 Air

In the pneumatic systems, compressed air is controlled by a pressure regulator valve from the compressor. Tank or chamber as an accumulator stores compressed air or the energy in the compressed air, and can prevent surges in pressure [9]. An orifice and a long pipe are usually flow resistance in the pneumatic circuit and result in a pressure drop through them. There is no doubt that the characteristics of the pneumatic system depend on these pneumatic components, especially the pressure regulator valve [10].

According to the application of the air pressure regulator, it is classified into several types, namely general purpose type, precision type, high-pressure type, vacuum type, and special fluid or deionized water type. According to the action principle, air pressure regulator can also be classified into direct-operated type and pilot-operated type. Nozzle flapper is the basic structure in air pressure regulators in spite of different classifications. Nowadays, SMC, CKD, PISCO in Japan, AIRTAC in Taiwan, FESTO in Germany are the famous companies who manufacture the air pressure regulator.

Research on the pressure response of air in the pneumatic components, such as the tank, pipe, and regulator, will improve the air pressure control equipment and promote pneumatic technology. To this end, Kagawa and his group performed several studies on the dynamic characteristics and transient response of air in a chamber, nozzle flapper, and pipe 30 years ago [11-13]. At the beginning of the 21st century, many researchers are still devoted to the air pressure control subjects. A study by Li et al. illustrated that the excessive pressure surges generated in the valve tend to be damped out in the pipe main and the valve connections tend to experience higher pressure surges for potential breakages [14]. Mohsen Shiee et al. developed an approach using sliding mode control for controlling pressure, they proposed that servo system possesses more robust characteristics than that of proportional pressure regulator-included system [15]. Lilia

Badykova et al. analyze dynamics of an air pressure reducing valve with a muffler installed at its output [16].

1.2.2 Methane and propane

Generally, the pressure in a city gas pipeline which transports natural gas (methane) is controlled by a pressure regulator called gas governor unit in Japan [17]. A higher pressure in main city gas pipeline should be set as far as possible in order to improve the transmission efficiency. On the other hand, an appropriate pressure needs to be maintained in each consumer places according to the usage conditions. Therefore, the city gas is transported to each consumer place through the pressure dropping scheme step by step. City gas is output by a high pressure from the factory which gasifies the liquefied natural gas (LNG). They are transferred to the factory by a medium pressure from 150 to 300 kPaG. And then the pressure is down to about 2.3 kPaG step by step using the gas governor unit in people's household [18]. The city natural gas transmission scheme is showed in Figure 1.2.

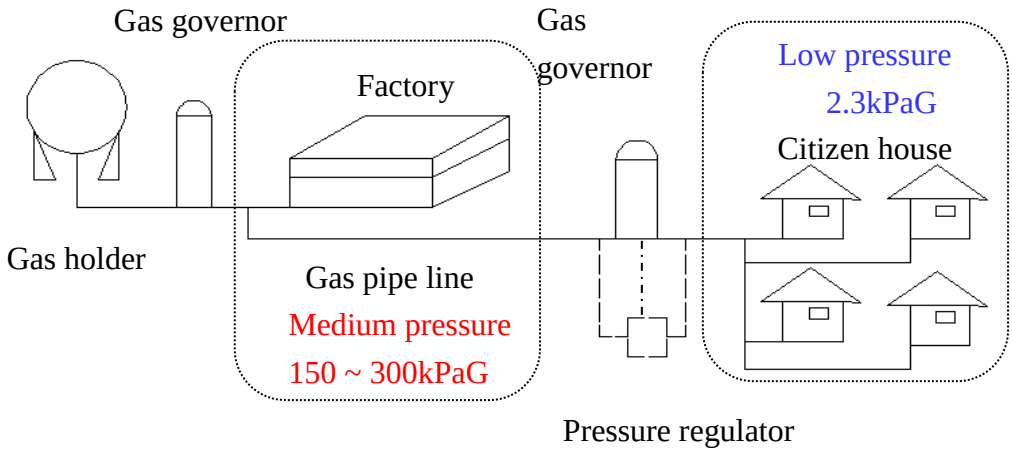

Fig.1.2 City natural gas transmission scheme

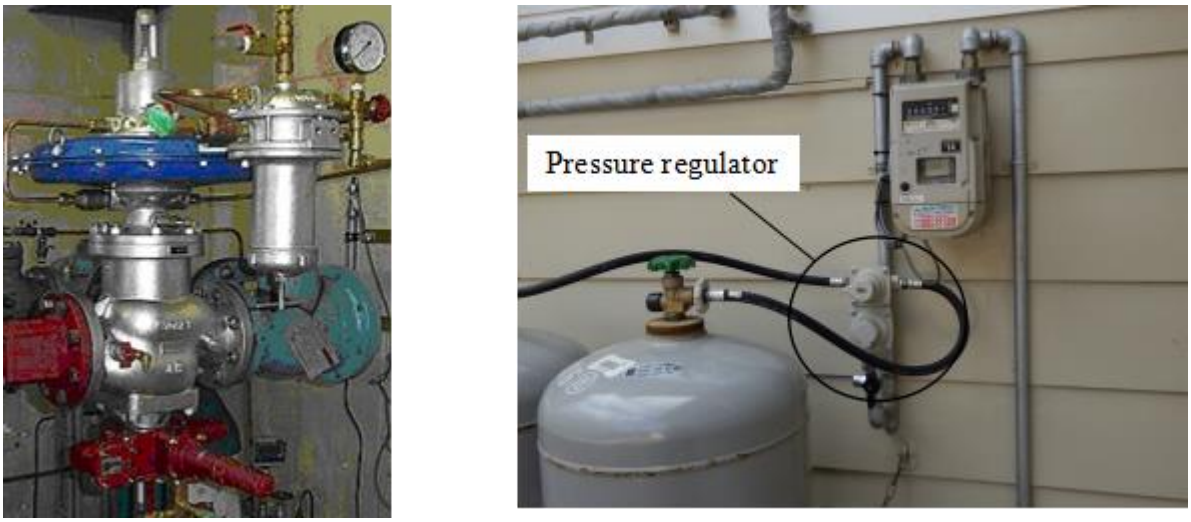

a) Gas governor b) LP gas pressure regulator

Fig.1.3 Methane and propane pressure regulator

Comparing with methane, the pressure control system of the propane in household is not so complicated because its transport uses a gas bombe. The pressure is maintained about 2.3~3.3 kPaG by the LP gas pressure regulator from the bombe whose inner pressure reaches up to 0.4~1.2 MPaG. The gas governor unit system and the LP gas pressure regulator are shown in Figure 1.3.

In fact, the gas governor unit is also composed of the gas pressure regulator or the pressure reducer valve and other gas components. There are many famous gas pressure regulator manufacturers, for example, KATSURA Co., Ltd, ITOKOKI Co., Ltd, Azbil Kimmon Co., Ltd, and Aichi Tokei Denki Co., Ltd in Japan; Fisher, RegO, AMCO by American Meter, and BelGAS by Marsh Bellofram Group of Companies in the USA; ITRON and ELSTER in Germany.

1.2.3 Hydrogen

Hydrogen is not a widely used energy source in industry because it is inflammable and combustible. Like the propane, hydrogen is also storage in a bombe and controlled by a

simple pressure regulator. Meanwhile, hydrogen is a newly-developing energy source and carrier for a fuel cell vehicle, thus the pressure control technology in this situation is not mature enough at present. Schlapbach indicates that a conventional hydrogen storage is a high-pressure tanks made of fairly cheap steel, and it is tested up to 30 MPa and regularly filled up to 20 MPa in most countries [19]. In recent studies, the pressure in the storage is up to 70MPa. However, the pressure needs to be controlled within about 10 kPaG in the fuel cell from the hydrogen storage which owns the ultra-high pressure [20]. Many manufacturers and researchers are developing a new type of pressure regulator and bombe. Mizuno et al. did a simulation study of radial slits pressure regulator for hydrogen gas [7]. Nakano et al. investigated the absorption/desorption characteristics of a metal hydride tank with boil-off gas from liquid hydrogen, and confirmed that the effect of the heat conversion was very small and boil-off gas could be treated as normal hydrogen for practical application [21].

1.3 Valve systems in Gas governor unit

Gas governor unit system is important for pressure control of natural gas as mentioned above. With the growing demand of natural gas, a gas governor unit system with an excellent performance is demanded by gas companies. The gas governor unit system also includes fitter, shutoff valve and other component parts; in this thesis, we primarily discuss the pressure regulator valve in it. Gas governor units are classified into two types: direct-acting valve system and pilot valve system.

1.3.1 Direct-acting valve system

Direct-acting valve system is the most common type of gas governor unit because it is easy to handle and has an uncomplicated structure. A direct-acting valve system is

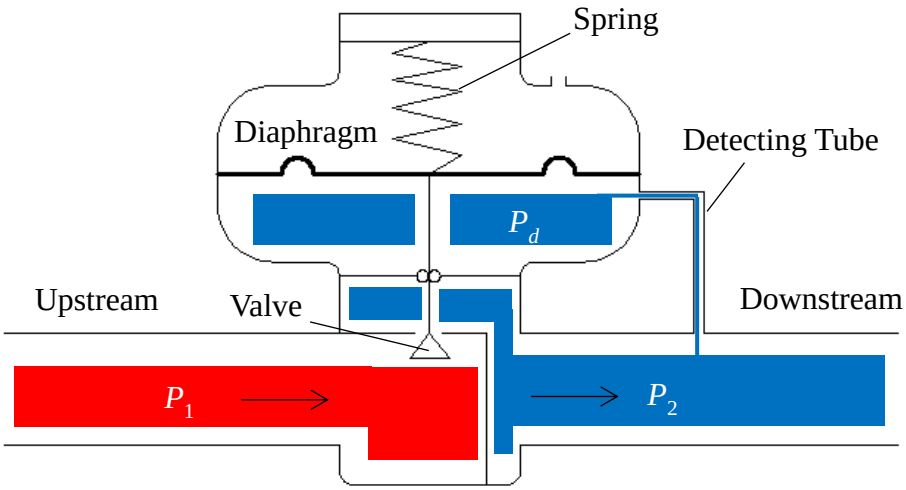

Fig.1.4 Direct-acting valve system

showed in Figure 1.4. The downstream pressure is generally called secondary pressure. The action principle of this system is summarized as follows:

1) The secondary pressure P_2 decreases when the consumption of gas increases.

2) The pressure in diaphragm chamber P_d also decreases through a detecting tube, and the pressure force which acts on the diaphragm drops. Then, the diaphragm is depressed down by the spring force.

3) Valve opens with the plug, and the flow rate increases.

4) The secondary pressure recovers to the set pressure, and arrives to a new steady state.

It is not difficult to see that the secondary pressure is the driving force of the valve. Therefore, when the flow rate is very large, it requires a large driving force to open the valve.

1.3.2 Pilot valve system

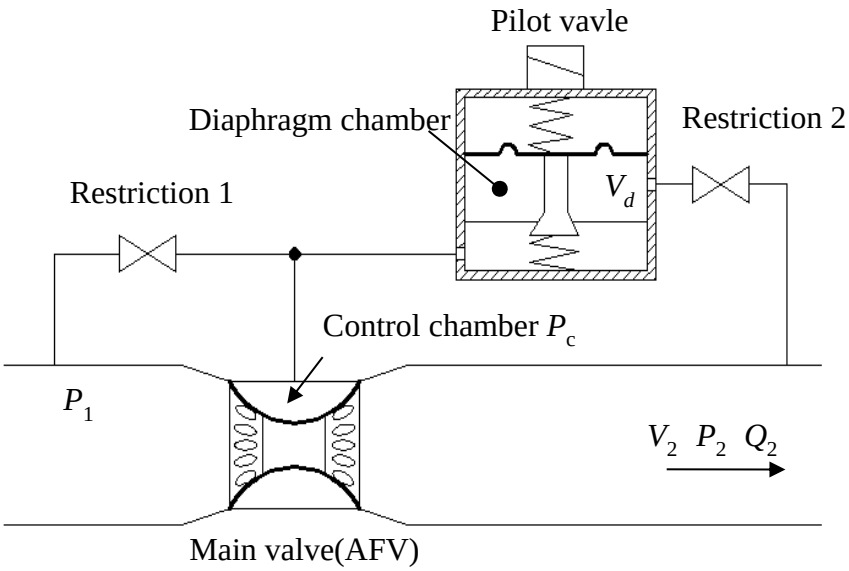

Fig.1.5 Pilot valve system

In pilot valve system, there are two control valves, a main valve controls the flow rate of the main pipeline and a pilot valve controls the flow rate of the pilot line. The secondary pressure is directly sensed by the pilot valve, and the driving force by the control pressure in the diaphragm chamber of the main valve is amplified by the pilot valve. Therefore, the secondary pressure is indirectly controlled by the main valve. Comparing with the direct-acting valve system, the pilot valve system have a small off-set [22] in the secondary pressure.

Figure 1.5 shows a common pilot-type gas governor system. The main valve, termed the axial flow valve (AFV) [23-25], is installed in the main pipeline, and the pressure P_c in its control chamber is regulated by the pilot valve, which is installed in the pilot line. When the flow demand increases, the downstream pressure P_2 decreases. Subsequently, the pressure P_d in the diaphragm chamber of the pilot valve drops through the tube, which is restricted by an orifice or some other restrictions. As a result, the pilot valve opens by the adjustable spring force and allows the gas to flow into the pilot line. This flow leads

to a drop in P_c and makes the main valve open. Eventually, P_2, P_d, and P_c achieve an equilibrium state by this feedback control system.

1.3.3 Evaluation indicator of gas governor unit

In order to review the property of the gas governor unit, there are some evaluation indicators to help engineers to handle it.

(1) *P*-*Q* characteristics

Generally, the flow rate of the gas governor unit is a function of the secondary pressure. In addition, the pressure difference between the pressure at the maximum flow rate and the setting pressure, is called an offset. The offset is smaller, and the precision of the control pressure is higher. Accordingly, the *P*-*Q* characteristics curve is an important characterization of precision in the gas governor unit. Additionally, there is usually a lock up pressure from the gas governor starting to the setting pressure. Figure 1.6 shows a *P*-*Q* characteristics curve of a gas governor.

(2) Response speed and stability

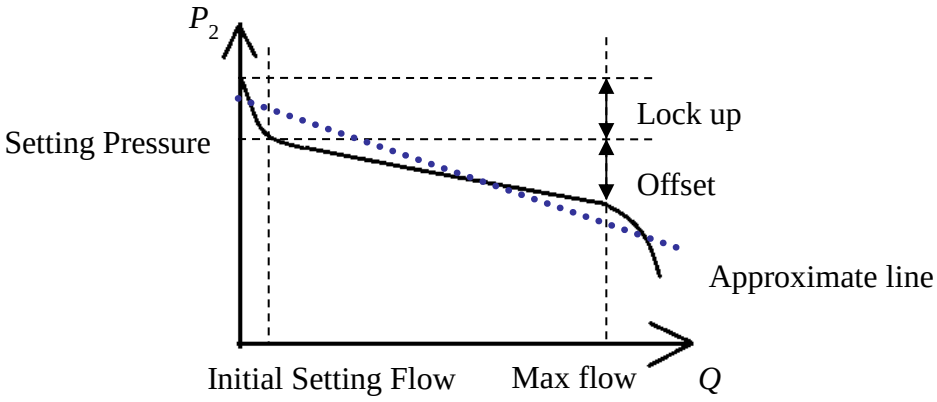

Fig.1.6 *P*-*Q* characteristics curve of a gas governor

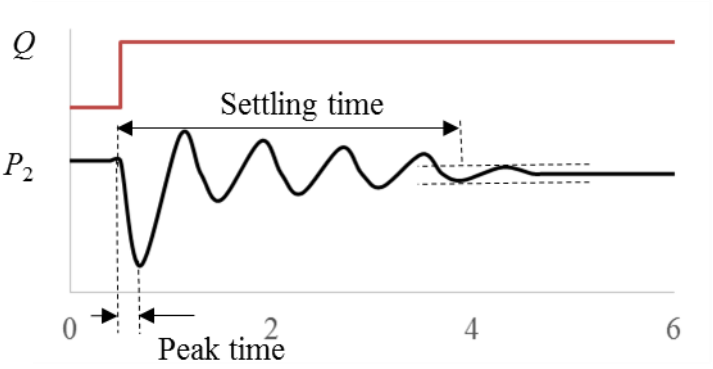

Fig.1.7 Step response in gas governor system

When the gas consumption suddenly changes, the secondary pressure will also have a change response to the flow rate surge. Commonly, a step response experiment is carried out to examine the response speed and stability of the gas governor unit as shown in Figure 1.7. The delay time, rise time, and peak time can reflect the response speed, and the settling time can reflect the stability [26]. If we know the dynamic model of the valve system, we can judge the property of the gas governor by simulation.

1.4 Problems in pilot valve system

Pilot valve system in a governor unit is an effective approach for reducing the offset of the pressure regulator for a medium and low pressure gas pipeline [27]. However, some problems in the working pressure of the gases are constantly occurred in this system and puzzle the consumers and gas suppliers. The primary problems are the pressure vibration in the downstream pipes and the unsatisfactory dynamic characteristics when the downstream flow loads abrupt changes. [28-30].

1.4.1 Pressure vibration

In Figure 1.5, the pilot valve contains a tube that connects its diaphragm chamber to the downstream pipeline, and this tube is used to detect the secondary pressure and

provide feedback signal for adjusting the control pressure of the main valve. It is known that resonance occurs in an air column at its inherent frequency called gas column vibration. Correspondingly, gas column vibration also occurs in the detecting tube. The downstream pressure vibration caused by the gas column vibration is shown in Figure 1.8. In addition to this vibration, the secondary pressure often oscillates because of the dead-band [31] and the phenomenon of flow choking at the restrictions of the pressure-reducing elements [32]. Earney summarized that all the components in a given pressure system are contributing factors to any instability of the pressure control [33]. All these vibrations could affect the control pressure in the main valve, lead to secondary pressure instability, and generate valve noise. Feedback can amplify the vibration, which in turn would make the gas equipment unusable [34].

These problems were studied in some previous works, including that of Zafer and Luecke [35], who established a linearized model to study the stability of a gas regulator

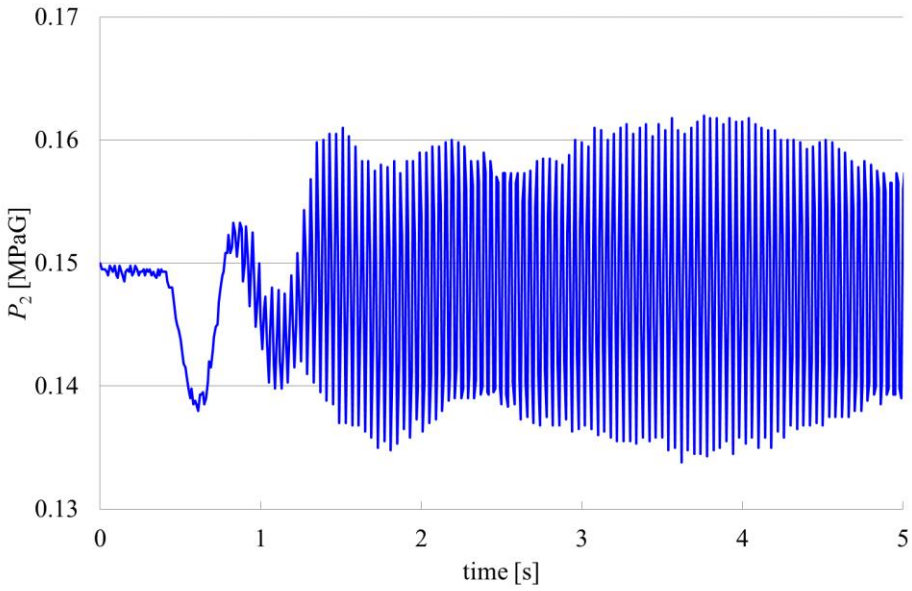

(Data from Tokyo gas Co., Ltd)

Fig.1.8 Pressure vibration in pilot valve

system with changes in various design parameters. Ng [36] reported that reduction of the acoustical energy at the source is the most direct approach for overcoming the valve noise problem, most quiet valves are based on the concept of reducing and redistributing acoustical energy by dividing the flow into several smaller streams. Rami, et al. [37] established a pressure regulating station model, and pointed that the amplitude of the pressure oscillation increases dramatically for small volumes. Generally, field modifications for stabilizing an installation include relocation of the pressure-sensing tap, redesign of the downstream piping to provide more volume, and restriction of the pressure feedback line [38]. A flow resistance such as an orifice or a needle valve is installed in the tube by manufacturers in order to constitute a pneumatic RC circuit with the diaphragm chamber. This method is used to curb the effects of the downstream pressure vibration and has been employed in several previously patented pilot valves [39-41].

However, the pneumatic RC circuit, which uses an orifice as the restriction, also has some disadvantages. The flow resistance, that is the flow rate characteristics of the orifice, is nonlinear as shown in Figure 1.9. The flow rate equation indicates that it is square

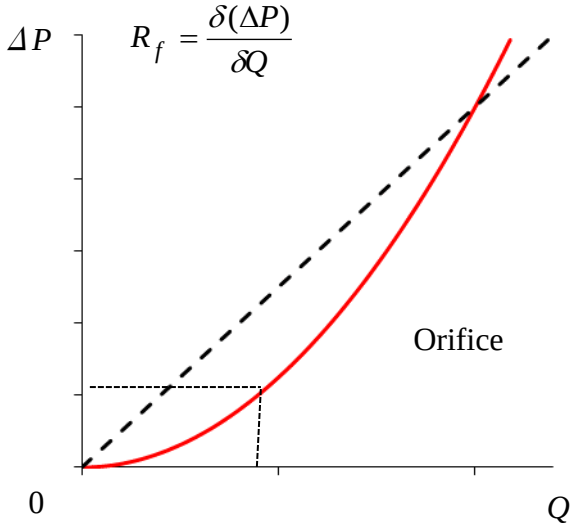

Fig.1.9 Different flow rate characteristics

characteristics. According to the definition of flow resistance R_f as shown in this figure, the flow resistance is very small with a diminutive pressure difference, and the small resistance could result in a large flow rate. The main valve in the gas governor unit will act by this large flow rate. Thus, a small pressure vibration also causes the main valve action and leads to an unstable pressure problem. On the other hand, the flow resistance gradually increases with the increases of the pressure difference. In fact, it is hoped to be a small flow resistance with a large pressure difference, which can make the gas governor act quickly. In addition, because of the nonlinear flow rate characteristics of the orifice, the gain of the pressure response changes with changing amplitude of the pressure vibration [42] [43]. The nonlinear behavior in the control system is inconvenient for the design of the pressure control system.

1.4.2 Unsatisfactory dynamic characteristics with abrupt load change

Except the pressure vibration, some pressure problems occur on the moment that the amount of gas consumption suddenly changes, which is known as abrupt load changes. As we know, most valves use a spring to control the displacement of the valves, so that the motion principle of the valves is essentially a spring oscillator system. Hence, if we choose a stable valve, a long time delay of the pilot valve movement will occur due to its large damping. Consequently, the secondary pressure, which keeps the gas equipment working, will experience a large pressure drop when the gas consumption suddenly increases as showed in Figure 1.10. Because the valve is still closed or not fully open yet, the flow rate can't satisfy the large pressure drop. The gas equipment can't work at this low pressure state. If we choose a pilot valve that responses fast, the stability will be

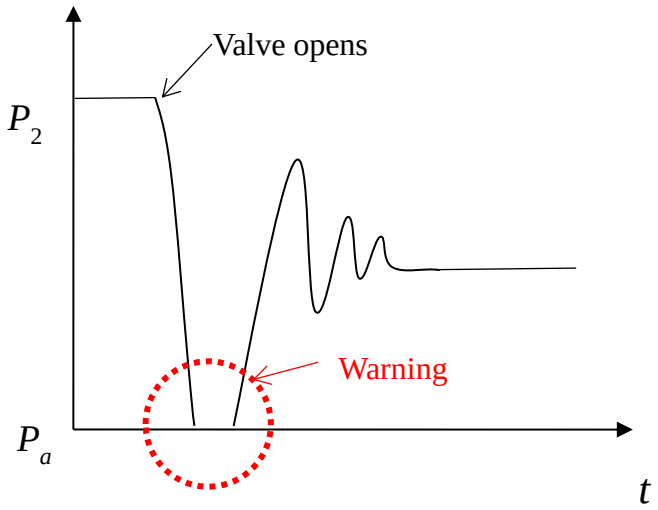

Fig.1.10 Pressure drop at valve opens

unsatisfactory, and it will cause a pressure surge in the downstream pipeline. Furthermore, it will result in a pressure resonant problem.

Krope, et al. [44] state that incorrect choice of pipe dimensions leads to too high or too low pressure drops and consequently increases maintenance costs caused by disturbances in operation. But it is sometimes difficult to change the pipe diameter. Dong and Li [45] developed a novel parallel-spool pilot operated high-pressure solenoid valve with high flow rate and high speed. But the solenoid valve can't be used in the flammable gas pressure control system. To solve these unsatisfactory dynamic characteristics problems, A parallel pilot valve system has been proposed to be applied in the gas governor unit 40 years ago [46]. However, the product of the parallel pilot system has not been manufactured. And it dynamic characteristic was not clear, because there was no mathematical model of the parallel pilot valve system. In order to analyze the dynamic characteristics of this complicated system, a mathematical model of the parallel pilot valve system is established, and the simulation is implemented by the MATLAB.

1.5 Research purposes

The conventional pilot valve system in gas governor unit can't solve these problems adequately in pressure control process. And with the increasing application of hydrogen, the studies on various gas pressure control and pressure equipment design become more and more important. Therefore, the purposes of this thesis are:

(1) We propose a method that employs porous materials for improving the characteristics of a gas pressure control system called pneumatic RC circuit owing to their linear flow rate characteristics as shown in Figure 1.9 with the dash line, which cause the gas flow state to change to laminar in the micro-holes. It is seen that the resistance of the linear flow characteristics is larger than orifice when the pressure difference is small, and it is smaller than orifice when the pressure difference is large. These characteristics can filter the small pressure vibration and ensure the response speed of the gas governor unit. On the other hand, the flow resistance of the porous material is a constant with the change of the pressure difference.

First, a static flow rate characteristics experiment was performed in order to compare the flow characteristics of porous materials with those of an orifice. And the linear flow rate characteristics of the porous materials were confirmed. Then, a series of dynamic pressure response experiments were performed to examine the dynamic characteristics of the porous materials and an orifice in the pneumatic RC circuit. The experiments provided some conclusions in the relationship of the pressure gain and the amplitude of the downstream pressure vibration. These results demonstrate porous materials are conducive to change the pressure control system into a linear system instead of the nonlinear system because of the linear flow rate characteristics. And it can be employed in place of an orifice in the gas pressure control systems in order to improve their stability.

However, pneumatic RC circuit is only a constituent part in a pilot valve system. In order to examine the conclusions above, whether they are suitable for a pilot valve system. A test pilot valve was manufactured and a pilot valve system was developed in our laboratory. A mathematical model of the pilot valve system using porous materials and an orifice was simulated in MATLAB. A series of dynamic pressure response experiments were performed to examine the dynamic characteristics of the porous materials in the pilot valve system. It is hoped that the porous materials can be used in the pilot valve system instead of an orifice to improve its dynamic characteristics.

(2) On the other hand, a parallel pilot valve system which uses two diaphragm type pressure regulators was proposed to solve the dynamic pressure response problem in a gas governor unit as explained in the section 1.4.2. However, there is no theoretical analysis of the parallel pilot valve system so far. Hence, we established a mathematical model of these two pressure regulators. The static characteristics of two regulators are verified by a static experiment, and the simulation model shows a good agreement with the results. The dynamic characteristics of the parallel pilot valve system was simulated using these models by MATLAB, and this study can help the manufacturers to develop this new type gas governor unit preferably.

(3) Engineers generally use air in their research and experiments for developing new pressure control equipment for gas because while it is a convenient and safe source, the properties of air are similar to those of city gas. Of course, the researches mentioned above also use air to implement experiments although the gas governor and valve system are prepared for natural gas. On the other hand, there were few experiment data and literatures dealing with the pressure response of hydrogen and its special fluid property. The pneumatic resistance, such as an orifice, nozzle flapper, and pipe with the capacity, is the

most important constituent of pneumatic and gas pressure control systems. Therefore, we investigated the effect of different gas properties on the pressure response in a pneumatic resistance capacitance system in the last part of this thesis. Four gases—air, hydrogen, methane, and propane—were chosen to perform a static flow rate characteristic experiment and two dynamic pressure response experiments. The flow rate equation for an orifice with the four gases was confirmed based on the experimental data, and the pressure response speed with various gases in the pneumatic resistance capacitance system was discussed. Finally, changes in the time delay and gas column vibration in the pressure propagation through a pipe with the various gases were studied. The research findings can be applied in the design and manufacture of different gas systems and equipment, particularly in the application of the hydrogen.

1.6 Structure of this thesis

This thesis is composed of six chapters, the introduction in chapter 1, and the contents of other chapters are briefly prompted as follows:

Chapter 2 will introduce a method that uses porous materials to improve the characteristics of the pressure control system. The mathematical model of these systems and the experiment method will be illustrated, respectively. Some interesting results will be shown by a Bode diagram.

Chapter 3 will continue to propose this method to apply in a pilot valve system, and examine the effectiveness of this method. A pilot valve system is established in our laboratory, and a simulation model of this system is also completed by our team. The analysis of experiments and simulation results will help us to confirm the superior capability of porous materials when they are employed in the pilot valve system.

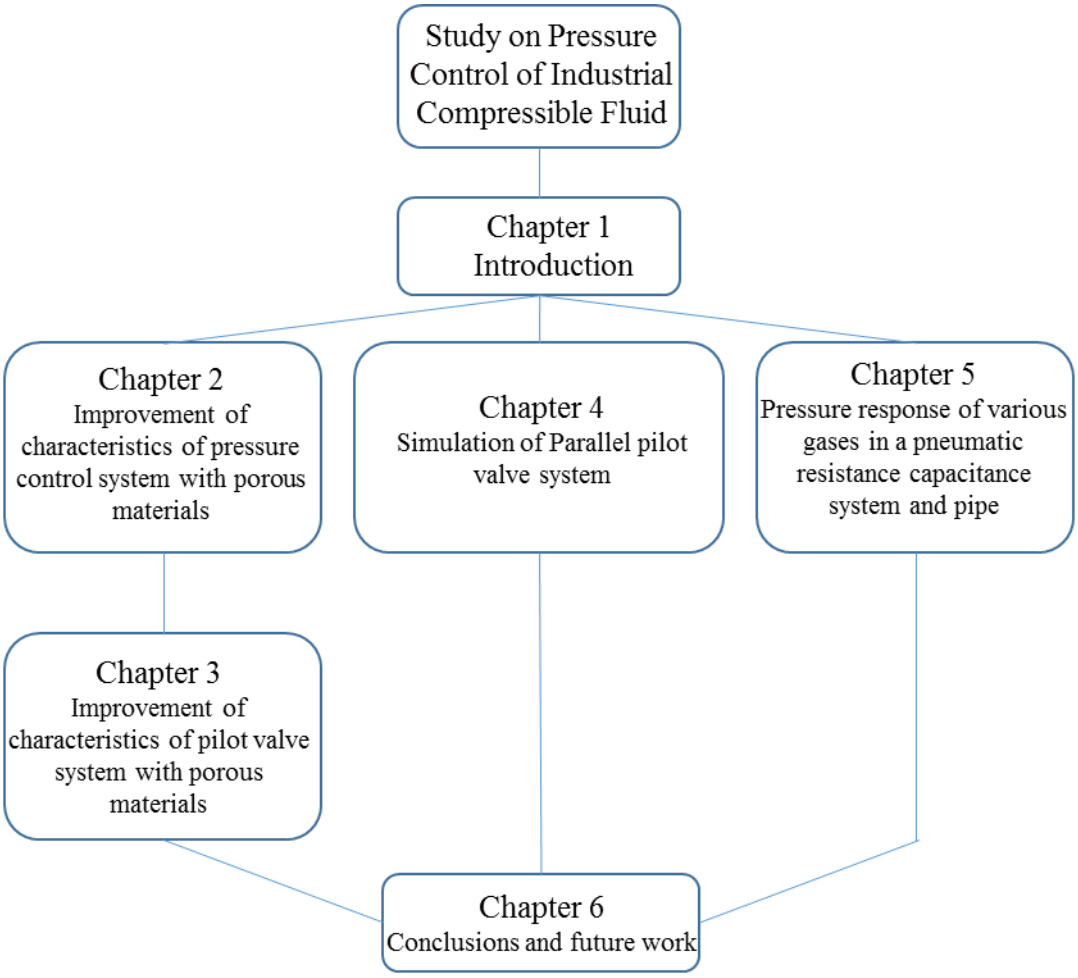

Fig.1.11 Structure of this thesis

Chapter 4 will provide a mathematical model of the parallel pilot valve system. And this simulation will be carried out on the MATLAB. Some flow rate and pressure measurement experiments with the diaphragm type pilot valve will be carried out to help the simulation obtain the physical parameter.

Chapter 5 will investigate the difference in the pressure response experiment with four gases, namely air, methane, propane, and hydrogen. Particularly, it will demonstrate an amazed pressure response results with the hydrogen.

Chapter 6 summarizes the research above, and proposes some work what needs to be done in the future.

A structure diagram of thesis is showed in Figure 1.11.

Chapter 2 Improvement of characteristics of pressure control system with porous materials

2.1 Pneumatic RC circuit

Pneumatic RC circuit is a basic constituent part in pressure control systems. In pilot valve system (Figure 1.5), restriction 2 and the diaphragm chamber constitute a pneumatic RC circuit, as shown in Figure 2.1. The volume of the chamber is similar to the volume of the diaphragm chamber V_d. In the pneumatic RC circuit, as is the case in an electric RC circuit, the restriction is equal to the resistance, and the chamber is equal to the capacitance. In consequence, the change in pressure P_d in the chamber is delayed from the downstream pressure P_2 because of the integral of the flow rate. The specific mathematical formula will be clarified in section 2.4. If the restriction is stronger and the frequency of the pressure vibration is higher, the time delay will be larger. That is, the pressure gain of P_d will decrease with an increase in the frequency of the pressure vibration P_2 and the resistance of the restriction. However, unlike the characteristics of electrical resistance, the resistance characteristics of a pneumatic restriction such as an orifice are nonlinear.

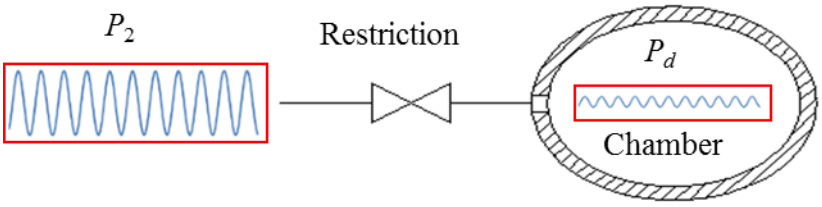

Fig.2.1 Pneumatic RC circuit

2.2 Nonlinear and linear flow rate characteristics

The flow resistance characteristics of a pneumatic restriction refer to its flow rate characteristics, that is, the *P*-*Q* characteristics. The relationship of the pressure with the flow rate *G* in an orifice is summarized in the well-known flow rate equation [48]:

$$G(S_e, P_U, P_D) = \begin{cases} S_e P_U \sqrt{\dfrac{\kappa}{R\theta_1}\left(\dfrac{2}{\kappa+1}\right)^{\frac{\kappa+1}{\kappa-1}}}, & \dfrac{P_D}{P_U} \le 0.5283 \\ S_e P_U \sqrt{\dfrac{2\kappa}{\kappa-1}\cdot\dfrac{1}{R\theta_1}\left[\left(\dfrac{P_D}{P_U}\right)^{\frac{2}{\kappa}} - \left(\dfrac{P_D}{P_U}\right)^{\frac{\kappa+1}{\kappa}}\right]}, & \dfrac{P_D}{P_U} > 0.5283 \end{cases} \tag{2.1}$$

$$S_e = C_D \frac{\pi d^2}{4} \tag{2.2}$$

where S_e is the effective area, d is the diameter of the orifice, C_D is the discharge coefficient, R is the gas constant, P_U is the upstream pressure, P_D is the downstream pressure, θ_1 is the flow temperature, and κ is the specific heat ratio.

Some disadvantage of the nonlinear flow rate characteristics in an orifice with compressible fluid is mentioned in 1.4.1. In fact, engineers prefer a linear characteristics in a control system. Thus, a linear flow rate characteristic is expected to be applied in the pilot valve system. As we know, the flow rate is proportional to the pressure difference when the flow state is transformed to a laminar flow in some micro structures with a low Reynolds number. The linear flow rate characteristics of a laminar-flow pipe, which has a small inner diameter, can be determined from the Hagen–Poiseuille equation:

$$Q = \frac{\pi r^4 \Delta P}{8\mu L} \tag{2.3}$$

where Q is the volumetric flow rate, r is the radius of the pipe, L is the length of the pipe, μ is the dynamic viscosity, and ΔP is the differential pressure.

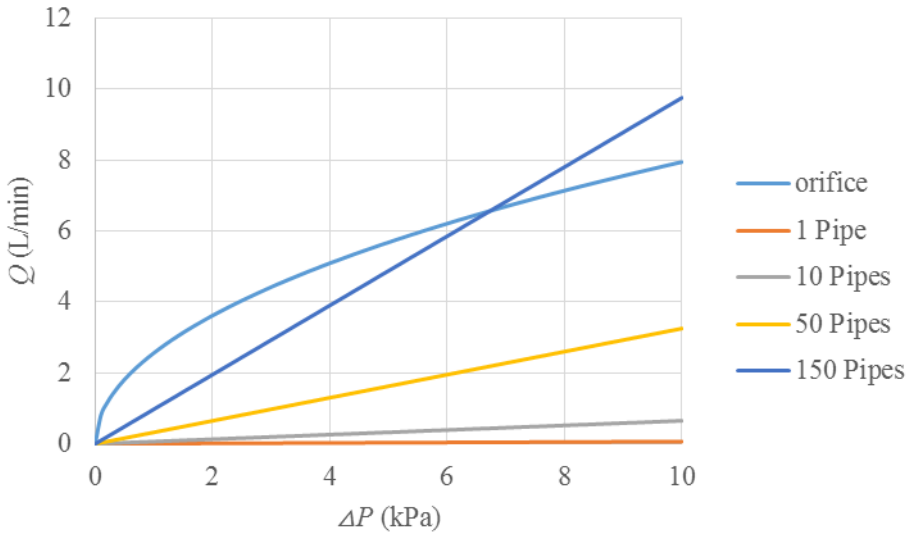

(Pipe: ϕd = 0.2 mm, L = 20 mm; Orifice: ϕd = 1 mm)

Fig.2.2 Flow rate comparison with orifice and micro pipes

However, from Figure 2.2, it is found that the flow rate in the micro pipe is extremely small. And 150 pipes, that are 20 mm in length and 0.2 mm in diameter, would be required to achieve a flow rate corresponding to a 1 mm orifice. It is difficult to manufacture such a large number of micro pipes.

Fortunately, some researchers find that porous materials also have a linear flow rate characteristics when viscous effects govern the flow which is called the Darcy regime [49-54]. That is, it produces the same effect as the micro pipes, i.e., of converting the flow state to laminar due to its large viscous. Figure 2.3 shows a porous material with a hollow cylindrical shape, manufactured by SMC; its dimensions are labeled in this figure. The filter precision of the porous material is only 2 μm. The figure on the right shows the flow route in our experimental apparatus, wherein it can be observed that the effective flow area is the cylinder's inner wall.

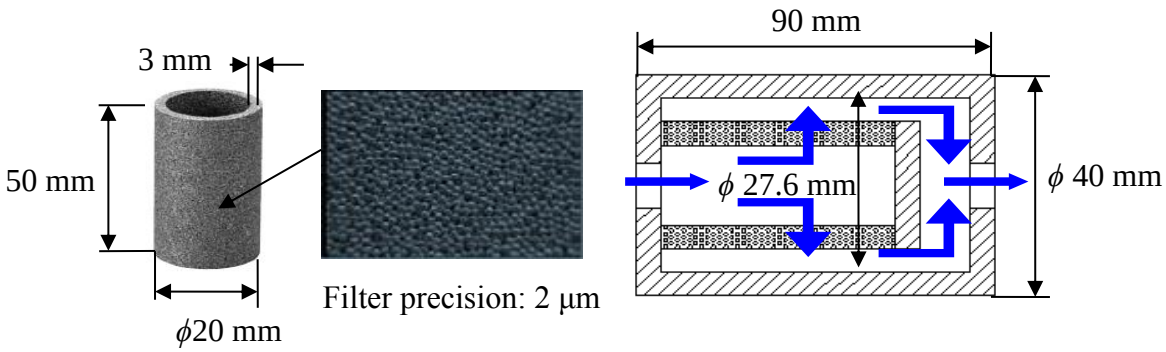

Fig.2.3 Specimen of porous material

2.3 *P*-*Q* characteristics of porous materials

Theoretically, it is difficult to determine the flow rate characteristics of the porous materials by calculation, because of its complicated microstructure. Therefore, a flow rate measurement experiment is indispensable.

2.3.1 Static experiment

A static *P*–*Q* characteristics experiment was performed to determine the actual flow rate characteristics of the porous material and the orifice. The schematic of the experimental setup is shown in Figure 2.4. In this experiment, the type of the porous materials is ESP-20-50-3-2 by SMC. Two orifices of different diameters (3.2 mm and 2.8 mm) were employed, for the flow rate was almost the same as that for the hollow porous cylinder under a certain differential pressure. The natural gas was replaced with air because of their thermodynamic similarity. The difference of this two gases will be discussed in chapter 5. The other reasons are that air is security and convenience.

The upstream pressure was set to a constant value of 90 kPaG by the regulator, because the working pressure will be held on 90 kPaG in the next dynamic experiment. The downstream pressure could be adjusted by the control valve. The upstream pressure and

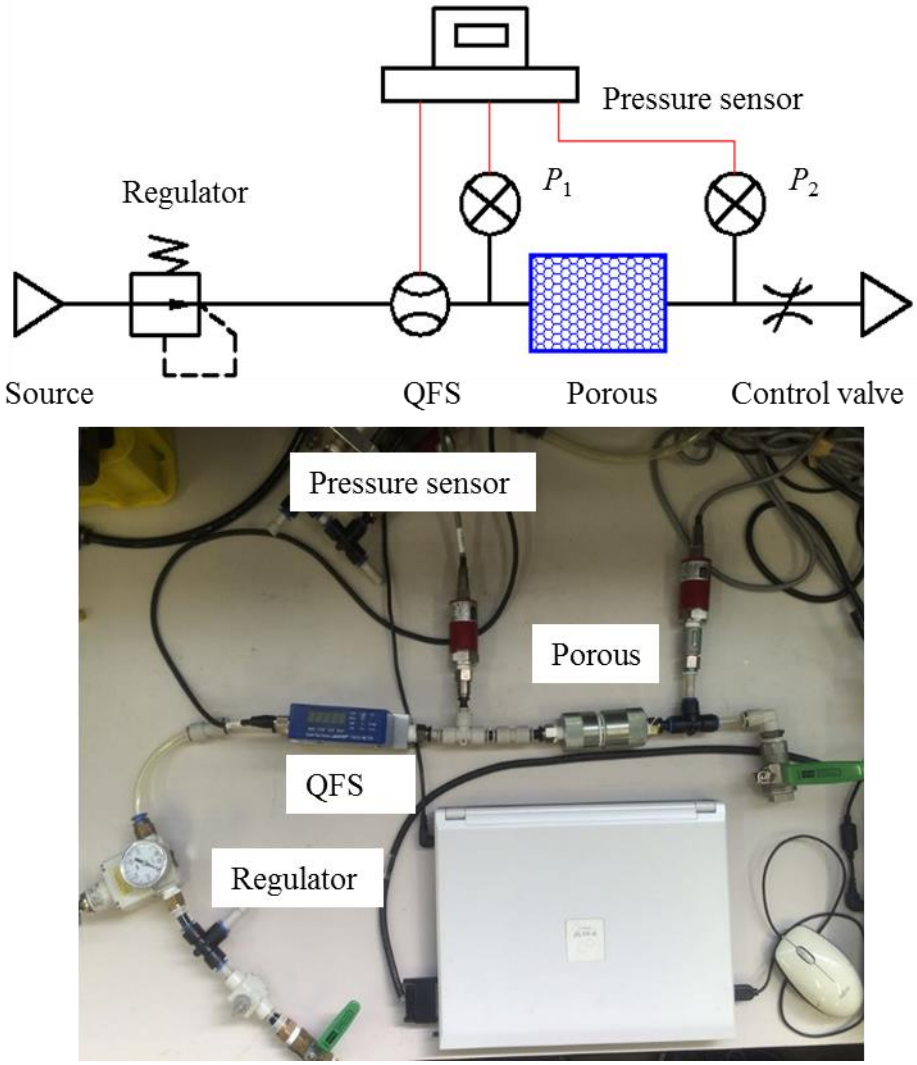

Fig.2.4 Schematic of experimental setup

downstream pressure were measured by pressure sensor P_1 and P_2, respectively. The flow quantity Q was measured by a quick flow sensor (QFS) [55].

2.3.2 Experiment results

Figure 2.5 shows the P–Q characteristics curves of the porous material and the orifice. In this figure, the diamonds, circles, and squares indicate the experimental data for the porous material, 2.8 mm orifice, and 3.2 mm orifice, respectively. The negative signs of ΔP and Q represent a reversed flow. It can be clearly seen that the trend of the

experimental data for the porous material is a straight line and that for the orifice is a curve. The straight line in this figure is the linear fitting of the data points for the porous material. Furthermore, the calculated curves were obtained using Eq. (2.1), for which purpose C_D was obtained from the experimental data points of the orifice, C_D is calculated to 0.98 in the 3.2 mm orifice and 0.93 in the 2.8 mm orifice. The resultant equations of the line and curves were used in the simulation of the dynamic response described in the next section 2.4.

The *P*–*Q* characteristics curve of the orifice indicates that the flow rate increases rapidly when the differential pressure is small, and the increasing speed gradually reduces when the differential pressure increases. However, the response of porous material remains unchanged because of its linear characteristics. That is, the pneumatic resistance of the orifice is smaller than the porous material when the pressure difference is small. And, a slight change in a pressure difference results in a considerable change in the flow rate through the orifice and generates a pressure oscillation in the chamber of the pneumatic RC circuit. But when the pressure difference becomes larger, the pneumatic resistance of the orifice also becomes larger, and it allows less flow rate than the porous material. Meanwhile, the pneumatic resistance of the porous material is always invariable. The amplitude change of the pressure vibration affects the pressure difference, and then, affects the pneumatic resistance of the orifice. Therefore, the amplitude of oscillation of the pressure P_2 affects the dynamic response of the pressure P_d in the chamber with the orifice, but it does not affect the dynamic response of P_d in the chamber with the porous material.

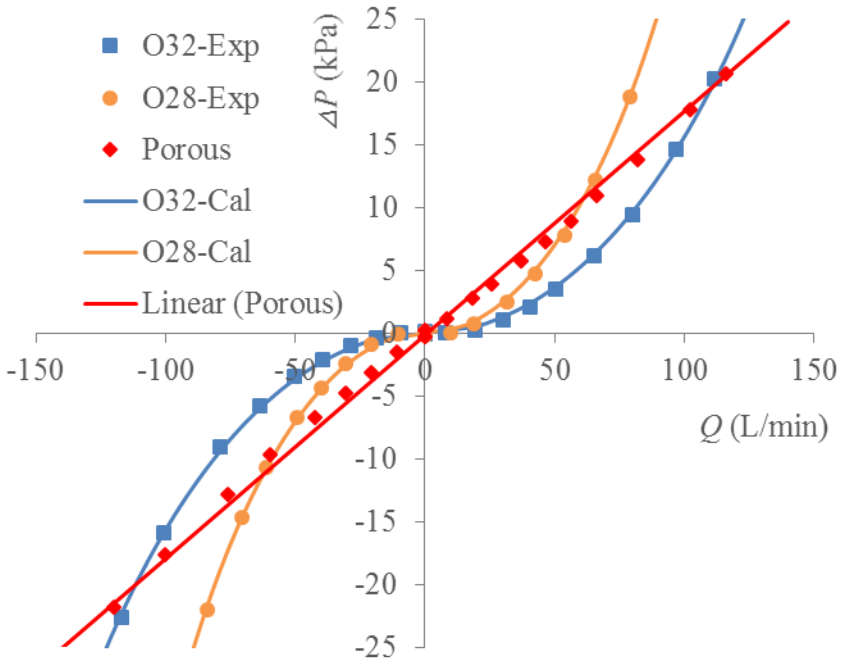

Fig.2.5 *P*–*Q* characteristics curves

2.4 Simulation of the pneumatic RC circuit

The pneumatic RC circuit with a porous material and orifice was simulated by MATLAB. The pressure vibration source P_2 was replaced by a sine signal. The mathematical model is shown in Figure.2.6.

Firstly, the restriction model of the porous material and orifice was obtained from their *P*–*Q* characteristics curves. From Fig. 2.5, the discharge coefficient C_D was calculated to be 0.98 in orifice for the model which used Eq. (2.1). The fitted equation of *P*–*Q* characteristics curve in the porous material was determined to be:

$$Q_{porous} = K_{p1} * \Delta P \tag{2.4}$$

Here, Q_{porous} is the quantity of flow in the porous material. The pressure and flow rate units are kPa and L/min respectively. K_{p1} is the flow rate constant, K_{p1} = 6.2 [L/(min·kPa)].

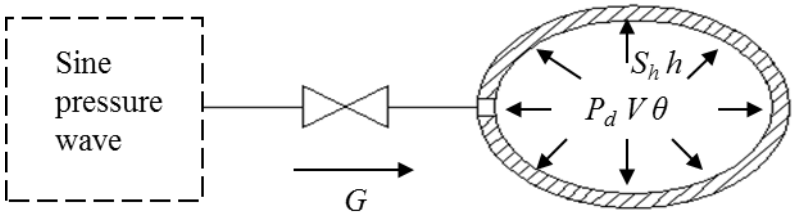

Fig.2.6 Mathematical model

Secondly, in the chamber, the ideal gas equation was differentiated with respect to time:

$$P_d V = mR\theta \tag{2.5}$$

$$\frac{VdP_d}{dt} = R\theta\frac{dm}{dt} + mR\frac{d\theta}{dt} \tag{2.6}$$

Where P_d is the pressure in the chamber, V is the volume of chamber, m is the mass of the air in the chamber, θ is the average temperature in chamber, and R is the ideal gas constant.

In the vacant chamber, the temperature change needs to be added. Thus, considering the enthalpy in the chamber and the energy change on the wall of the chamber, the energy equation was obtained from the first law of thermodynamics. Thus:

$$q = P_d\frac{G}{\rho} - C_v\rho V\frac{d\theta}{dt} \tag{2.7}$$

G is the mass flow rate, ρ is the average density of air in the chamber, C_v is the constant volume specific heat capacity, and C_v = 718 J/(kg·K). q is the heat transfer on wall, from the Newton's law of cooling,

$$q = hS_h(\theta - \theta_a) \tag{2.8}$$

θ_a is the temperature of atmosphere, h is the thermal conductivity, S_h is the heat transfer area of the chamber. Eq. (2.8) was substituted to Eq. (2.7):

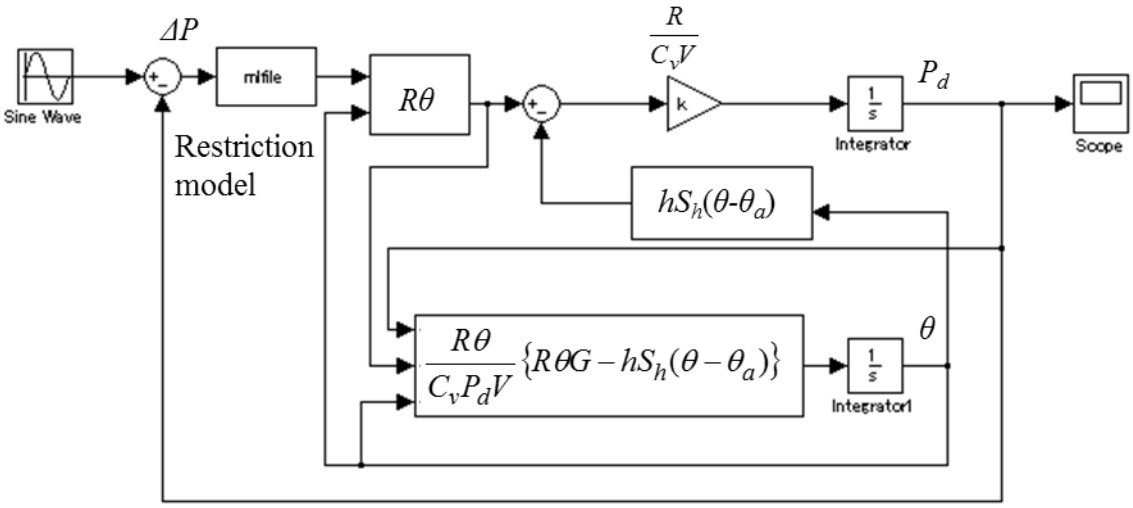

Fig.2.7 Diagram of simulation block with vacant chamber model

$$\frac{d\theta}{dt}=\frac{R\theta}{C_vP_dV}\left\{R\theta G-hS_h(\theta-\theta_a)\right\} \tag{2.9}$$

Eq. (2.9) was substituted to Eq. (2.6), and using the equation $R=C_p$ - C_v, C_p is the constant pressure specific heat capacity. C_p =1005 J/(kg·K). Our equation is:

$$\frac{dP_d}{dt}=\frac{R}{C_vV}\left\{C_p\theta G-hS_h(\theta-\theta_a)\right\} \tag{2.10}$$

Figure.2.7 shows the simulation block diagram of Eq. (2.4), Eq. (2.9) and Eq. (2.10).

In the isothermal chamber, the temperature change can be neglected. And equation (2.6) ~ (2.9) is canceled. $d\theta/dt=0$. Furthermore, $dm/dt=G$, where G is the mass flow rate. Therefore, Eq. (2.10) was changed to

$$\frac{dP_d}{dt}=\frac{R\theta}{V}G,\ \text{integral form is,}\ P_d=\int\frac{R\theta G}{V}dt \tag{2.11}$$

Figure 2.8 shows the simulation block diagram.

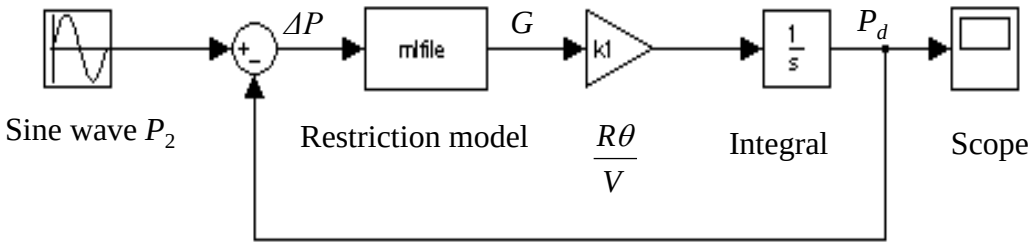

Fig.2.8 Diagram of simulation block with ITC model

$$K_d = 20\log_{10}(\frac{A_d}{A_2}) \tag{2.12}$$

where A_d, and A_2 are the amplitudes of P_d, and P_2, respectively. The phase difference $\Delta\phi_d$ is also considered with respect to the input pressure P_2. That is,

$$\Delta\phi_d = \phi_d - \phi_2 \tag{2.13}$$

Here, ϕ_d and ϕ_2 are the phases of P_d and P_2, respectively.

2.5 Dynamic experiment

The pressure response experiment is carried out in a vacant chamber and an isothermal chamber. Each experiment is divided into two steps, one uses the porous material as a restriction to investigate the pressure response and the other one uses an orifice.

2.5.1 Experiment setup

In our experiment, a sine pressure generator was used to provide the pressure input by regulating the inflow and outflow from a servo valve using feedback PI control [56]. The generator produced a sine pressure wave whose frequency can be adjusted to 50 Hz, and amplitude can reach to 30 kPa. The volume of the isothermal chamber was 200 mL with a bundle of copper wires in it. The actual volume was 180 mL. Therefore, when the copper wires were taken out to be placed in a vacant chamber, a 20 mL solid metal block was put in it for keeping the volume to 180 mL.

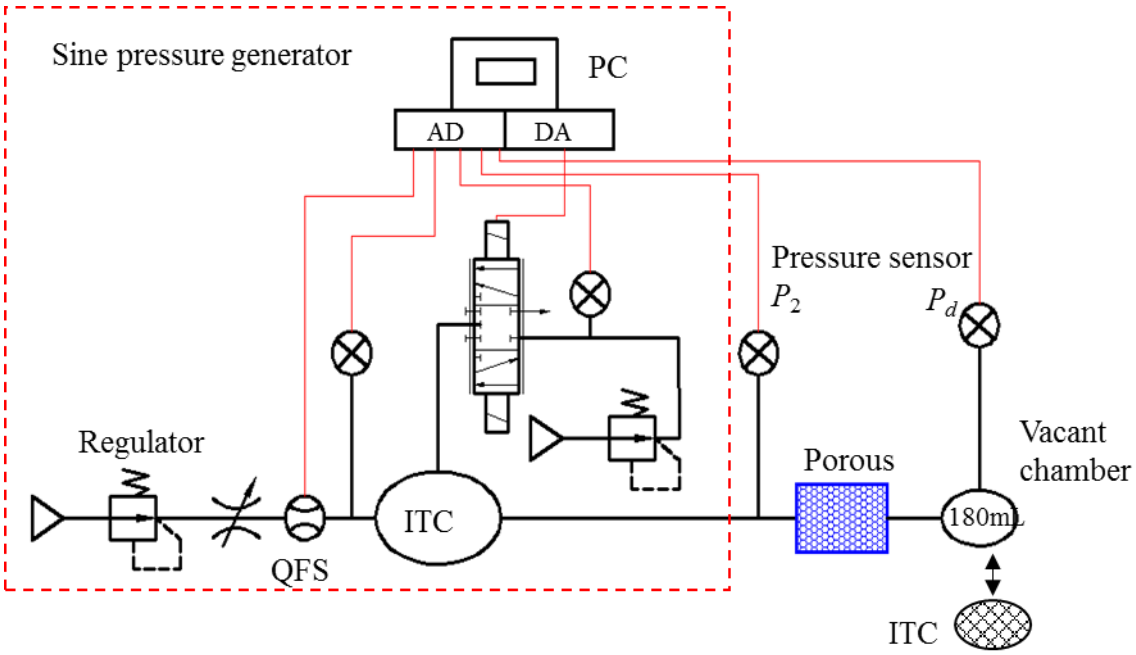

Fig.2.9 Pneumatic circuit diagram of frequency response experiment

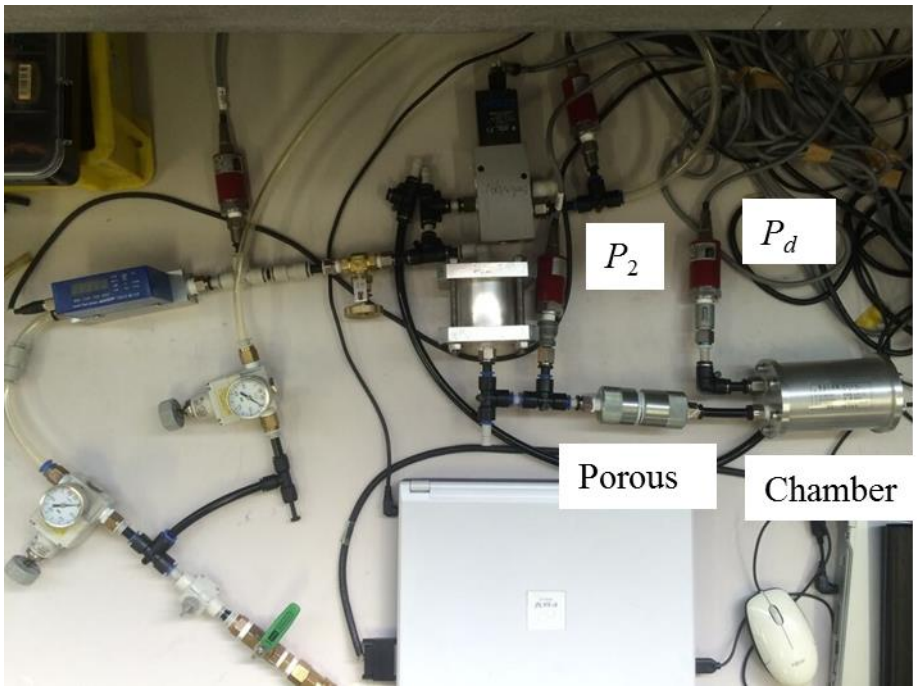

Fig.2.10 Dynamic experiment apparatus

Figure 2.9 shows the pneumatic circuit of the pressure response experiment. The pressure generator is in the red block, and the generated pressure was measured by pressure sensor P_2. The response pressure in the chamber was measured by pressure

Table 2.1 Specifications of experimental equipment

Equipment	Range	Type
Pressure P_2	0–500 [kPa]	FP101-B31-C20A*B (YOKOGAWA)
Pressure P_d	0–200 [kPa]	FP101-A31-C20A*B (YOKOGAWA)
Flow rate	0–200 [L/min(ANR)]	QFS-200 (TOKYO METER)
ITC	180 [mL]	ITC-0.2(TOKYO METER)

sensor P_d. Figure 2.10 presents an image of this experimental apparatus. Table 2.1 shows the primary specification of the equipment in this experiment.

The experimental conditions are listed in Table 2.2. The experiment process is illustrated as follows:

1) First, the amplitude of the generated pressure P_2 was set to a constant value of 1 Hz, the base pressure is set to 90 kPaG.

2) Start the pressure generator, and the data of P_2 and P_d were recorded.

3) Then, a data were recorded every 5 Hz with increasing frequency to 40 Hz.

4) The amplitude was then changed and the above steps were repeated.

5) After the completion of a restriction test, the restriction was changed and the procedure returned to the first step.

6) Change the vacant chamber to ITC, and record the data following the procedures above.

Table 2.2 Experimental conditions

Chamber	Test restriction	Frequency [Hz]	Amplitude [kPa]
Vacant	Porous material	1–40	5,10,20
	3.2 mm Orifice	1–40	5,10,20,30
ITC	Porous material	1–40	5,10,20
	3.2 mm Orifice	1–40	5,10,20,30
	2.8 mm Orifice	1–40	5,10,20,30

2.5.2 Data of the pressure wave

A series of pressure waves in this dynamic experiment was recorded. Figure 2.11 illustrates a series of pressure response waves change with frequency when the restriction is applied to porous material. The amplitude of the sine pressure vibration is set to 10 kPa, it is seen that the amplitude of the response pressure P_d gradually decreases while the frequency increases. For example, when the frequency reaches to 25 Hz, the amplitude of P_d is almost one third of P_2, and the gain of P_d is calculated to be -10.07 dB, the phase difference is -72.31°.

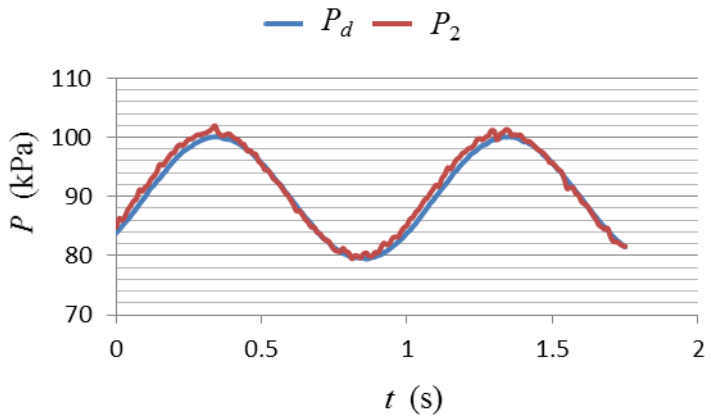

a) 1 Hz

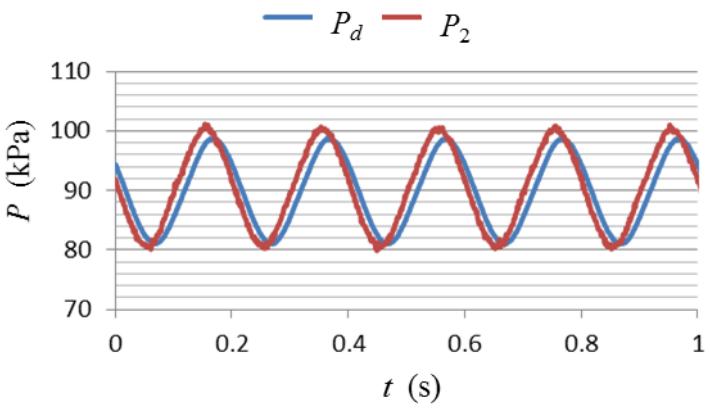

b) 5 Hz

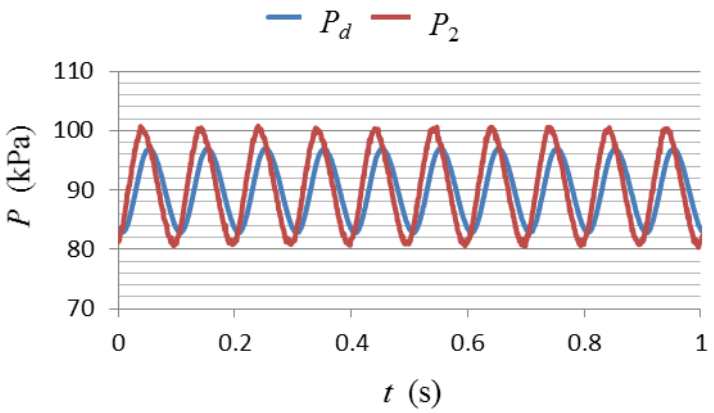

c) 10 Hz

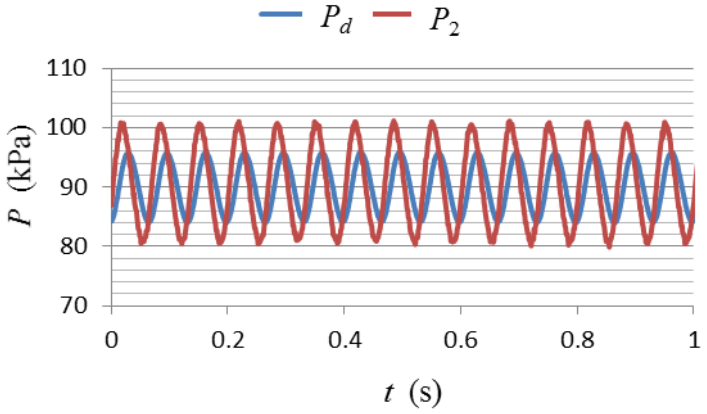

d) 15 Hz

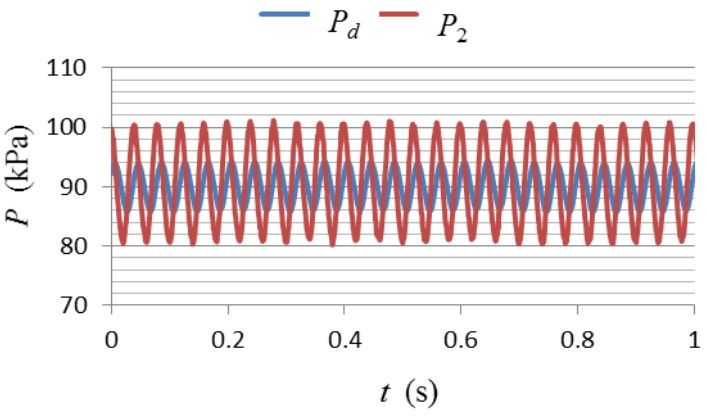

e) 25 Hz

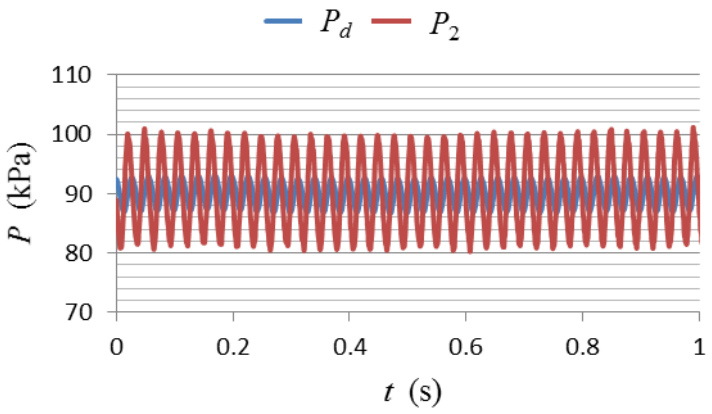

f) 35 Hz

Fig.2.11 Pressure response wave with frequency in porous materials (A_2=10kPa)

Figure 2.12 shows the response pressure wave with different amplitude of input pressure at the same frequency when the restriction is applied to porous material. The amplitude of P_d are all 0.33 times of P_2, and the phase difference are all -72°. Figure 2.12 (b) is looked like to be stretched from Figure 2.12 (a) in proportion.

In Figures 2.11 and 2.12, the pressure wave is not a standard sine wave, because there are some errors in the pressure generator. These tiny pressure vibration in the pressure wave will affect the calculation of the amplitude and phase. Hence, the data were processed with a harmonic analysis by FFT to confirm its accurate amplitude and phase. Figure.2.13 shows an example of the amplitude calculation by FFT which uses the data of Figure 2.12 (a). It can be seen that the response pressure wave P_d is very smooth, but the input pressure wave P_2 appears two small noise waves at 50 Hz and 75 Hz, respectively. The calculation program was manufactured to an m-file by MATLAB. We can use this program to investigate the accurate amplitude and phase of each data. By the way, these pressure wave examples are all in the vacant chamber.

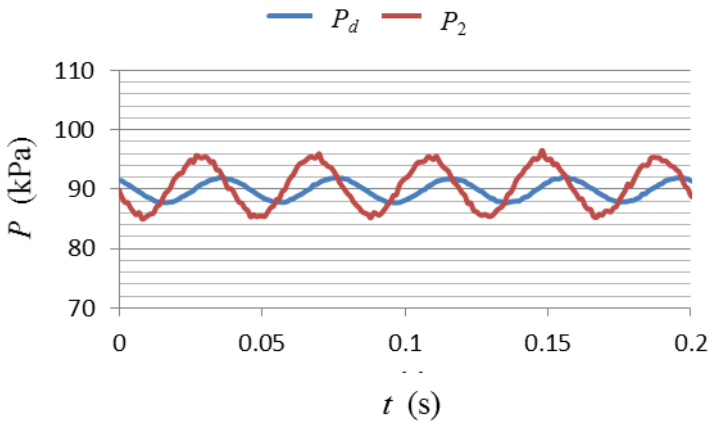

a) A_2=5kPa

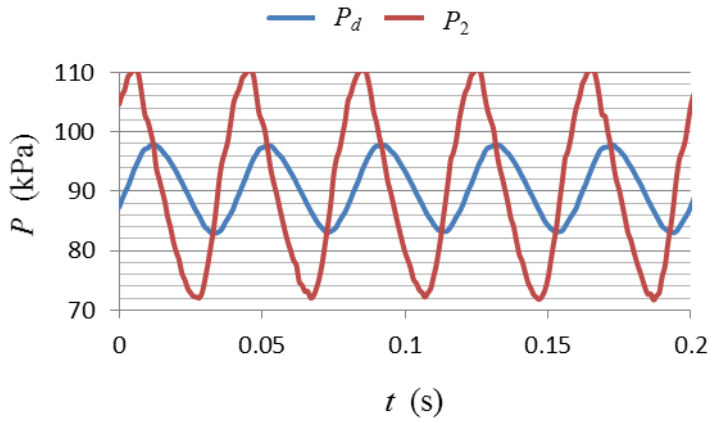

b) A_2=20 kPa

Fig.2.12 Pressure response with different amplitude in porous materials (f = 25 Hz)

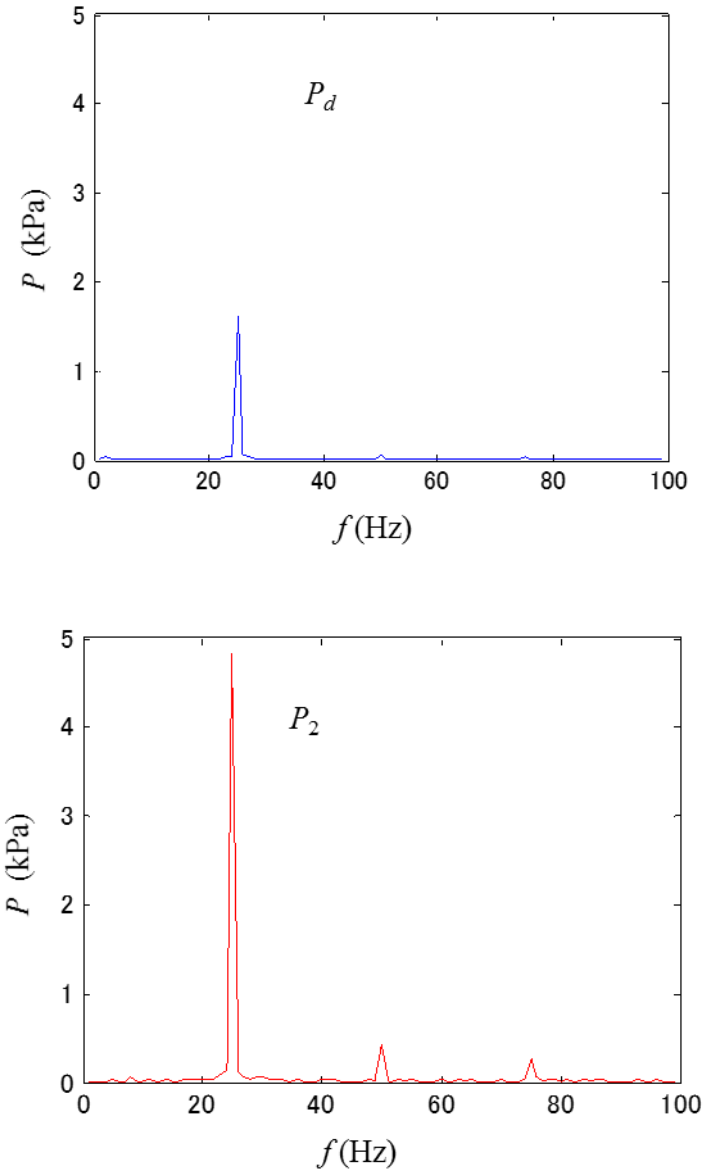

(A_2 = 5kPa; f = 25 Hz; Porous material)

Fig.2.13 FFT analysis with pressure response

2.5.3 Dynamic experiment results and analysis

The Gain and phase difference of the response pressure were calculated by Eq. (2.12) and Eq. (2.13) at each frequency, as shown in the Bode diagram. Firstly, the simulation and experiment results with the vacant chamber are shown in Figures 2.14 and 2.15.

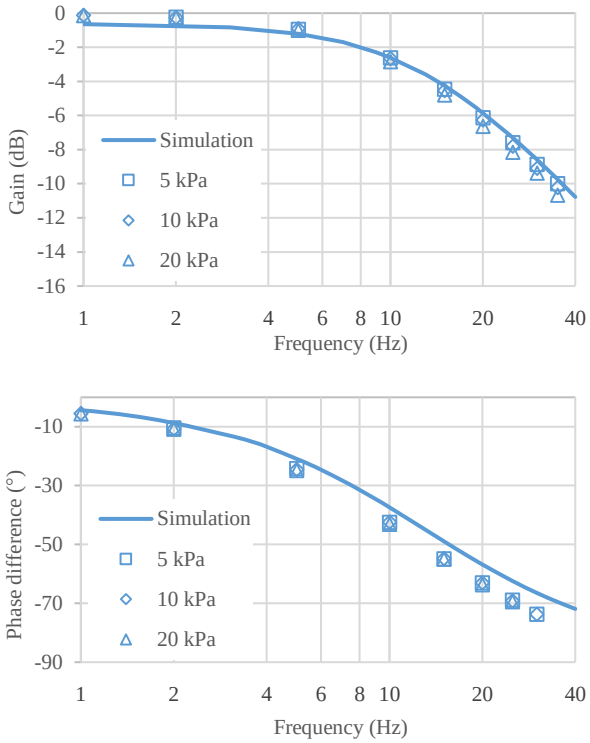

Fig.2.14 Bode diagram of porous material

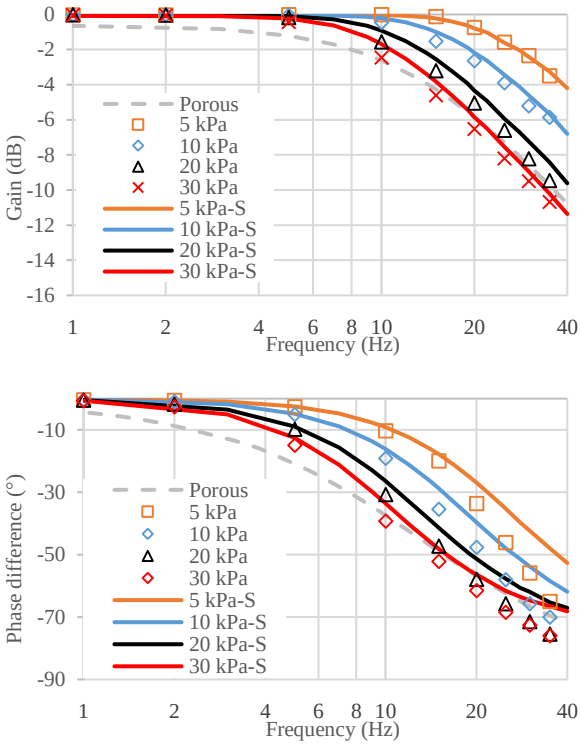

Fig.2.15 Bode diagram of orifice

Figure 2.14 shows the frequency response of the porous material, and Figure 2.15 shows the frequency response of the orifice. The points based on the experimental data and the markers represent the different amplitude conditions of the input pressure. The solid curves are the simulation results. In addition, the top graph shows the gain changes and the bottom graph shows the phase changes.

The results shows how the pressure gain drops and the phase delay increases with frequency no matter what the restriction is. In the simulation, the magnitude of the gain drop in the porous restriction is invariable with respect to the amplitude of input pressure. Therefore, the simulation results form only one curve in Figure 2.14. Also, the experiment data is in agreement with it when the input pressure amplitudes are 5, 10, and 20 kPa. However, in the right picture, the pressure gain curve of the orifice drops at a different rate if the amplitude of the input pressure changes. There is a small discrepancy between the experiment data and the simulation results because of the experimental error. The reason is thought to be the linear and nonlinear characteristics in porous materials and orifice, respectively. Because of the linear *P*–*Q* characteristics of the porous restriction, the quantity of flow into the chamber will increase in proportion to the differential pressure. If the amplitude of the input pressure changes, the flow rate changes by the same proportion, and the amplitude of the pressure response P_d also has the same proportional change. However, in an orifice, these changes cannot stay proportional because of the nonlinear behavior. In short, the flow rate resistance is a constant in a porous material but not in an orifice. This phenomenon can be also seen in the change of the phase difference. In addition, the dash curve in the right picture represents the porous material for comparison. It shows that the gain of pressure is lower than that of the orifice when the amplitude of the input pressure is small, such as 5–20kPa. That is, if the vibration of the

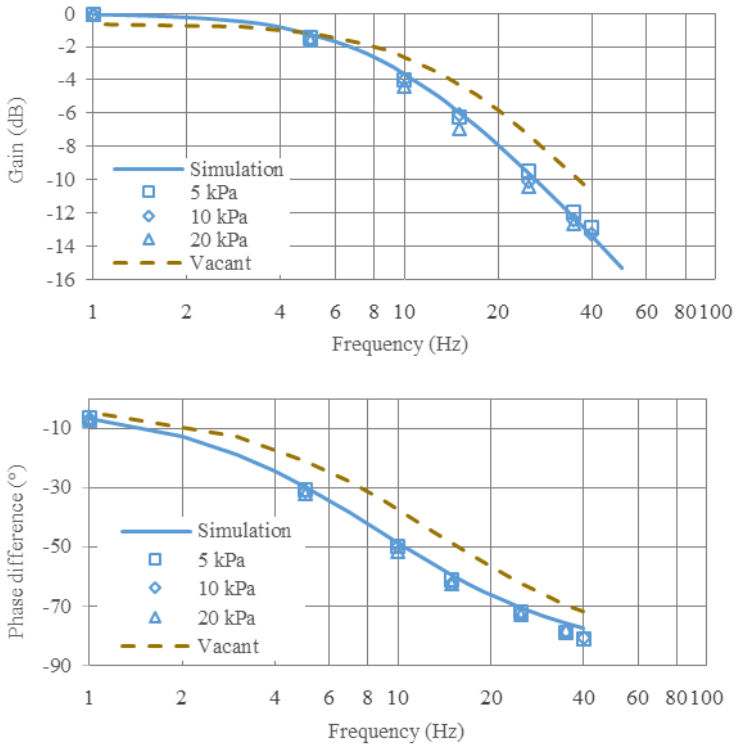

Fig.2.16 Bode diagram of porous material with ITC

downstream pressure P_2 is small, there will be a large oscillation in the diaphragm chamber with an orifice, while the porous material has no such problems.

Figure 2.16 shows the results of porous material with an isothermal chamber. The variation tendency of the gain and phase difference is also in accordance with the results of vacant chamber, but slightly lower than them at the high frequency domain because of the significant heat exchange. These difference is also in the results of the orifice, but it is not shown in the next figures because the large number of curves.

Figure 2.17 shows the results of two orifices with the isothermal chamber. Referring to the dash curve, the gain and phase difference of 2.8 mm orifice is lower than that of 3.2 mm orifice because of its larger pneumatic resistance. And the curve of the porous material is is demonstrated by the gray dash lines in the left figures. It indicates that the position of the gain and phase difference curves only depend on the magnitude of their

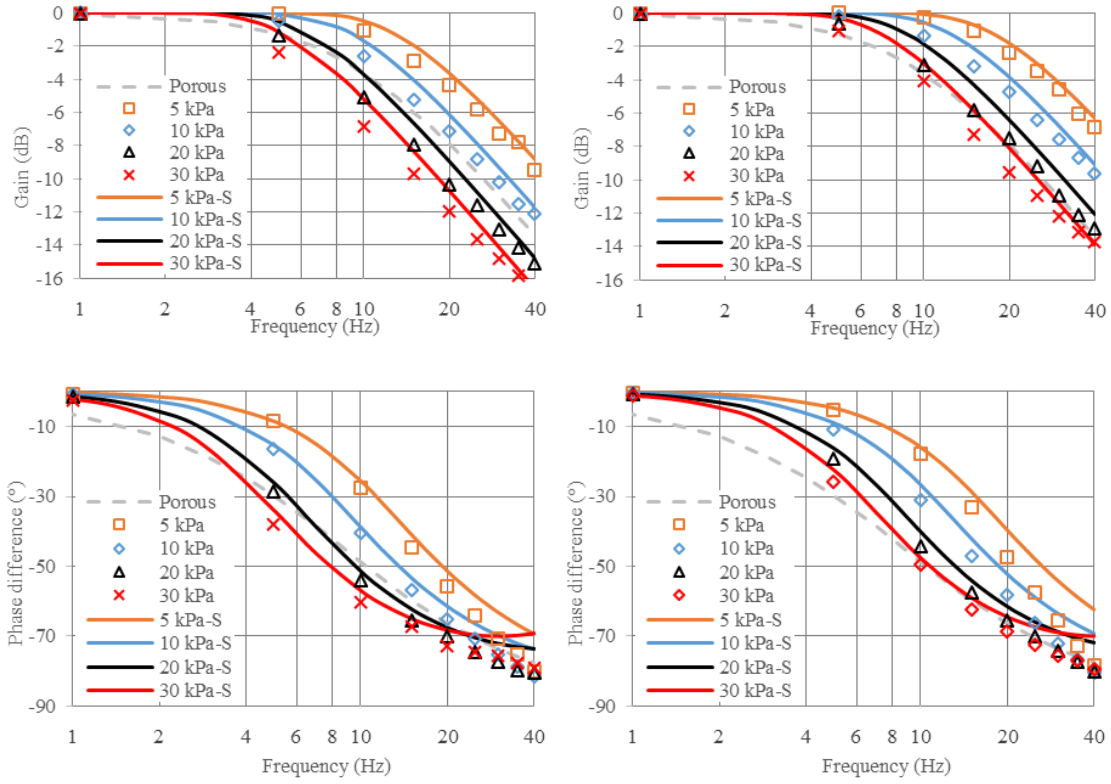

d = 2.8 mm　　d = 3.2 mm

Fig.2.17 Frequency response of orifices with ITC

flow rate. Therefore, we could select a feasible porous material to match with the original orifice in the pilot valve system according to their flow rate characteristics.

From these results, it is not hard to see that the porous materials are conducive to change the pressure control system into a linear system instead of the nonlinear system, and this linear performance will help the engineers to design the pressure control system. At the same time, its flow resistance is larger than the orifice with a small pressure difference, and the pressure vibration can be effectively restrained.

2.6 Conclusions

In this chapter, we proposed a method for improving the characteristics of a gas pressure control system, such as a pilot valve governor unit, by using porous materials and an isothermal chamber. A static characteristics experiment with a porous material and an orifice was performed to confirm their *P*–*Q* characteristics. A frequency response experiment was also performed to estimate their dynamic responses. The results of the experimentation were in close agreement with the simulation results. Finally, the following conclusions were drawn from the study:

(1) The *P*–*Q* characteristics of porous materials are linear, but those of the orifice are nonlinear. The flow rate increases rapidly when the differential pressure in the orifice is small, and it gradually reduces with increasing differential pressure. However, for the porous material, the increase rate remains invariable.

(2) In the case of a pneumatic RC circuit with a porous restriction, the curves of the pressure gain and phase difference in the frequency response experiment are invariable with respect to changes in the amplitude of the input pressure. However, they are variable in the case of a pneumatic RC circuit with an orifice, because of the nonlinear flow rate characteristics of the orifice.

(3) The pressure gain in the chamber with porous materials is lower than that with an orifice when the amplitude of the input pressure is small. The employment of porous materials instead of orifices helps reduce the pressure oscillation in a pneumatic chamber when the input pressure vibration is small.

(4) It indicates that the pressure control system can be linearized by using the porous material easily.

Chapter 3 Improvement of characteristics of pilot valve system with porous materials

3.1 Test pilot valve system

The linear effect of the porous materials is verified in the pneumatic RC circuit as discussed in Chapter 2. In this chapter, the effect of the porous materials is examined in a test pilot valve system established in our laboratory. Needless to say, the experimental gas is also air, for the same reason as discussed in the previous chapter.

In a gas governor unit, the flow rate of more than 2000 m^3/h is extremely large in the main pipe, and it is not possible to generate such a flow rate in our laboratory. Therefore, only the block part indicated by a dash line in Figure 3.1 is retained in the test pilot valve system; the rubber chamber of the main valve (axial flow valve) was replaced with an isothermal chamber (ITC) and the main pipe was removed. The pressure in the ITC was still referred to as the control pressure P_c. A sine-wave pressure P_i, instead of the downstream oscillation, was provided by a pressure generator. The upstream pressure P_1 was kept constant by the pressure regulator. To evaluate the characteristics of the test pilot valve system, the pressure responses of P_c and P_d relative to P_i were measured with different test restrictions. In this test system, it is easy to observe the pressure response results under the same experimental conditions. The pressure P_i can be maintained as a sine wave because there is no feedback flow to affect it.

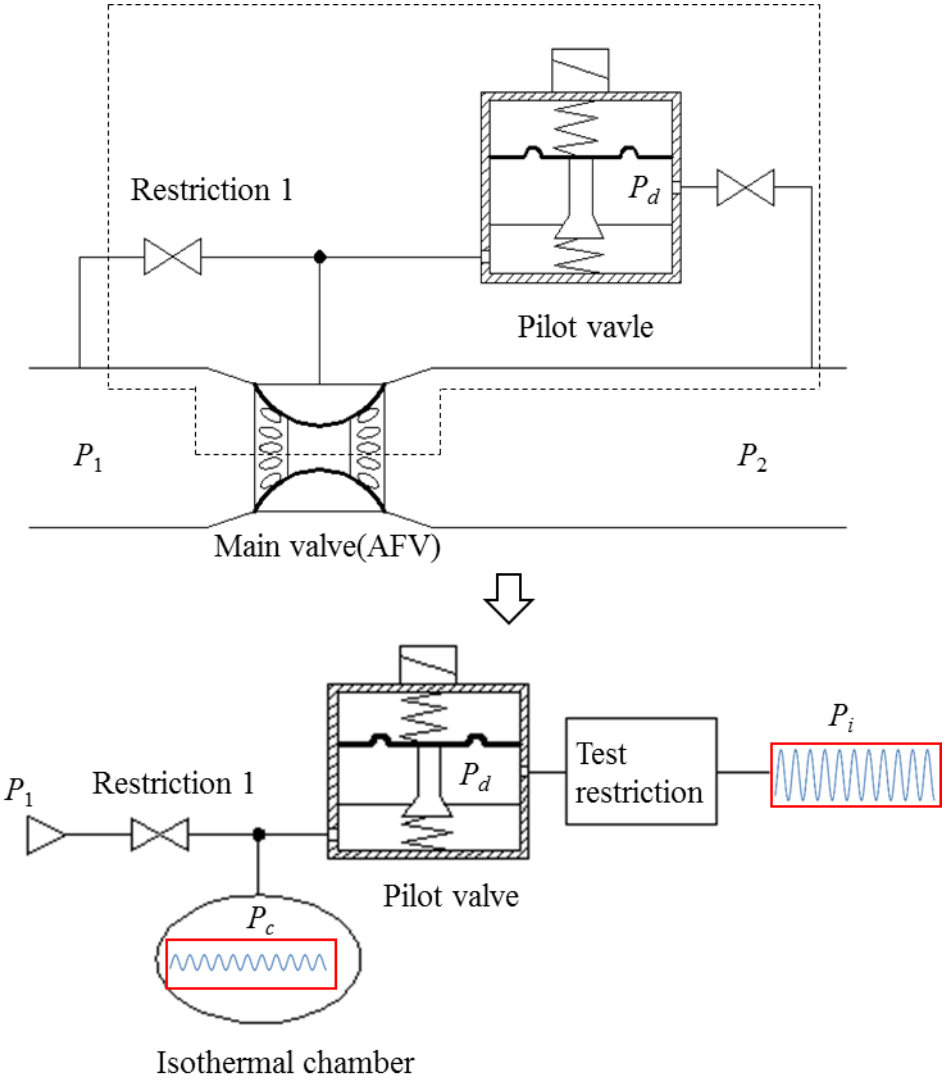

Fig.3.1 Test pilot valve system

3.2 Test restriction

There is a limited pressure in the test pilot valve, if the pressure in the diaphragm chamber exceeds or goes below this pressure limit, the valve will be fully open or completely closure. The valve will get to a saturation condition and the flow rate will be out of control. Thus, the amplitude of input pressure P_i needs to be controlled in a range to avoid the saturation condition. In this test valve, it needs to be controlled below 10 kPa. Due to this reason, the maximum pressure difference of the pressure P_i and P_d can't

exceed 10 kPa. Therefore, the flow rate characteristics of the test porous material and orifice are matched under this pressure difference. By the way, the work pressure in the diaphragm chamber is 150 kPaG, that is, the base pressure of the input pressure also needs to be set to this valve.

The diameter of the test orifice is also 2.8 mm in the same way as the previous experiment. A porous material with a hollow cylindrical shape (Figure 3.2) was used as a test restriction in this experiment. The dimensions are shown in the figure, and its wall thickness is changed to 2 mm to increase its flow rate, because the effective area is the cylinder's inner wall and the size of packed vessel is difficult to change. And the filter precision of the porous material is also 2 μm. The flow rate linear fitting equation of the porous material can be obtained through the *P*–*Q* characteristic experimental data. The flow rate characteristics experiment was implemented in the same manner as section 2.3.1.

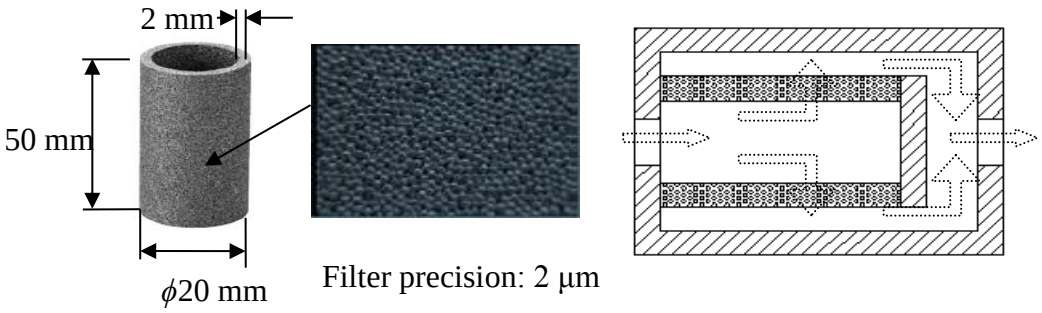

Fig.3.2 Porous material specimen

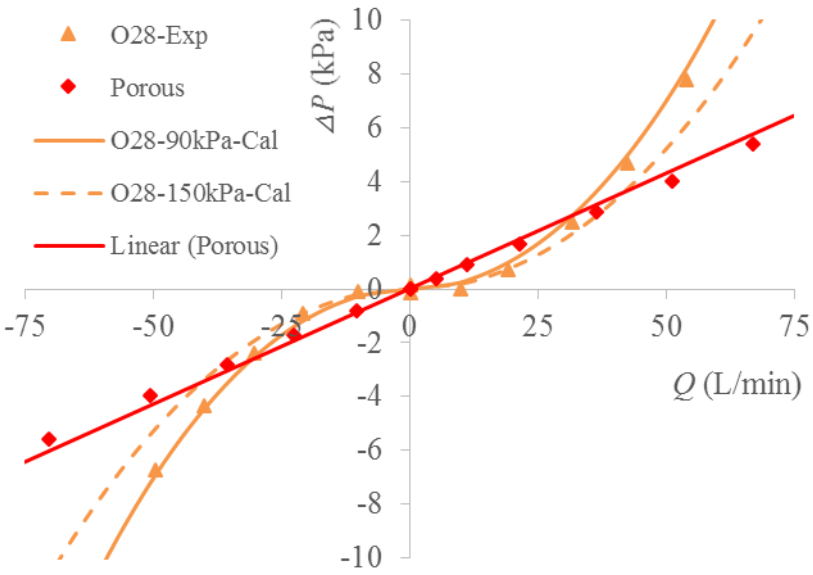

Fig.3.3. *P*–*Q* characteristic curves

Figure 3.3 shows the *P*–*Q* characteristic curves for the new porous material and orifice. The diamond- and triangle-shaped points represent the experimental data of the porous material and orifice, respectively. The *P*–*Q* characteristic curves (solid curve) of the orifice are obtained from the experiment data when the upstream pressure is set to 90 kPaG. For an upstream pressure of 150 kPaG, the *P*–*Q* characteristic curve for the orifice is represented by the dash curve in Figure 3.3. In the next dynamic experiment, we use the dash curve to simulate the experiment process because the working pressure is 150 kPaG. The fitted equation of the *P*–*Q* characteristics (straight line) for the porous material was determined to be

$$Q_{porous} = K_{p2} * \Delta P \tag{3.1}$$

Here, Q_{porous} is the quantity of flow and ΔP is the differential pressure. The pressure and flow rate units are kPa and L/min, respectively. K_{p2} is the flow rate constant, K_{p2} = 11.6 [L/(min·kPa)].

3.3 Simulation

The test pilot valve was manufactured by Tokyo Gas Co., Ltd. (Figures 3.4 and 3.5). An orifice 2 (restriction 1 in Figure 3.1) located upstream is embedded in the inlet of the valve. The diaphragm chamber is isolated from the downstream volume to avoid the effect of the downstream pressure. The control chamber is connected to an ITC to enlarge the volume and to eliminate the change in temperature. The mathematical model of this system is constituted with three parts: the pneumatic RC circuit with the restriction and diaphragm chamber, pilot valve model, and control chamber isothermal model.

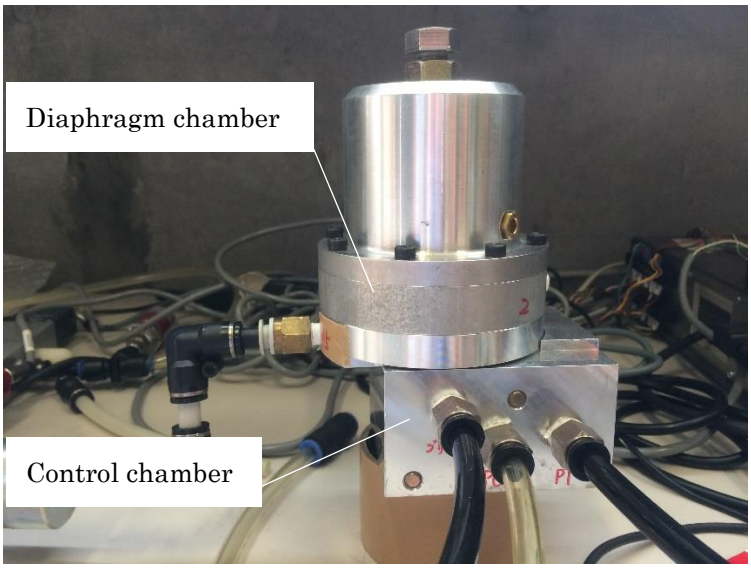

Fig.3.4 Photo of test pilot valve

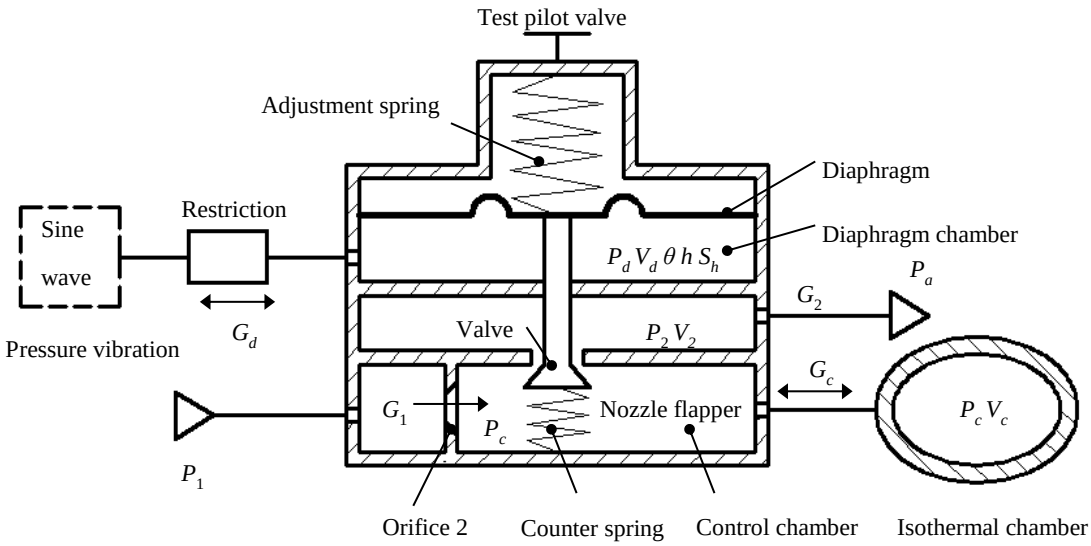

Fig.3.5 Model of test pilot valve system

3.3.1 Mathematical model of pneumatic RC circuit

The pressure vibration was simulated by a sine-wave pressure source. The mass flow rate G_d through the orifice and porous materials was obtained from Eqs. (2.1) and (3.1). In the diaphragm chamber, the volume was assumed to be constant and the ideal gas equation was differentiated with respect to time:

$$P_d V_d = mR\theta \tag{3.2}$$

$$\frac{V_d dP_d}{dt} = R\theta \frac{dm}{dt} + mR\frac{d\theta}{dt} \tag{3.3}$$

where P_d is the pressure in the diaphragm chamber, V_d is the volume, m is the mass of the air in the chamber, and θ is the average temperature. Note that dm/dt is just the mass flow rate G_d.

Considering the enthalpy in the diaphragm chamber and the energy change along the wall, the energy equation was obtained from the first law of thermodynamics:

$$q = P_d \frac{G_d}{\rho} - C_v \rho V_d \frac{d\theta}{dt} \tag{3.4}$$

where ρ is the average density of air in the diaphragm chamber, C_v is the constant volume specific heat capacity, C_v = 718 J/(kg·K), and q is the heat transfer along the wall. Using the Newton's law of cooling, q is defined as

$$q = hS_h(\theta - \theta_a) \tag{3.5}$$

where θ_a is the temperature of the atmosphere, h is the thermal conductivity, and S_h is the heat transfer area of the diaphragm chamber. Eq. (3.5) is substituted in Eq. (3.4) to obtain

$$\frac{d\theta}{dt} = \frac{R\theta}{C_v P_d V_d}\left\{R\theta G_d - hS_h(\theta - \theta_a)\right\} \tag{3.6}$$

By substituting Eq. (3.6) in Eq. (3.3) and using the equation $R = C_p - C_v$, where C_p is the constant pressure specific heat capacity (C_p = 1005 J/(kg·K)), the following equation is obtained:

$$\frac{dP_d}{dt} = \frac{R}{C_v V_d}\left\{C_p \theta G_d - hS_h(\theta - \theta_a)\right\} \tag{3.7}$$

3.3.2 Mathematical model of test pilot valve

The mass flow rate G_N through the nozzle flapper of the valve can also be obtained using Eq. (2.1). That is, $G_N = G(S_{ex}, P_c, P_2)$. Here, S_{ex} is the effective area of the nozzle flapper and is defined as

$$S_{ex} = C_D \pi d_N x \tag{3.8}$$

where x is the displacement between the nozzle and flapper and d_N is the diameter of the nozzle. x depends on the dynamic equation of the valve, and thus,

$$m_v \frac{d^2x}{dt^2} + c\frac{dx}{dt} + (k_1 + k_2)x = (P_d - P_{set})S_d \tag{3.9}$$

where m_v is the total mass of the moving part, including the mass of the flapper and center plates and one third of the sum of the spring mass. c is the damping coefficient, k_1 is the spring constant of the adjustment spring, k_2 is the spring constant of the counter spring, P_{set} is the setting pressure of the valve, and S_d is the effective area of the diaphragm. The Coulomb friction was neglected in this equation because it was too small in the test valve.

3.3.3 Mathematical model of ITC

In the ITC, the temperature is constant. Therefore, removing the temperature term, Eq. (3.3) can be written as

$$\frac{V_c dP_c}{dt} = R\theta_a (G_1 - G_N) \tag{3.10}$$

where V_c is the sum of the volumes of the ITC, control chamber, and pipe; P_c is the control pressure; G_1 is the flow rate through orifice 2 in the valve; $G_1 = G\ (S_{e2}, P_u, P_c)$; and S_{e2} is the effective area of orifice 2.

Finally, to simplify the calculation, the ITC is still used for the downstream volume because it is not an important part of this simulation. Thus,

$$\frac{V_o dP_o}{dt} = R\theta_a (G_N - G_2) \tag{3.11}$$

where V_o is the downstream volume, P_o is the downstream pressure, G_2 is the mass flow rate through the outlet of the valve, $G_2 = G\ (S_{e3}, P_o, P_a)$, and S_{e3} is the effective area of the outlet.

The gain of P_c and P_d is defined as

$$K_c = 20\log_{10}(\frac{A_c}{A_i}),\ \ K_d = 20\log_{10}(\frac{A_d}{A_i}) \tag{3.12}$$

where A_c, A_d, and A_i are the amplitudes of P_c, P_d, and P_i, respectively. The phase difference $\Delta\phi_c$ and $\Delta\phi_d$ are also considered with respect to the input pressure. That is,

$$\Delta\phi_c = \phi_c - \phi_i,\ \ \Delta\phi_d = \phi_d - \phi_i \tag{3.13}$$

Here, ϕ_c, ϕ_d, and ϕ_i are the phases of P_c, P_d, and P_i, respectively.

The simulation was implemented in MATLAB, and Figure 3.6 shows the simulation block diagram.

Some parameters of the simulation condition are shown in Table 3.1.

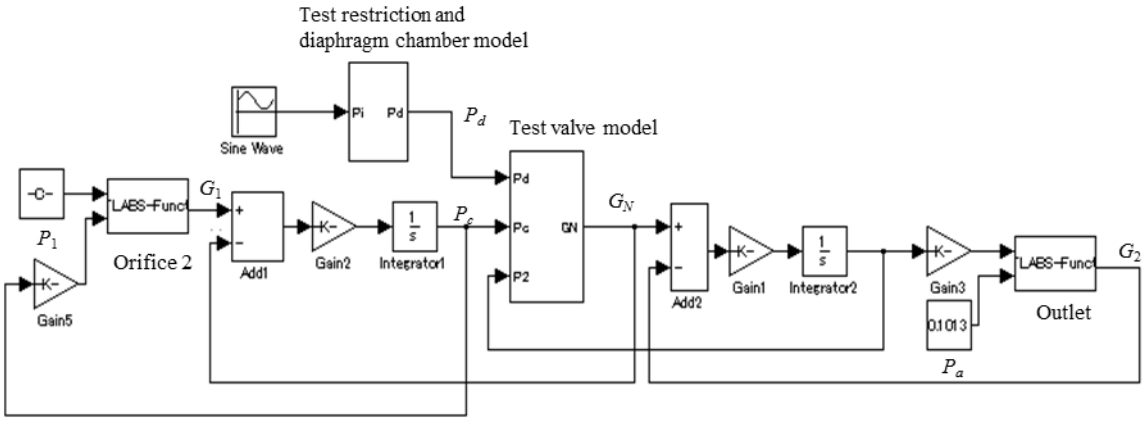

Fig.3.6 Simulation block diagram

Table 3.1 Simulation conditions

Parameters	Value	Parameters	Value
V_d (mL)	155	S_d (m^2)	0.0031
V_c (mL)	220	d_N (mm)	3.2
m_v (kg)	0.15	d_2 (mm)	1.25
k_1 (N/mm)	196	c (N·s/m)	0.98
k_2 (N/mm)	5	P_{set} (kPaG)	161

3.4 Dynamic experiment

A frequency response experiment was performed to investigate the dynamic response of the test pilot valve system using the porous materials and orifice.

3.4.1 Experimental apparatus

Figure 3.7 shows the pneumatic circuit used in the frequency response experiment. A sine-wave pressure generator was designed to provide the pressure input by regulating the inflow and outflow from a servo valve using PI feedback control. The generated input pressure P_i was measured by a pressure sensor. The response pressures in the diaphragm chamber (P_d) and ITC (P_c) were measured by pressure sensors. Figure 3.8 presents an image of the experimental apparatus. Table 3.2 lists the primary specifications of the equipment used in the experiment.

Table 3.2 Specifications of experimental equipment

Equipment	Range	Type
Pressure P_i	0–500 kPa	FP101-B31-C20A*B (YOKOGAWA)
Pressure P_d	0–200 kPa	FP101-A31-C20A*B (YOKOGAWA)
Pressure P_c	0–1 MPa	AP-13S (KEYENCE)
Flow rate	0–200 L/min (ANR)	QFS-200 (TOKYO METER)
ITC	180 mL	ITC-0.2 (TOKYO METER)

Table 3.3 Experimental conditions

Test restriction	Frequency [Hz]	Amplitude [kPa]
Porous	1–25	2, 5, 10
Orifice	1–25	2, 5, 10

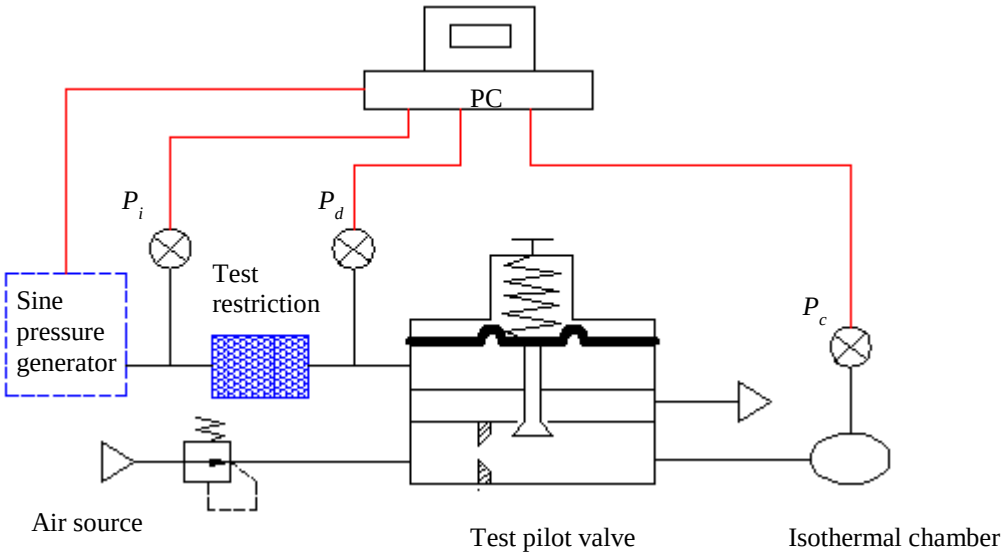

Fig.3.7 Pneumatic circuit diagram of dynamic experiment

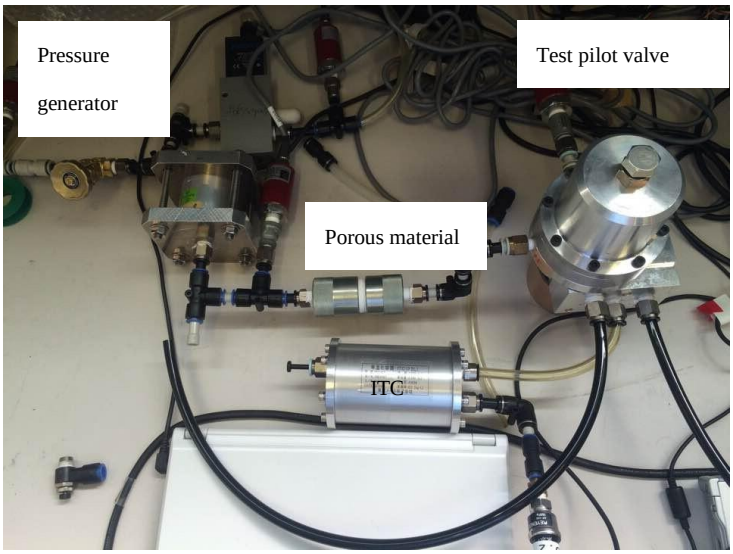

Fig.3.8 Photograph of experimental apparatus

The experimental conditions are listed in Table 3.3. All the pressure values are recorded relative to the pressures in the following part of the apparatus. The data of P_i, P_c, and P_d were recorded while increasing the frequency at the same input amplitude. The test valve started to open at the set pressure of 161 kPaG, and the base value of P_i was set

to 150 kPaG. Therefore, the amplitude was limited to 10 kPa because the valve reached full-open and full-close states when the amplitude exceeded 10 kPa.

3.4.2 Pressure wave

The dynamic experiment was conducted to record the response pressure wave at each frequency with different amplitude of input pressure. Figure 3.9 shows a series of pressure wave change with frequency in porous materials, when the amplitude of the input pressure P_i is set to

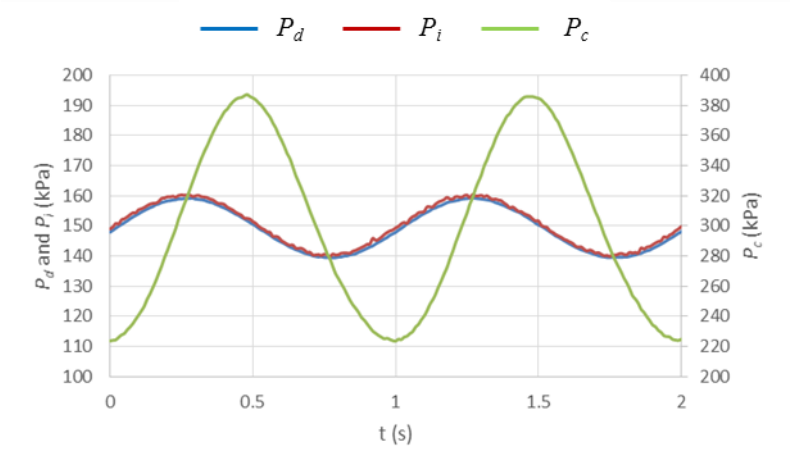

a) 1 Hz

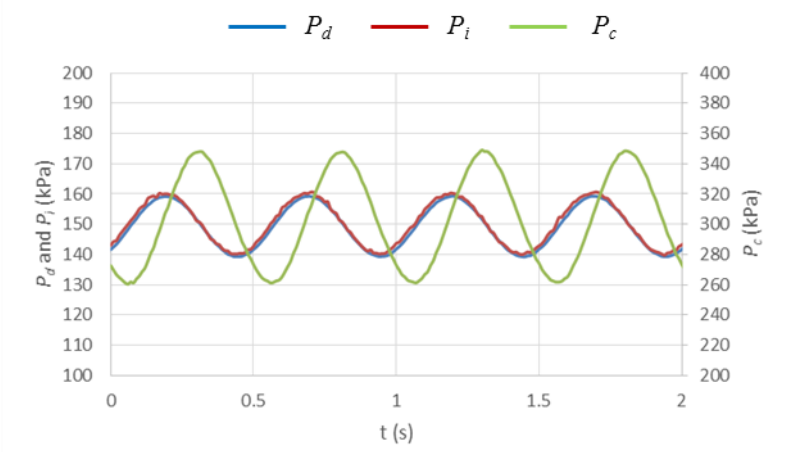

b) 2 Hz

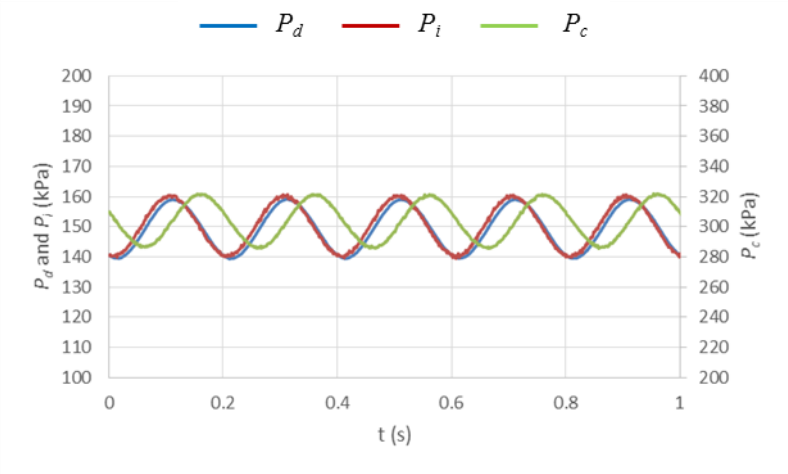

c) 5 Hz

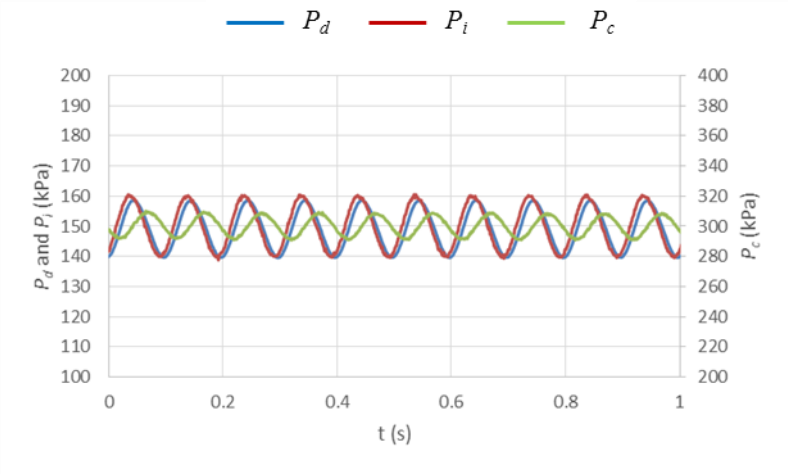

d) 10 Hz

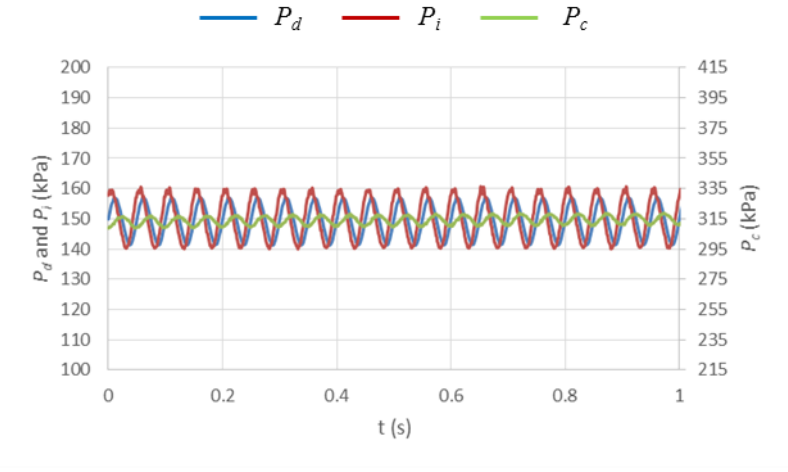

e) 20 Hz

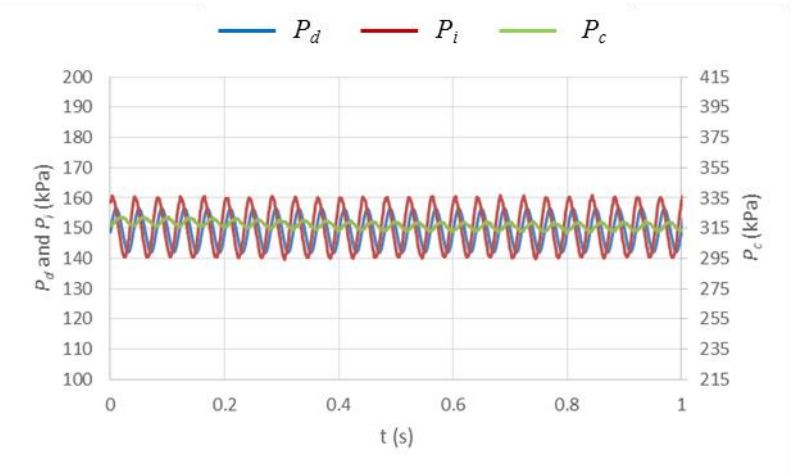

f) 25Hz

Fig.3.9 Pressure response wave with frequency in porous materials (A_i=10kPa)

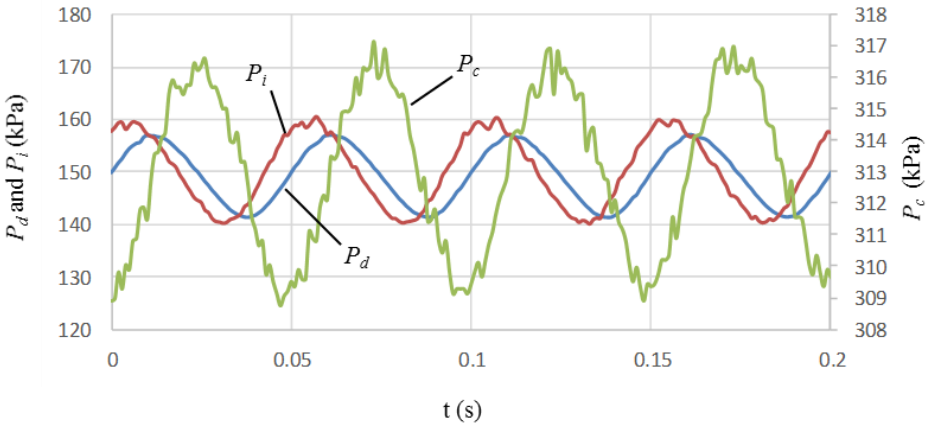

Fig.3.10 Pressure wave with small time scale (f = 20 Hz, A_i = 10 kPa)

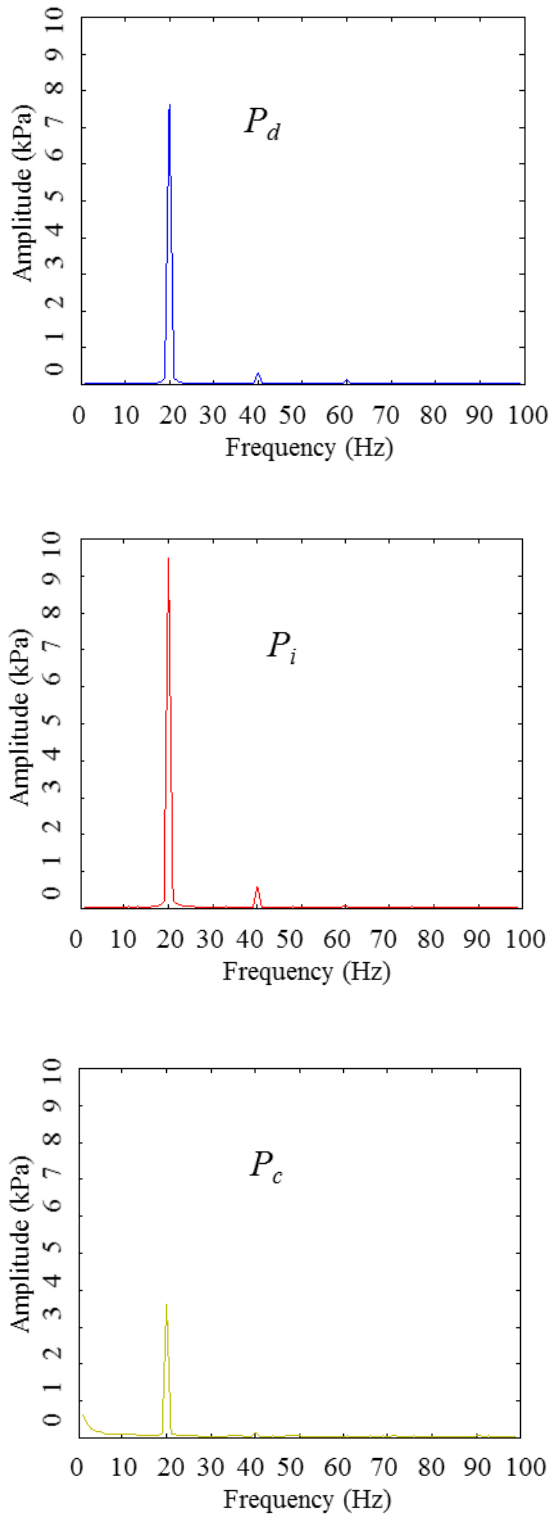

Fig.3.11 Amplitude analysis by FFT

10 kPa. The amplitudes of P_d and P_c decrease as the frequency increases because of the damping of the pneumatic RC circuit and the test pilot valve.

The pressure generator can produce a good sine-wave pressure P_i at low frequencies but not at high frequencies, as shown in Figure 3.10 (frequency: 20 Hz). Therefore, the data were processed by carrying out harmonic analysis based on the FFT technique to confirm the amplitude and phase accuracy. Figure 3.11 shows the FFT results of the amplitude of each pressure wave in frequency domain.

3.5 Results and discussion

Based on the definitions in Eq. (3.12) and Eq. (3.13), the changes in the gain and phase difference of P_c with the frequency are shown in the Bode diagram of Figure 3.12. The points represent the experimental data, whereas the markers represent the different amplitude conditions of the input pressure. The colors represent different restrictions. The red dash curve represents the simulation results of the porous material when the amplitudes of the input pressure P_i are 2, 5, and 10 kPa. The simulation results show that the variation in the gain drop of P_c as the frequency increases is constant with respect to the amplitude of the input vibration when the porous material is used as the test restriction. The experimental data for different amplitudes of the input pressure were in agreement, considering that the points were all located nearly on the same curve. However, for the orifice, the gain curves are of three different forms at high frequencies for different input amplitudes. The simulation results represented by the three blue solid curves and the distribution of the experimental data are also almost in agreement with these curves. Thus, if the amplitude of the input pressure changes, the pressure gain P_c of the orifice drops at a different rate. In addition, the width of the gain difference is nearly 5 dB at 25 Hz at input amplitudes between 2 and 10 kPa. This phenomenon can be also seen in the change

in the phase difference (Figure 3.12 (b)). The obvious difference of the pressure response between the porous material and orifice is demonstrated in this section.

At low frequencies, the gain and phase difference changes are almost the same irrespective of the restriction used because by now, the primary influencing factor is the pilot valve damping. On the other hand, these curves become different at high frequencies. This is thought to be because the flow rate gain in the RC pneumatic circuit is affected by the nonlinear flow characteristics of the orifice, but it isn't affected by the linear flow characteristics of the porous material at this time. When using the porous material, the quantity of flow into the diaphragm chamber increases in proportion to the differential pressure, as shown in Figure 3.3. If the amplitude of the input pressure P_i changes, the flow rate changes proportionally and the amplitude of the pressure response P_d also changes proportionally. However, when using an orifice, these changes do not remain proportional because of the nonlinear behavior. In short, the flow rate resistance is constant in a porous material but not in an orifice.

The gain of the diaphragm chamber pressure P_d is shown in Figure 3.13. In theory, the experimental data should be distributed along a single simulation curve for different input amplitudes when the porous material is used as the restriction. However, the red data points are slightly spread out in the figure. This is probably because of the small volume change in the chamber due to the motion of the diaphragm; however, this volume is considered to be constant in the theoretical calculations. Although the data points are spread out, the width of the gain difference at input amplitudes between 2 and 10 kPa is smaller than the width of the gain difference in orifice.

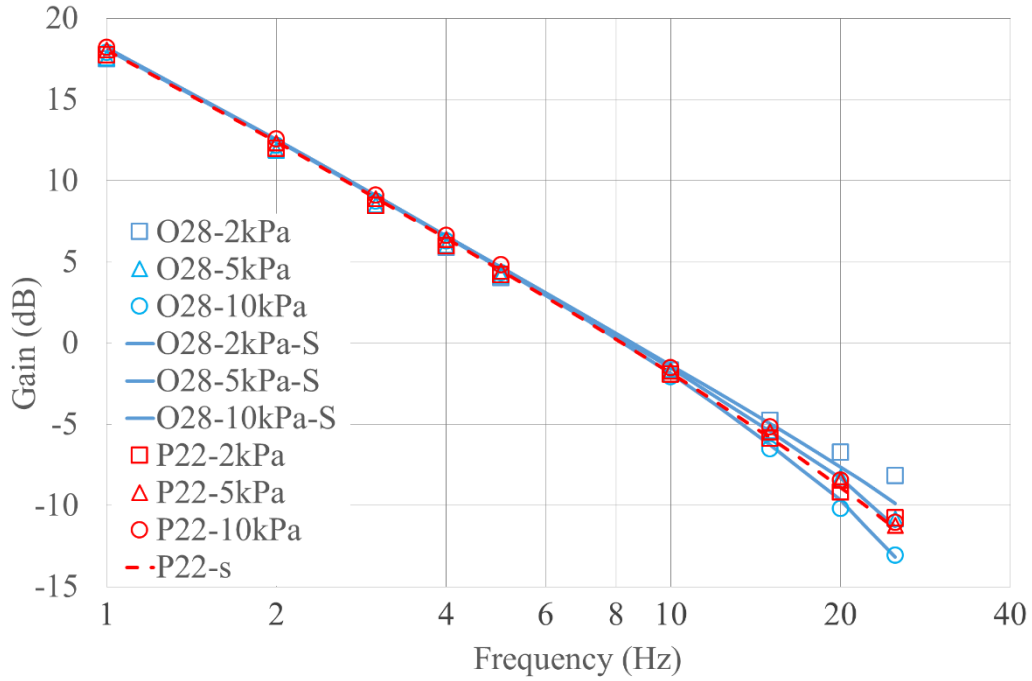

(a) Gain

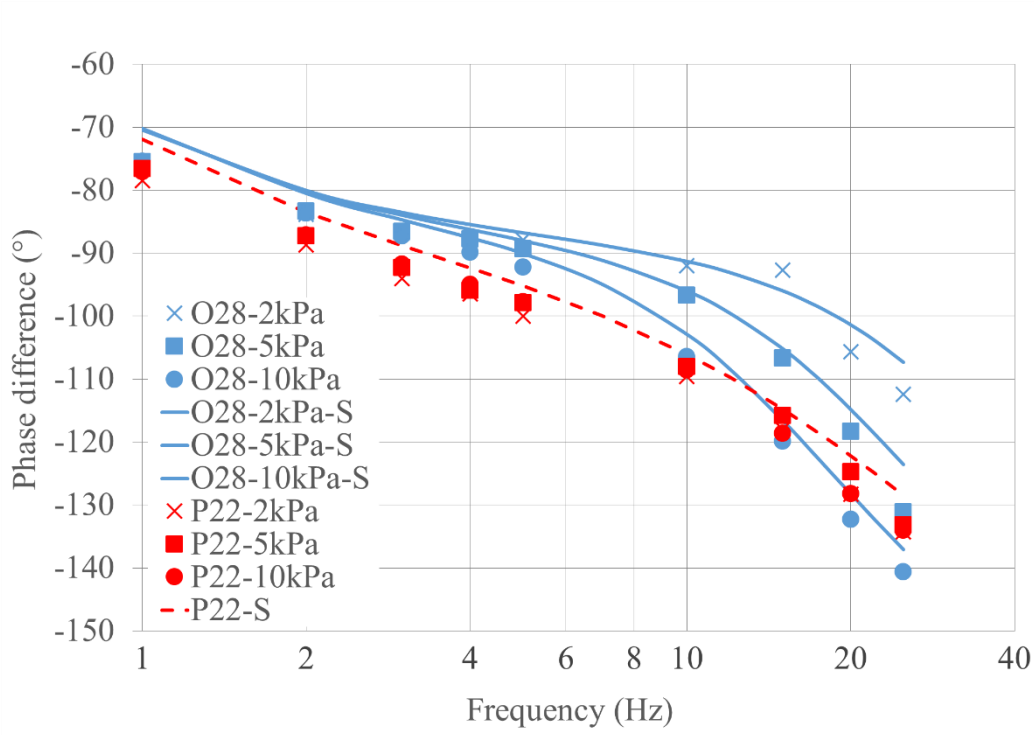

(b) Phase difference between P_c and P_i

Fig.3.12. Bode diagram of control pressure P_c

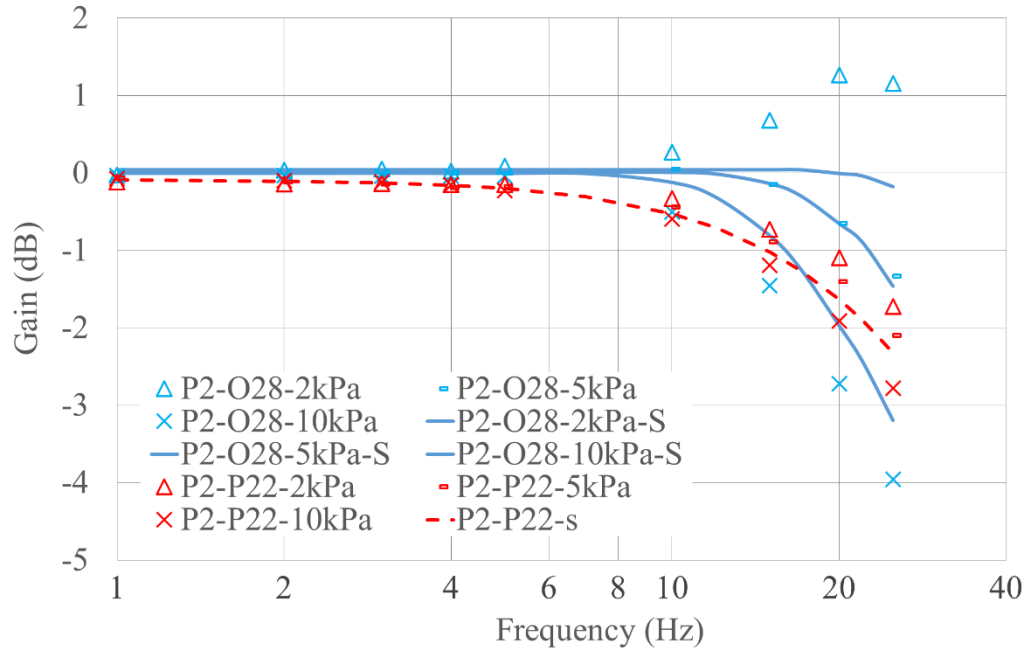

(a) Gain

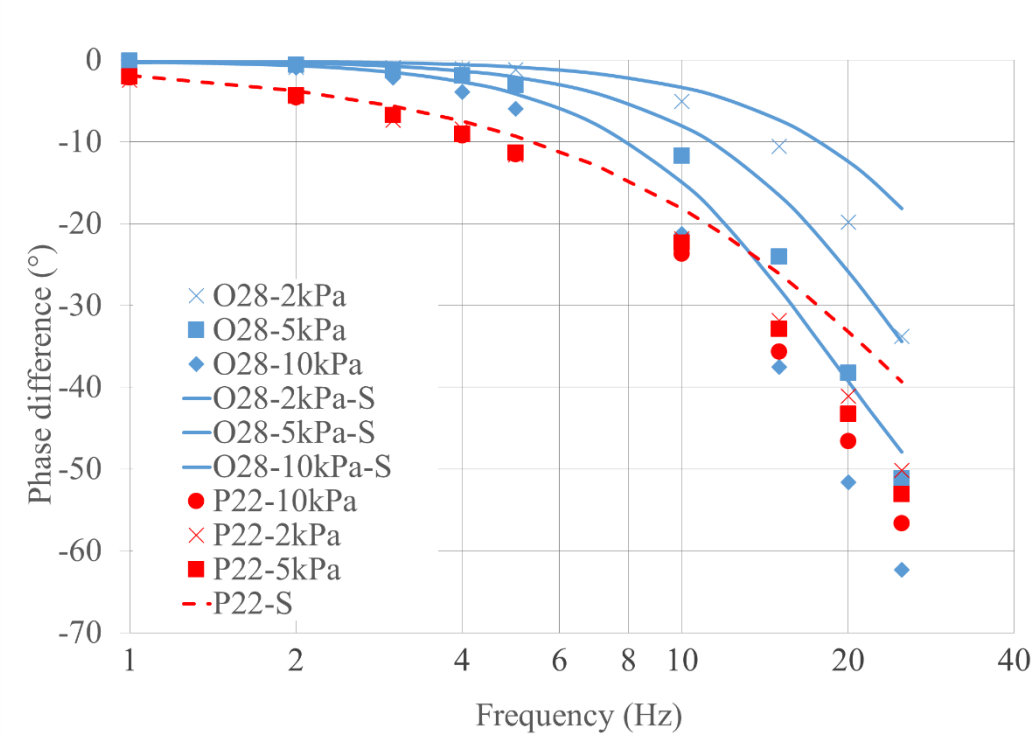

(b) Phase difference between P_d and P_i

Fig.3.13. Bode diagram of diaphragm chamber pressure P_d

In summary, because of the linear flow characteristics of the porous material, the gain of the pressure response in the diaphragm chamber does not change regardless of the changing pressure vibration amplitude. Consequently, the change in the vibration amplitude also does not affect the gain of the control pressure P_c. However, the orifice does not exhibit this property. These results show that porous materials can be used in the pilot valve system instead of an orifice to improve its dynamic characteristics.

3.6 Conclusions

In this chapter, we proposed a new method that employed porous materials to improve the characteristics of a pilot valve system used in a gas governor unit. An experiment was performed to confirm the static *P–Q* characteristics using a porous material and an orifice. A test pilot valve was manufactured, and a frequency response experiment was performed to estimate its dynamic response. A mathematic model of the test pilot valve system was developed in MATLAB. The experimental results were in close agreement with the simulation results. Finally, we obtained the following conclusions:

(1) The static flow characteristics of new type porous materials are also linear.

(2) In the frequency response experiment, the gain and phase difference of the diaphragm chamber pressure P_d remain constant with changes in the amplitude of the input vibration because of the linear flow characteristics of the porous material. As a result, the control pressure is not affected by the changes in the amplitude of the input vibration. However, the control pressure changes in the case of the orifice because of its nonlinear characteristics.

(3) The motion of the valve diaphragm will slightly affect the results of the dynamic response.

(4) Therefore, porous materials can be used in the pilot valve system instead of an orifice to improve its dynamic characteristics by making it to be a linear system easily. And the invariable flow resistance will help engineers to choose the restrictions more easily in the process of designing the pilot valve system.

Chapter 4 Simulation of Parallel pilot valve system

4.1 Parallel pilot valve system

The gas governor unit discussed in chapter 2 and chapter 3 is used for the medium pressure pipeline in city gas supply system. The downstream pressure is needed to be controlled in about 150 kPaG. In this chapter, we will deal with our study on the gas governor unit system for low pressure pipeline. The downstream pressure in this system is generally controlled in 2.3 ~ 2.8 kPaG. Therefore, the type and structure of the pilot valve are different from the formers.

In the gas governor unit, the dynamic characteristics of pilot valve are important as it is directly determined the response speed and stability of the system. Generally, a stable pilot valve which owns a large damping is preferentially employed in the gas governor unit to ensure the stability of the downstream pressure. In consequence, the downstream pressure will have a large pressure drop when the consumption of the gases suddenly increases as introduced in section 1.4.2. The sustaining low pressure makes the gas equipment such as the gas stove invalid.

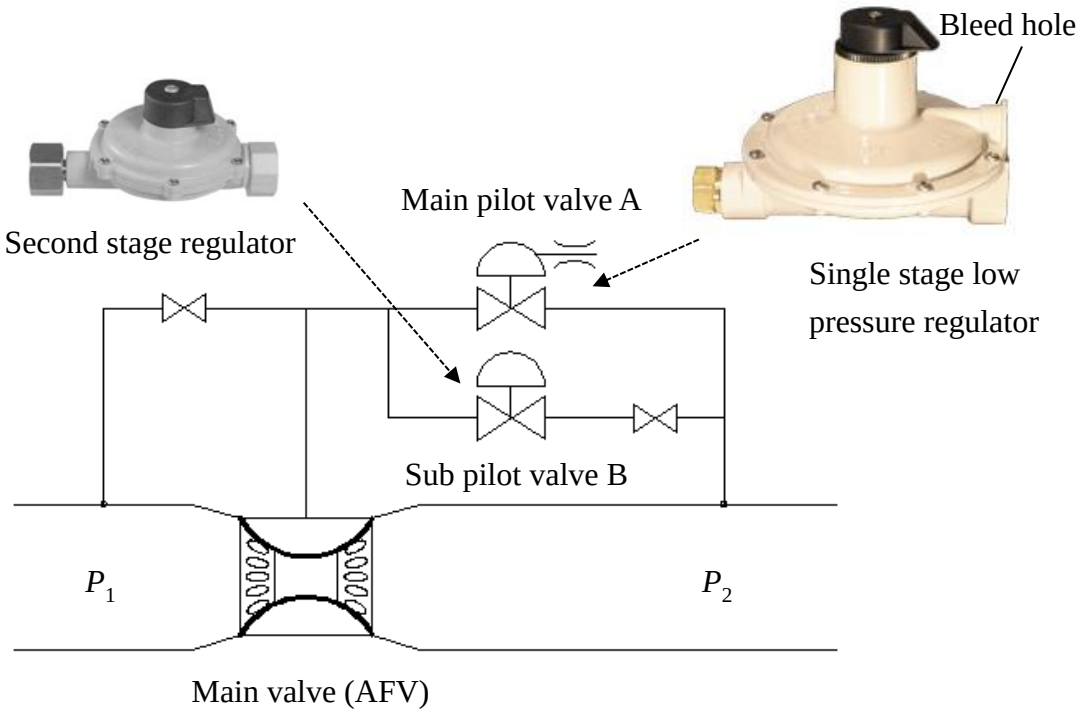

Fig.4.1 Parallel pilot valve governor system

To solve this problem and improve the dynamic characteristics of the gas governor unit, a parallel pilot valve system was proposed as shown in Figure 4.1. In this system, two diaphragm type pressure regulators were installed on the pilot line in parallel. A large capacity single stage low pressure regulator is marked as a main pilot valve A, and a small capacity second stage regulator is marked as a sub pilot valve B. A bleed hole which is connected to the upper diaphragm chamber is set up in the pressure regulator. The principle is like the injection orifice in the injector. If the injection orifice is blocked, the piston is difficult to move. The bleed hole of the main pilot valve A is restricted adequately to owns a large damping and ensure its stability. At the same time, the sub pilot valve B isn't restricted, but its response speed is faster than the former. The system is expected to implement the following functions. When the downstream pressure suddenly decreases, the sub pilot valve B opens firstly because of its small damping and

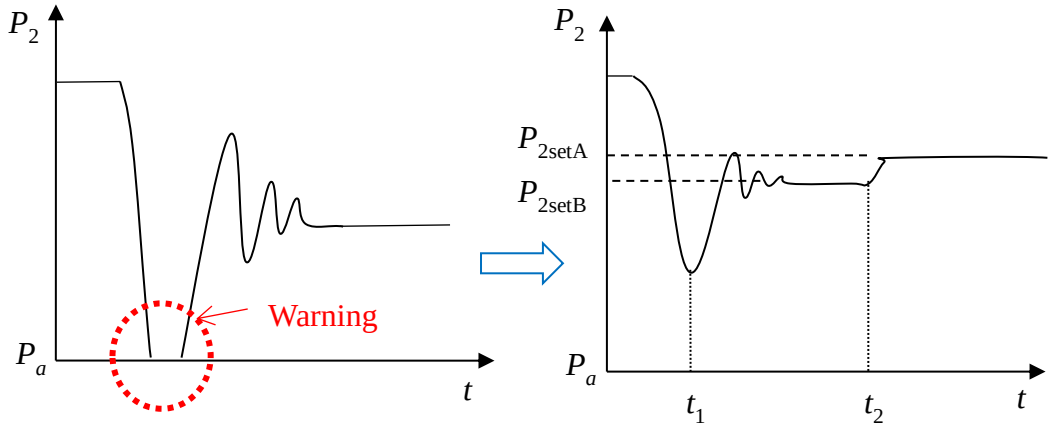

Fig.4.2 Improved pressure response curve

then it makes the main valve open. As a result, the pressure will recover to the setting pressure P_{2setB}, rapidly. Then, the main pilot valve A opens. And the pressure is gradually controlled by the main pilot valve and reach to the setting pressure P_{2setA}. Finally, the sub pilot valve B closes because the downstream pressure exceeds the setting pressure P_{2setB}, and the system is controlled by the main pilot valve A completely. The expected pressure response curve is shown in Figure 4.2.

Next, the mathematical models of the two pilot valves are established and a simulation is carried out to analyze the dynamic characteristics of the parallel pilot valve system.

4.2 Mathematical models

Generally, the static model of the pressure regulator from its *P*–*Q* characteristics curve provides enough information to judge its performance for engineers. But the dynamic model of the regulator is important in the parallel pilot valve system, because it is imperative for the investigation of the pressure response in time domain.

4.2.1 Mathematical model of sub pilot valve B

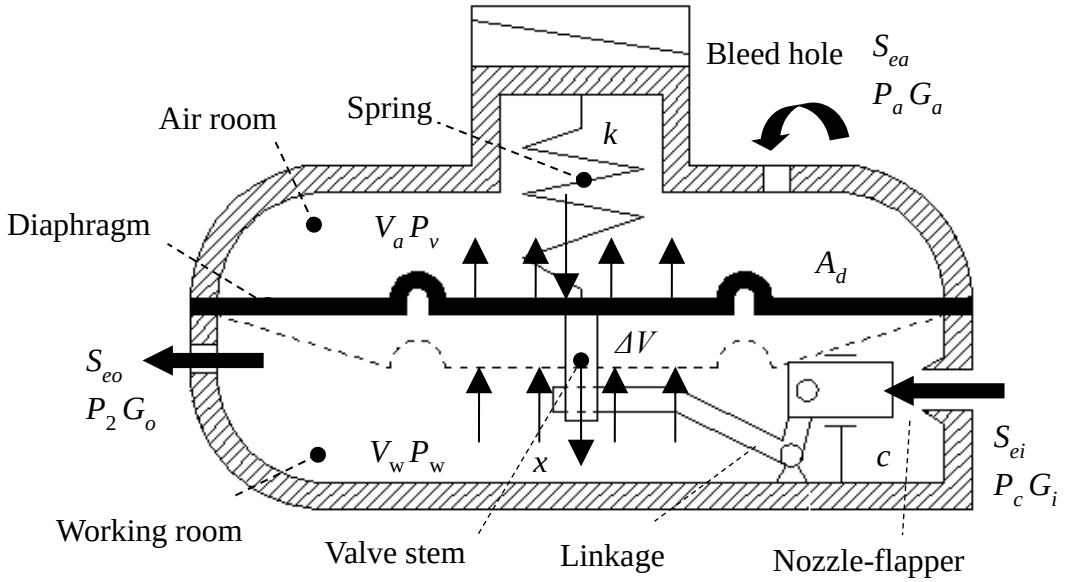

Fig.4.3 Mathematical Model of sub pilot valve B

Firstly, the mathematical model of the sub pilot valve B is shown in Figure 4.3. This model is constituted with four parts of model. They are the valve motion model, air room model, working room model, and restriction model. The simulation adopts air to replace the natural gas, which is assumed to be an ideal gas. The temperature changes slightly because the range of the pressure change is only thousands of Pascal in the regulator. Therefore, the simulation is assumed as an isothermal process.

(1) Valve motion model

The flow rate of the valve is determined by the effective area S_{ei} of the nozzle-flapper. The effective area S_{ei} changes with the displacement x of the valve motion. The motion equation is:

$$m_e \frac{d^2x}{dt^2} + c\frac{dx}{dt} + P_v A_d + k(x + x_0) = P_w A_d \tag{4.1}$$

where c is the viscous damping coefficient, P_v is pressure in the air room, P_w is the pressure in the working room, k is the spring constant. x_0 is the initial length of the spring.

m_e is the equivalent mass of the motion parts that contains the diaphragm, the valve stem, and the spring. In particular, only one third of the total mass of the spring is added to m_e. Thus:

$$m_e = m_d + m_v + \frac{1}{3}m_s \tag{4.2}$$

m_d is the mass of diaphragm, m_v is the mass of valve stem, and m_s is the mass of spring.

A_d is the equivalent area of the diaphragm, it is defined as:

$$A_d = \frac{\pi}{4}D_e^2 \tag{4.3}$$

where D_e is the equivalent diameter of the diaphragm, by using the diameter of the diaphragm D_1 and the diameter of the diaphragm metal disc D_2, it can be simply calculated by:

$$D_e = \frac{D_1 + D_2}{2} \tag{4.4}$$

(2) Air room model

In the air room, the change of temperature is neglected, and it uses the atmosphere temperature θ_a, the ideal gas state equation is:

$$P_v V_a = m_A R\theta_a \tag{4.5}$$

where V_a is the volume of the air room, m_A is the mass of air in the air room, R is the gas constant. Considering the change of P_v and V_a, the ideal gas equation is differentiated with respect to time:

$$V_a \frac{dP_v}{dt} + P_v \frac{dV_a}{dt} = \frac{dm_A}{dt} R\theta_a \tag{4.6}$$

Rearranging the equation, and noticing that $\frac{dm_A}{dt} = G_a$, G_a is the mass flow rate through the bleed hole, we have:

$$\frac{dP_v}{dt} = \frac{G_a R\theta_a}{V_a} - \frac{P_v}{V_a}\frac{dV_a}{dt} \tag{4.7}$$

Using the initial volume of the air room V_{a0}, and the change volume of the air room ΔV, and

$$\Delta V = A_d x \tag{4.8}$$

we get:

$$V_a = V_{a0} + \Delta V = V_{a0} + A_d x \tag{4.9}$$

Therefore,

$$\frac{dV_a}{dt} = A_d \frac{dx}{dt} \tag{4.10}$$

Eq. (4.8) and Eq. (4.10) are substituted in Eq. (4.7), thus:

$$\frac{dP_v}{dt} = \frac{G_a R\theta_a}{V_{a0} + A_d x} - \frac{P_v A_d}{V_{a0} + A_d x}\frac{dx}{dt} \tag{4.11}$$

And, P_v can be obtained from

$$P_v = \int \frac{dP_v}{dt} dt \tag{4.12}$$

(3) Working room model

Similarly, in the working room, the ideal gas equation is written as:

$$P_w V_w = m_W R\theta_a \tag{4.13}$$

where P_w is the pressure in the working room, V_w is the volume of the working room, m_W is the mass of air in the working room. Then, Eq. (4.7) is changed to:

$$\frac{dP_w}{dt} = \frac{(G_i - G_o)R\theta_a}{V_w} - \frac{P_w}{V_w}\frac{dV_w}{dt} \tag{4.14}$$

where G_i is the mass flow rate which flows into the working room, G_o is the mass flow rate which flows out the working room. Here,

$$V_w = V_{w0} - \Delta V = V_{w0} - A_d x \tag{4.15}$$

where V_{w0} is the initial volume of the working room, the minus sign represents the change volume contrary to the change in the air room. And,

$$\frac{dV_w}{dt} = -A_d \frac{dx}{dt} \tag{4.16}$$

Eq. (4.15) and Eq. (4.16) are substituted in Eq. (4.14), we obtain:

$$\frac{dP_w}{dt} = \frac{(G_i - G_o)R\theta_a}{V_{w0} - A_d x} + \frac{P_w A_d}{V_{w0} - A_d x}\frac{dx}{dt} \tag{4.17}$$

And,

$$P_w = \int \frac{dP_w}{dt} dt \tag{4.18}$$

(4) Mass flow rate through the restrictions

The mass flow rate through the bleed hole, outlet, and the inlet nozzle is calculated by Eqs. (2.1) and (2.2), Thus:

$$G_a = G_a(S_{ea}, P_v, P_a), \quad G_i = G_i(S_{ei}, P_c, P_w), \text{ and } \quad G_o = G_o(S_{eo}, P_w, P_2) \tag{4.19}$$

where S_{ea} is the effective area of bleed hole, S_{eo} is the effective area of the outlet. They are constant, but the effective area S_{ei} changes with the displacement x of the valve motion by the linkage. The structure parameters of the linkage are difficult to be measured. Therefore, we directly find the function of the effective area S_{ei} with x.

4.2.2 Mathematical model of main pilot valve A

The size of the main pilot valve A is larger than the sub pilot valve B, and the structure is also different from it. The mathematical model of the main pilot valve is showed in Figure 4.4. One chamber called damping room is added below the diaphragm in this model. It connects with the working room by a damping hole. As a consequence, there are four parts: the valve motion model, the air room model, the working room model, and the damping room model.

(1) Valve motion model

In this model, the pressure P_d in the damping room replaces P_w acts on the undersurface of the diaphragm, the motion equation is only needed to change a little:

$$m_e \frac{d^2x}{dt^2} + c\frac{dx}{dt} + P_v A_d + k(x + x_0) = P_d A_d \tag{4.20}$$

The meanings of the other variables are same as section 4.2.1.

(2) Air room model

The air room model of the main pilot valve A is unchanged. So, Eq. (4.5) ~ Eq. (4.12) are all suitable for this valve.

(3) Damping room model

The role of damping room equals to the working room in the sub pilot valve B. Therefore, in the damping room model, we only consider the mass flow rate G_d through the damping hole. And Eq. (4.17) is changed to:

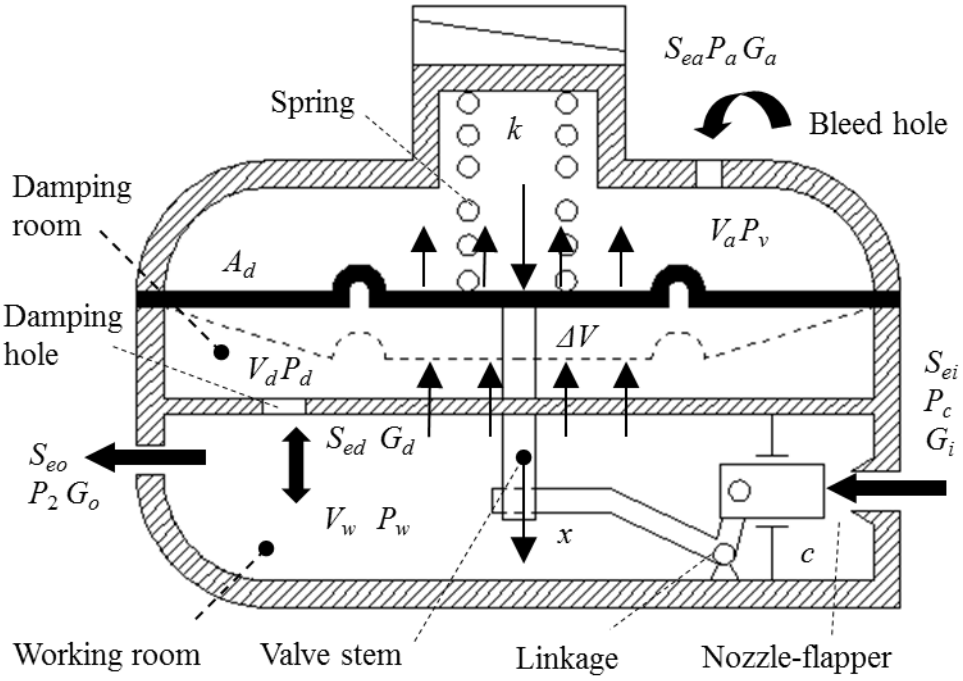

Fig.4.4 Mathematical model of main pilot valve A

$$\frac{dP_d}{dt} = \frac{G_d R\theta_a}{V_{d0} - A_d x} + \frac{P_d A_d}{V_{d0} - A_d x}\frac{dx}{dt} \tag{4.21}$$

where V_{d0} is the initial volume of the damping room.

(4) Working room model

In the working room, the volume V_w is a constant, and considering the mass flow rate G_i, G_o, and G_d. Eq. (4.7) is changed to:

$$\frac{dP_w}{dt} = \frac{(G_i + G_d - G_o)R\theta_a}{V_w} - \frac{P_w}{V_w}\frac{dV_w}{dt} \tag{4.22}$$

because $\frac{dV_w}{dt} = 0$, and substitute to Eq. (4.22):

$$\frac{dP_w}{dt} = \frac{(G_i + G_d - G_o)R\theta_a}{V_w} \tag{4.23}$$

The mass flow rate G_i, G_o, G_a, and G_d. is also calculated by Eqs. (2.1) and (2.2).

4.2.3 Effective area of pilot valve

The effective area S_{ei} of the nozzle-flapper in the pilot valve changes with the valve motion as mentioned above. Hence, we need to find a function of the relationship between the effective area and the displacement of the valve. The simplest method is to measure the displacement x of the diaphragm plate and the flow rate Q. The measurement experiment is shown in Figure 4.5.

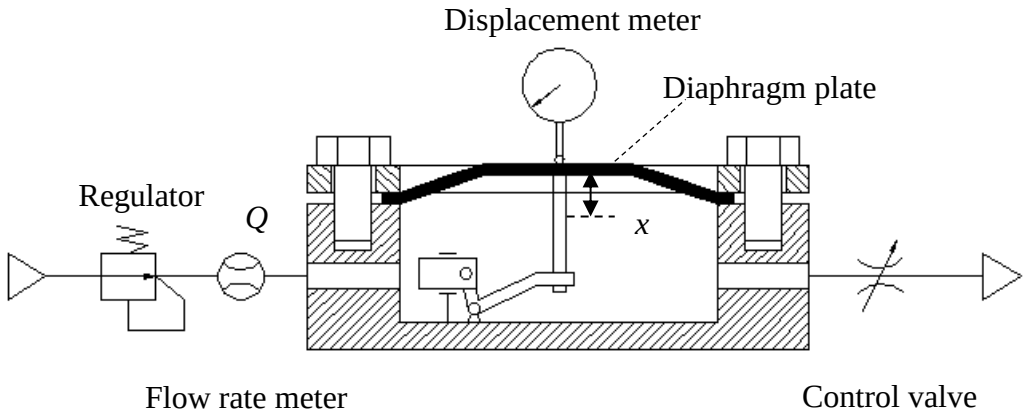

Fig.4.5 Effective area measurement experiment setup

Experiment process:

a) Set the upstream pressure to 200 kPaG by the regulator, slowly shut up the control valve until the flow rate is 0 L/min, and record the initial position x_0 by the displacement meter.

b) Gradually open the control valve, and record the flow rate Q_1 and the position x_1 at this time.

c) Turn up the control valve, and record Q_2, Q_3, … and x_2, x_3, …Hence, the displacements of the diaphragm plate are x_1 - x_0, x_2 - x_0, x_3 - x_0, …

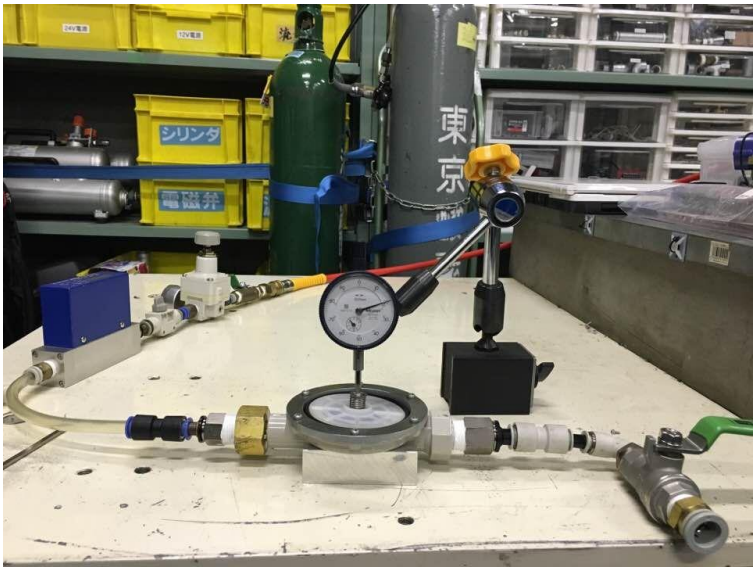

Fig.4.6 Photo of the effective area measurement experiment

The photo of the experiment is shown in Figure 4.6.

Figure 4.7 shows the experiment data. The triangle points represent the results of the main pilot valve A, and the circle points represent the results of the sub pilot valve B. In fact, there are some deviations in the probe of the displacement meter and the diaphragm plate. Consequently, we measure several sets of data for each pilot valve. Four sets of data show that they are located nearly on one curve. And their fitting functions of the curve are obtained by these data:

Main pilot valve A:

$$Q_A = M_1 x^4 + M_2 x^3 + M_3 x^2 + M_4 x \tag{4.24}$$

Sub pilot valve B:

$$Q_B = N_1 x^3 + N_2 x^2 + N_3 x \tag{4.25}$$

Where M_1, M_2, M_3, M_4 are the fitting coefficients for main pilot valve A, N_1, N_2, N_3 are the fitting coefficients for sub pilot valve B, their valves are:

M_1 = 738.40 [L/(min·mm^4)]; M_2 = -1079.00 [L/(min·mm^3)];

M_3 = 518.54 [L/(min·mm^2)]; M_4 = -1.27 [L/(min·mm)];

N_1 = -35.04 [L/(min·mm^3)]; N_2 = 67.16 [L/(min·mm^2)]; N_3 = 16.16 [L/(min·mm)].

In this experiment, the upstream pressure is set to 200 kPaG, and the downstream pressure is atmosphere. Therefore, the flow is chocked because the critical pressure ratio is lower than 0.5283. Eq. (2.1) is rewritten to calculate the effective area:

$$G(S_e, P_1, P_2) = S_e P_1 \sqrt{\frac{\kappa}{R\theta_1}\left(\frac{2}{\kappa+1}\right)^{\frac{\kappa+1}{\kappa-1}}} \tag{4.26}$$

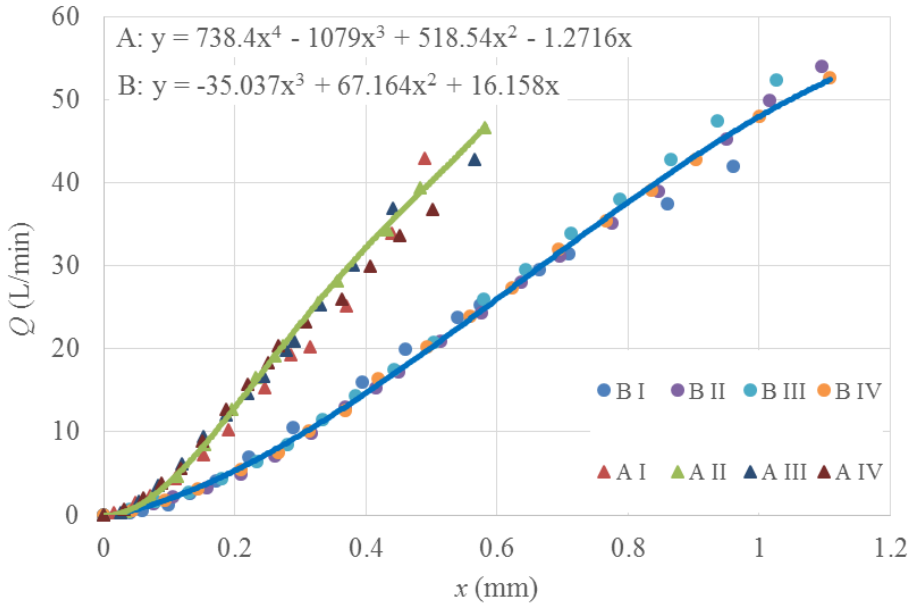

Fig.4.7 Relationship between x and Q (P_1=200 kPaG)

Using the volume flow rate, Eq. (4.26) is solved for S_e:

$$S_e = \frac{Q\rho}{P_1\sqrt{\frac{\kappa}{R\theta_1}\left(\frac{2}{\kappa+1}\right)^{\frac{\kappa+1}{\kappa-1}}}} \tag{4.27}$$

In this experiment, P_1 = 0.3 MPa (abs), ρ = 1.205 kg/m^3, R = 287 J/(Kg·K), θ = 293 K, κ = 1.4. Noticing the unit conversion, the effective area is calculated by:

$$S_e = \frac{Q}{35.28}(mm^2) \tag{4.28}$$

Eqs. (4.24) and (4.25) are substituted in Eq. (4.28), we get:

$$S_{eiA} = M_1^* x^4 + M_2^* x^3 + M_3^* x^2 + M_4^* x \tag{4.29}$$

$$S_{eiB} = N_1^* x^3 + N_2^* x^2 + N_3^* x \tag{4.30}$$

The unit of effective area is mm^2. Where M_1^*, M_2^*, M_3^*, M_4^* are the fitting coefficients for main pilot valve A, N_1^*, N_2^*, N_3^* are the fitting coefficients for sub pilot valve B, their valves are:

M_1^* = 20.9 [mm^{-2}]; M_2^* = -30.6 [mm^{-1}]; M_3^* = 14.7 [/]; M_4^* = -0.036 [mm];

N_1^* = -0.99 [mm^{-1}]; N_2^* = 1.90 [/]; N_3^* = 0.46 [mm].

4.3 Static characteristics

The pressure in the working room or the damping room was considered to be equal to the downstream pressure P_2, previously. However, according to the analysis above, it is believed that they are different. A static characteristics experiment is performed to verify this viewpoint.

4.3.1 Experiment

A hole was drilled on the wall of the pilot valve to measure the inner pressure. The experimental setup is shown in Figure 4.8. The downstream volume was replaced by an isothermal chamber. The upstream pressure was set to 200 kPaG. Through adjusting the control valve, the data of P_2, P_w, P_d changed with flow rate Q are measured by the pressure sensor. Figure 4.9 shows the photo of the experimental setup.

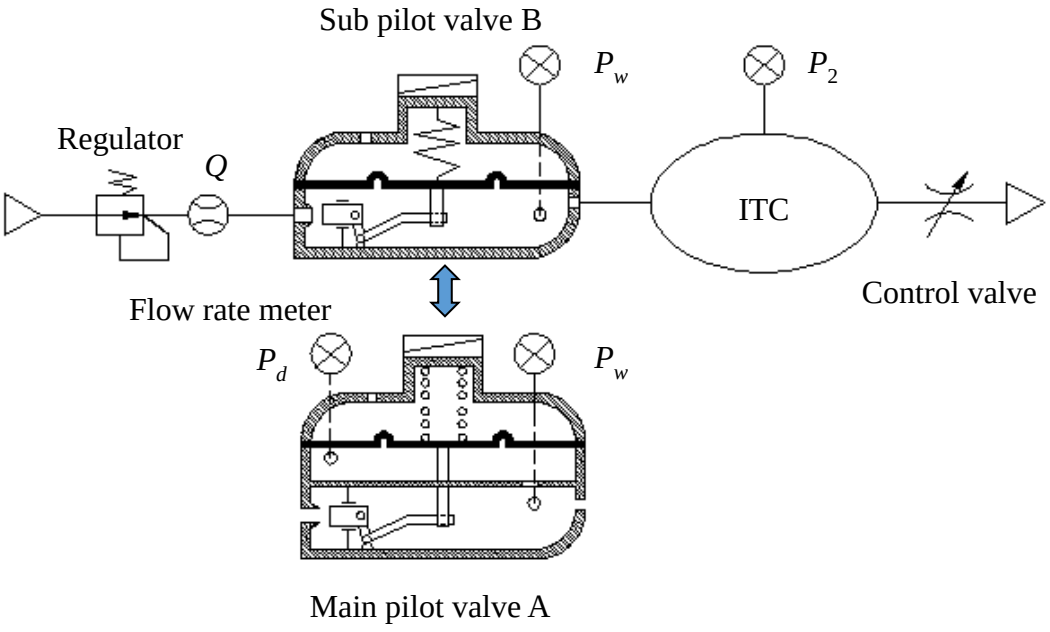

Fig.4.8 Experimental setup

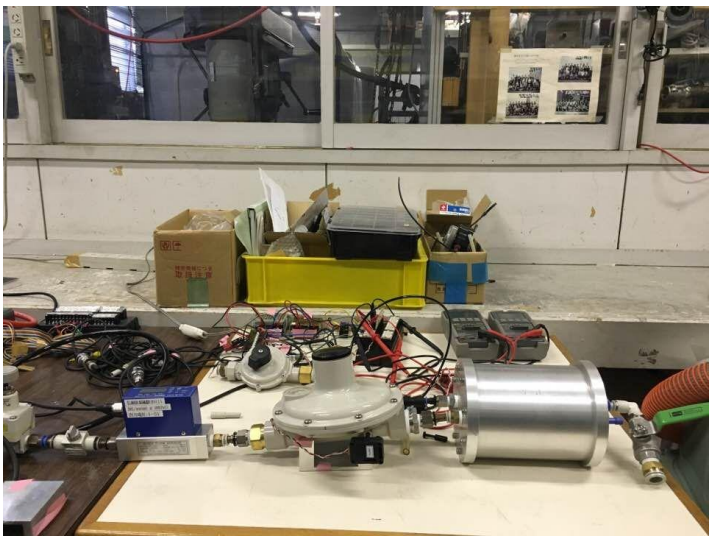

Fig.4.9 Photo of the static experiment

4.3.2 Results

Fig.4.10 shows the experiment results, and the curves are the results of simulation. The experimental data show agreement with the simulation results. The results indicate that the change of downstream pressure P_2 with flow rate is different from P_w in the working room of the pilot valve. And the pressure drop of P_2 is larger than P_w. The reason is presumably because the pressure in the working room is affected by the high upstream pressure. From the flow continuity equation, the mass flow rate G_i equals to G_o, while G_o is determined by P_w and P_2. Therefore, P_w must be higher than P_2, and the flow rate G_o just equals to G_i. In other words, the pressure difference between P_w and P_2 determines the flow rate G_i and G_o. On the other hand, the pressure change of P_w is the same as pressure P_d in the main pilot valve A. Because the working room is connected with the

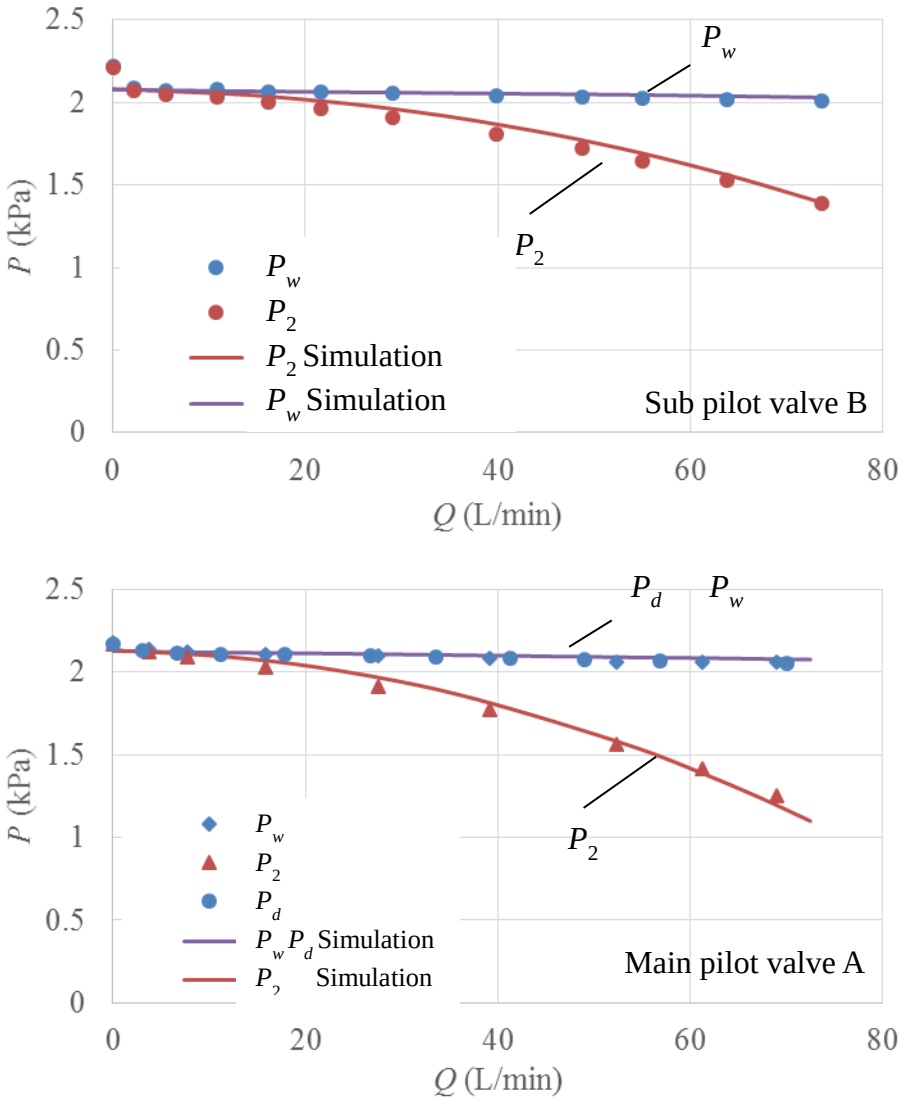

Fig.4.10 Results of the static experiment

damping room by the damping hole whose diameter is 6 mm. The flow rate can exchange rapidly. Therefore, P_w and P_d change together.

4.4 Simulation of dynamic response

Up to now, the mathematical model of the main valve (AFV) is unknown. That is, the simulation of the whole gas governor system is difficult. But the dynamic characteristics of the single pilot valve and the parallel pilot valve system can be simulated. A step

pressure response simulation was conducted to analyze the dynamic characteristics of the parallel pilot valve system.

4.4.1 Simulation model

The simulation model of the system is shown in Figure 4.11. The upstream pressure P_1 is set to 0.2 MPaG. And we uses an isothermal chamber (ITC 1) model to replace the rubber chamber in the main valve. A ϕd_1 = 2 mm orifice is installed in front ITC 1 to control the pressure P_c, and P_c is also the upstream pressure of the pilot valve. The setting pressure of the sub pilot valve B is 2.08 kPaG that is lower than the main pilot valve A. Noticing that the setting pressure is the pressure when the valve opens. The diameter ϕd_b of the bleed hole in the main pilot valve A is set to 0.5 mm, while it opens to 4 mm in the sub pilot valve B. An isothermal chamber (ITC 2) is used as the downstream volume and the flow rate is controlled by an on-off valve. The step response simulation starts as the diameter ϕd_2 of the on-off valve changes to 3.1 mm. The parameters of the simulation are shown in Table 4.1.

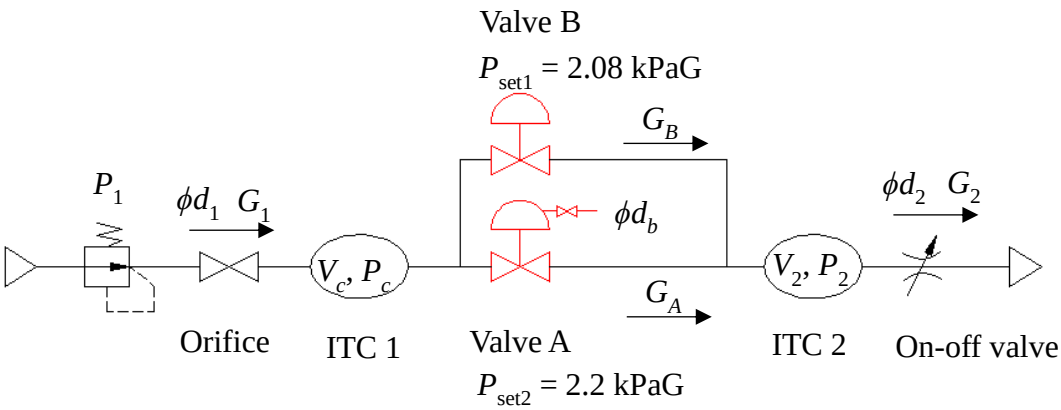

Fig.4.11 Simulation model

Table 4.1 Simulation parameters

Parameter	Values
V_c	200 mL
V_2	1 L
ϕd_1	2 mm
ϕd_b	0.5 mm
P_{set1}	2080 PaG
P_{set2}	2200 PaG

The mathematical models of the two pilot valves are illustrated in section 4.3. The flow rate of the pilot valve is determined by the control pressure P_c and downstream pressure P_2. In the isothermal chamber, Eq. (2.11) can be used to calculate P_c and P_2.

$$\frac{dP_c}{dt} = \frac{R\theta_a}{V_c}(G_1 - G_A - G_B) \tag{4.31}$$

$$\frac{dP_2}{dt} = \frac{R\theta_a}{V_2}(G_A + G_B - G_2) \tag{4.32}$$

where V_c and V_2 are the volume of the ITC 1 and ITC 2. G_1 and G_2 are the mass flow rate through the orifice and on-off valve. G_A and G_B are the mass flow rate of the main pilot valve A and the sub pilot valve B.

Using Eqs. (2.1) and (2.2), we get:

$$G_1 = G_1(S_{e1}, P_1, P_c), \quad G_2 = G_2(S_{e2}, P_2, P_a) \tag{4.33}$$

$$S_{e1} = C_{D1}\frac{\pi d_1^2}{4}, \quad S_{e2} = C_{D2}\frac{\pi d_2^2}{4} \tag{4.34}$$

where C_{D1} and C_{D2} are the discharge coefficient of orifice and the on-off valve, respectively. And we simply assume they are 0.85.

The simulation are implemented in MATLAB by three steps. Only one pilot valve is used to analyze the dynamic characteristics of the single pilot valve in the first two steps. Then, the parallel pilot valve system with the two regulators is implemented at the last step. Figure 4.12 shows the block diagram of the simulation.

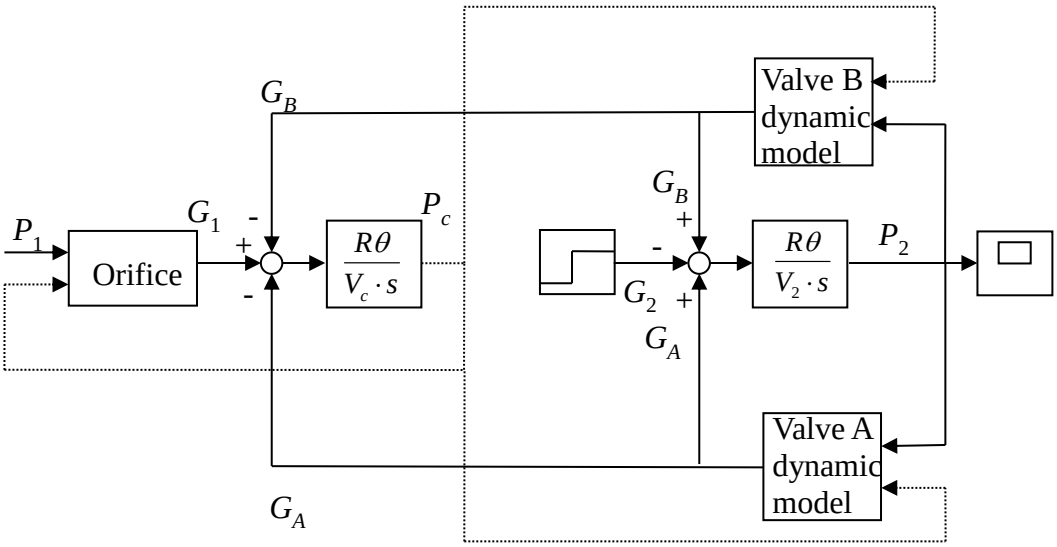

Fig.4.12 Block diagram

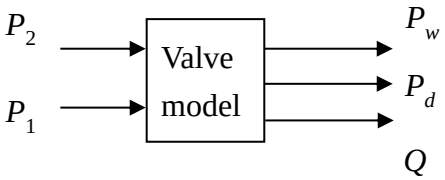

Fig.4.13 Block diagram

In addition, the simulation results of Figure 4.10 is the steady-state solution of the pilot valve model as shown in Figure 4.13. We can set different input pressure P_2 to solve the pressure P_w, P_d, and the flow rate Q.

4.4.2 Results of simulation and discussion

Figure 4.14 shows the simulation results of the step response with a single pilot valve. Figure 4.14(a) is the results of sub pilot valve B, while Figure 4.14(b) is the results of main pilot valve A. In addition, the flow rate response curves are G_A and G_B of the pilot valves, not the flow rate of the on-off valve G_2. It is seen that the recovery time of the downstream pressure P_2 to the setting pressure only takes 0.1 second with the single sub pilot valve B when the on-off valve opens. But it takes about 1 second with the single

main pilot valve A. The flow curves show that the flow rate increase fast in the sub pilot valve B, while it goes up slowly in main pilot valve A. That is, the response speed of the sub pilot valve A is much faster than the main pilot valve A.

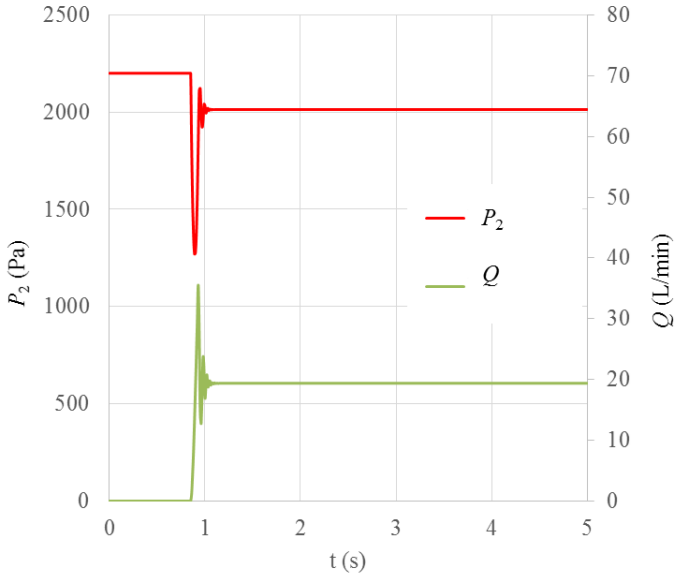

(a) Sub pilot valve B

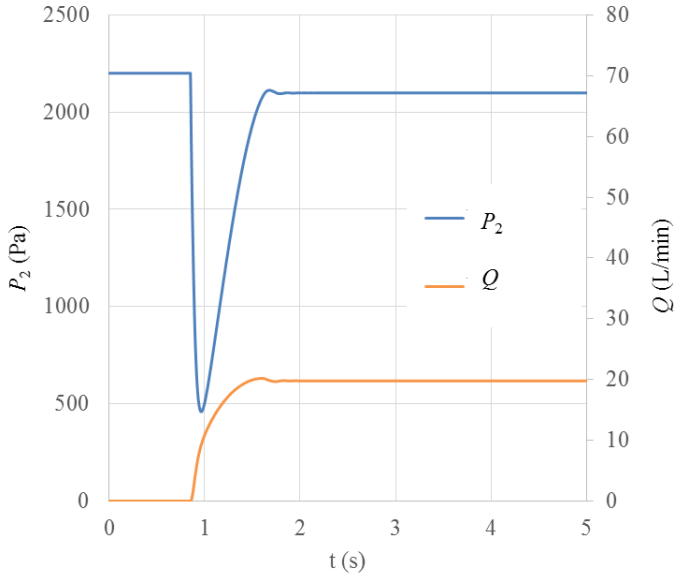

(b) Main pilot valve A

Fig.4.14 Simulation results of step response with single pilot valve

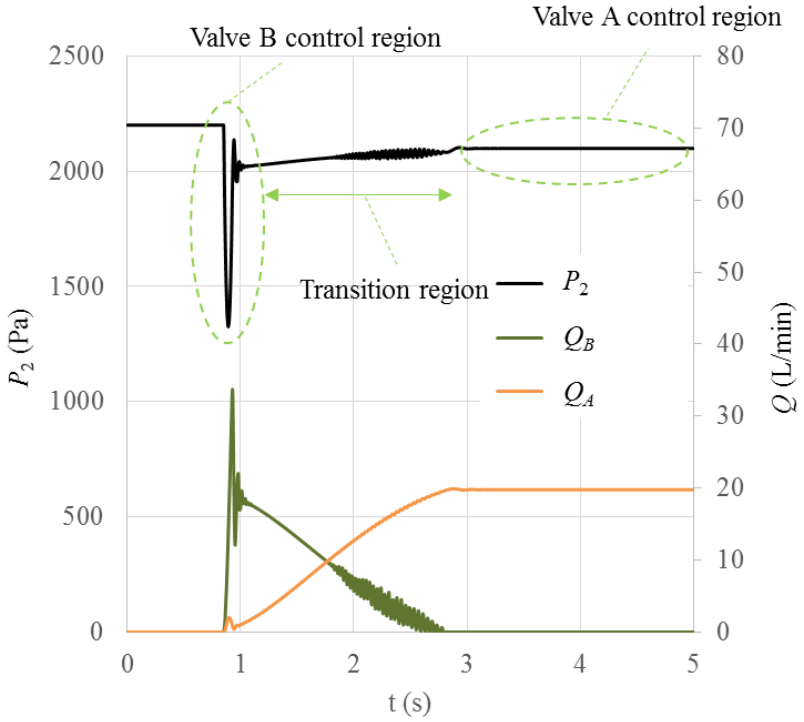

(a) Parallel pilot valve

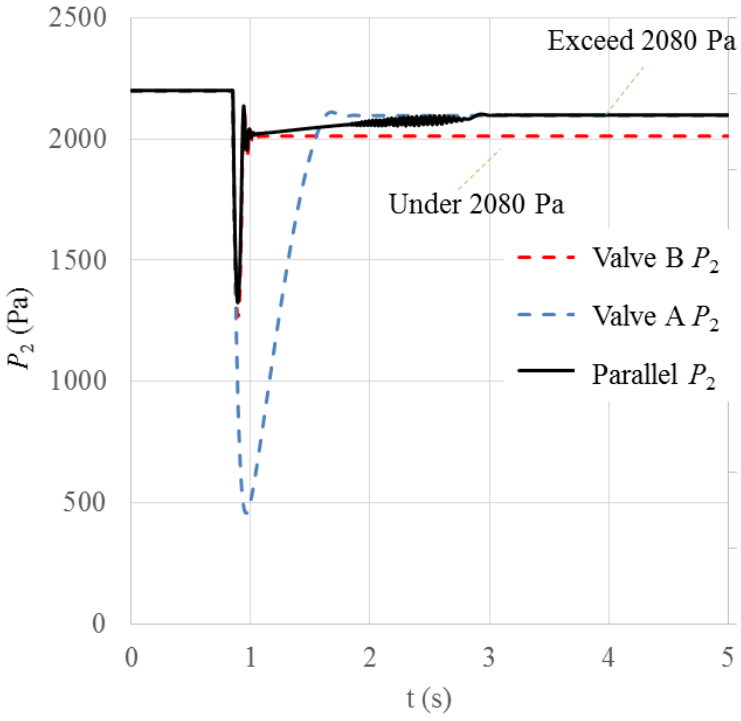

(b) Pressure response compare

Fig.4.15 Simulation results of step response with parallel pilot valve system

On the other hand, a pressure vibration and a flow rate over shoot are occurred with the sub pilot valve B, while not occurred with the main pilot valve A. These phenomenon indicates that the sub pilot valve B is more sensitive to the pressure than the main pilot valve A. The reason is probably that the damping of the main pilot valve is larger than the sub pilot valve B due to its bleed hole whose diameter is restricted to 0.5 mm.

Figure 4.15 shows the simulation results of step response with the parallel pilot valve system. Figure 4.15(a) demonstrates the response of volume flow rate Q_A and Q_B, which converted from the mass flow rate G_A and G_B. From the flow rate curves, it is seen that the sub pilot valve B opens firstly, then the main pilot valve A opens. And its flow rate gradually increases, while that of sub pilot valve B gradually decreases in the transition region. At last, sub pilot valve B closes, and the system is controlled by the main pilot valve A completely. Figure 4.15(b) includes the pressure response results in Figure 4.14 for comparison. In this figure, the downstream pressure curve of the parallel pilot valve system is overlapped with that of the single pilot valve B at the first 0.1 second after the system started. And then, it gradually increases from the setting pressure of the sub pilot valve B to the main pilot valve A. It indicates the downstream pressure is firstly controlled by the valve B, and recovered rapidly because of the fast response speed of it, and then controlled by the valve A because it reaches to the setting pressure of the valve A and it becomes stabilized. Thus, when the downstream pressure exceeds 2080 PaG, the pressure is completely controlled by the valve A, because the valve B is completely closed due to its setting pressure is set to 2080 PaG that lower than the valve A. And when the downstream pressure under 2080 PaG, the action of the valve B makes the downstream pressure recover rapidly. In a word, the simulation results indicate that the parallel pilot valve system owns a composite dynamic characteristics of these two pilot valves.

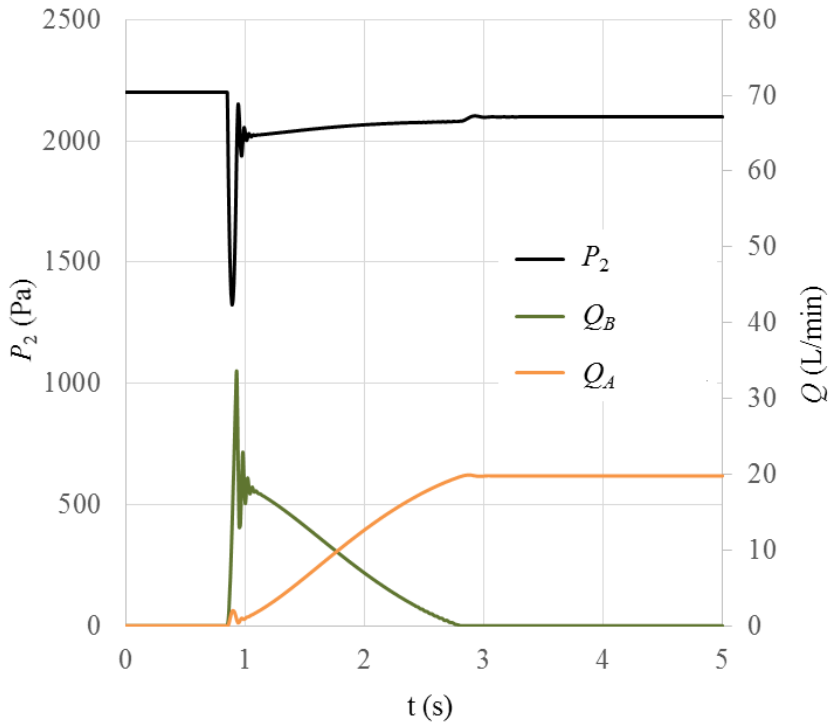

Fig.4.16 Response of parallel pilot valve (c = 10 [N·s /m])

In addition, there is a slightly large pressure vibration between 1.8 to 2.8 seconds. From the flow rate response curve, it is seen that the sub pilot valve B is gradually closing in this time period. That is, the speed of the diaphragm motion becomes slow, while the damping relates to the motion speed. The motion speed is smaller, and the damping is also smaller. Therefore, the unstable pressure phenomenon is occurred. If we set a larger damping coefficient with the sub pilot valve B, the vibration is disappeared as shown in Figure.4.16. Hence, the vibration is almost affected by the damping of the sub pilot valve B.

In the simulation results, the downstream pressures are all stable after the step signal, it is seem that the main pilot valve A, the sub pilot valve B, and the parallel pilot valve system all show a good stability. In fact, without the whole feedback gas governor unit system, the stability can’t be reflected in the results. However, up to now, we know the

response speed of the sub pilot valve B is faster than main pilot valve A. It indicates that the sub pilot valve B is more sensitive to the downstream pressure than the pilot valve A, the flow rate gain of the sub pilot valve B is larger than the main pilot valve A. Therefore, the unstable problem of the downstream pressure is more likely to occur with the single pilot valve B in the whole gas governor system. On the other hand, the parallel pilot valve system owns the composite characteristics of these two valves, it will possess the stability of the main pilot valve and the quick response of the sub pilot valve, simultaneously. Thus, the parallel pilot valve system will show a better characteristics than the single pilot valve in the gas governor system. The research on the stability of the parallel valve system in the gas governor unit will be conducted in the future work.

4.5 Conclusions

In this chapter, a simulation model of the parallel pilot valve system was proposed to analyze the dynamic characteristics of the gas governor unit. The mathematical models of the main pilot valve and the sub pilot valve were established. A static experiment was carried out to confirm the static characteristics of the pilot valve and to find the relationship of the downstream pressure and the pressure inside the pilot valve. Finally, a simulation by MATLAB was implemented to investigate the dynamic characteristics of the parallel pilot valve system. Some conclusions are summarized as follows:

(1) The simulation model of the regulator with an air room chamber and a bleed hole, can reflect the dynamic characteristics of two type pilot valves. The sub pilot valve B has a quick response, and the main pilot valve A has a slow response because its bleed hole is restricted, adequately. The sub pilot valve B is more sensitive to the pressure than the main pilot valve A.

(2) The simulation results indicate that the parallel pilot valve system owns a composite dynamic characteristics of these two pilot valves. It will possess the stability of the main pilot valve and the quick response of the sub pilot valve, simultaneously.

(3) The proposed simulation model can be helpful to analyze and design the parallel pilot valve system for quick and stable pressure control.

Chapter 5 Pressure response of various gases in a pneumatic resistance capacitance system and pipe

5.1 Properties of four gases

In the former chapters, we discussed the pilot valve system is used for natural gas, but the experimental gas is all air. Because air is easy to be supplied and it is a secure gas in a laboratory. However, the properties of these gases are different from each other. Therefore, in order to confirm the influence of different properties of various gases to the gas pressure control system, some pressure response experiments are conducted. In these research, four common industrial compressible fluid, air, methane, propane, and hydrogen, are used. The properties of these four gases are shown in Table 5.1.

In our experiments, we used a quick flow sensor (QFS; Figure 5.1) based on the laminar flow theory to measure the flow rate of the various gases. The flow rate calculation of the QFS uses the Hagen–Poiseuille equation:

$$Q = \frac{\pi r^4 \Delta P}{8 \mu L} \tag{5.1}$$

where Q is the volumetric flow rate, r is the pipe radius, L is the pipe length, μ is the dynamic viscosity, and ΔP is the differential pressure.

Table 5.1 Properties of various gases

Gas	Density ρ [kg/m^3]	Relative density	Viscosity μ [10^{-7} Pa·S]	Relative viscosity	Gas constant R [J/(kg·K)]	Specific heat ratio κ
Air	1.205	1.000	181	1.000	287	1.40
Methane	0.668	0.554	108	0.597	518.3	1.32
Hydrogen	0.083	0.068	88	0.486	4128.5	1.41
Propane	1.882	1.562	80	0.442	189	1.13

(Temperature = 20 °C at atmospheric pressure)

Fig.5.1 Laminar flow rate meter (QFS)

A flow rate meter is usually designed for air measurement because of its universality. Therefore, the parameters of the QFS can only be used for air measurements; that is, the dynamic viscosity μ is of air. The parameters of the QFS must be modified to enable measurements for other gases. Based on the experimental data Q_m obtained with the QFS, the real flow rate Q_{real} of various gases can be obtained with Eq. 5.2, which uses the relative viscosity μ^*. The relative viscosity of the four gases are shown in Table 5.1.

$$Q_{real} = \frac{Q_m}{\mu^*} \tag{5.2}$$

For example, if the measured data Q_m of hydrogen is 20 L/min shown in the display of the QFS, the real flow rate Q_{real} is 41.2 L/min, because the measured data is divided the hydrogen relative viscosity of 0.486.

In addition, four types of gas equipment are used in this research, such as orifice, isothermal chamber, nozzle-flapper, and pipe.

5.2 Flow rate characteristics of various gases

An orifice as a restriction is the most widely used pneumatic resistance. Firstly, it is necessary to confirm the difference of the flow rate through the orifice with various gases. The mass flow rate is determined by Eq. (2.1) with air, and it is observed that the critical pressure ratio is 0.5283 because the specific heat ratio of air is 1.4. In fact, the critical pressure ratio relates to the specific heat ratio, and the overwritten mass flow rate equations are shown as Eq. (5.3), (5.4), and (5.5).

when $\frac{P_D}{P_U} \le (\frac{2}{\kappa+1})^{\frac{\kappa}{\kappa-1}}$,

$$G(S_e, P_U, P_D) = S_e P_U \sqrt{\frac{\kappa}{R\theta_1}(\frac{2}{\kappa+1})^{\frac{\kappa+1}{\kappa-1}}} \tag{5.3}$$

and $\frac{P_D}{P_U} > (\frac{2}{\kappa+1})^{\frac{\kappa}{\kappa-1}}$

$$G(S_e, P_U, P_D) = S_e P_U \sqrt{\frac{2\kappa}{\kappa-1}\cdot\frac{1}{R\theta_1}\left[\left(\frac{P_D}{P_U}\right)^{\frac{2}{\kappa}} - \left(\frac{P_D}{P_U}\right)^{\frac{\kappa+1}{\kappa}}\right]} \tag{5.4}$$

$$S_e = C_D \frac{\pi d^2}{4} \tag{5.5}$$

where S_e is the effective area, d is the orifice diameter, C_D is the discharge coefficient, R is the gas constant, P_U is the upstream pressure, P_D is the downstream pressure, θ_1 is the flow temperature, and κ is the specific heat ratio.

If we propose the gas constant and simply note:

$$G(S_e, P_U, P_D) = \frac{1}{\sqrt{R}}\varphi(S_e, P_U, P_D) \tag{5.6}$$

Eq. (5.6) indicates that the mass flow rate is inversely proportional to the square root of gas constant R if the other parameters are constant. In addition, G (S_e, P_U, P_D) is simply noted as G, the volume flow rate can be calculated by:

$$Q = \frac{G}{\rho} \tag{5.7}$$

where ρ is the density. At the atmosphere (P_a), the ideal gas equation (2.5) is transformed to:

$$P_a V = mR\theta \tag{5.8}$$

$$\rho = \frac{P_a}{R\theta} \tag{5.9}$$

Here, m is the unit mass of air, V is the unit volume of air. Because $m/V = \rho$. Eq. (5.9) is substituted to Eq. (5.7) and uses Eq. (5.6):

$$Q = \frac{\sqrt{R}\theta\varphi(S_e, P_U, P_D)}{P_a} \tag{5.10}$$

Similarly, the volume flow rate is proportional to the square root of gas constant R if the other parameters of each gas are constant.

Generally, the discharge coefficient C_D is mostly dependent on the structure and dimensions of the orifice, while at times, it is affected by the Reynolds number. In this

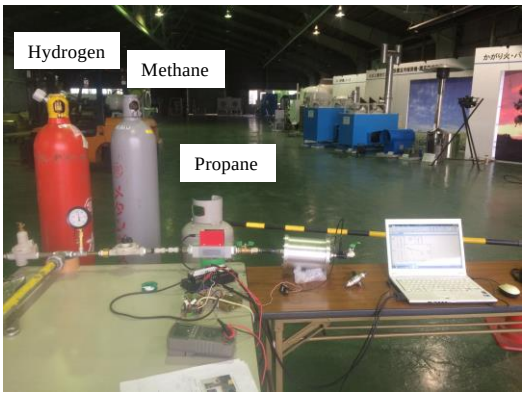

Fig.5.2 Experimental setup

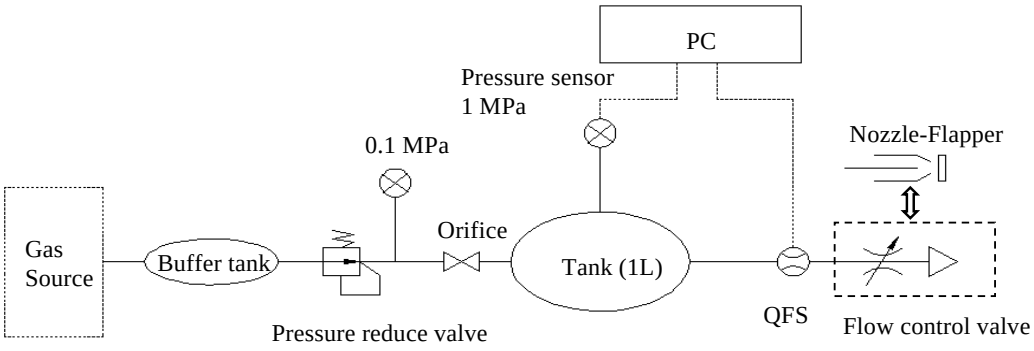

Fig.5.3 Pneumatic circuit of experiment

experiment, the orifice was not changed and the Reynolds number was large most of the time. At large Reynolds numbers, changes in C_D are very small. Therefore, to compare the primary factor of influence, C_D was set to a constant equal to the C_D of air. Curve fitting of the experiment data revealed that the discharge coefficient is 0.89 in the next experiment. On the other hand, the specific heat ratio κ of the different gases is almost the same; therefore, it is not a primary influencing factor compared with the gas constant. If the specific heat ratios of all gases are assumed to be the same as that of air, that is 1.4, it is not difficult to determine that the mass flow rate of the various gases is only dependent on the gas constant under a certain pressure difference from Eq. (5.6). Therefore, the calculation results from Eq. (5.10) indicate that the volume flow rates of hydrogen, propane, and methane were 3.80, 0.79, and 1.34 times those of air, respectively, under the same pressure difference. Note that we are talking about the volume flow rate, and not the mass flow rate.

A static experiment using a ϕ1 mm orifice was conducted to confirm the *P*-*Q* characteristic curve with various gases. The experimental location and sources of the various gases were shown in Figure 5.2. Figure 5.3 shows the pneumatic circuit of the static experiment. Here, the upstream pressure was set constant at 0.1 MPaG and the

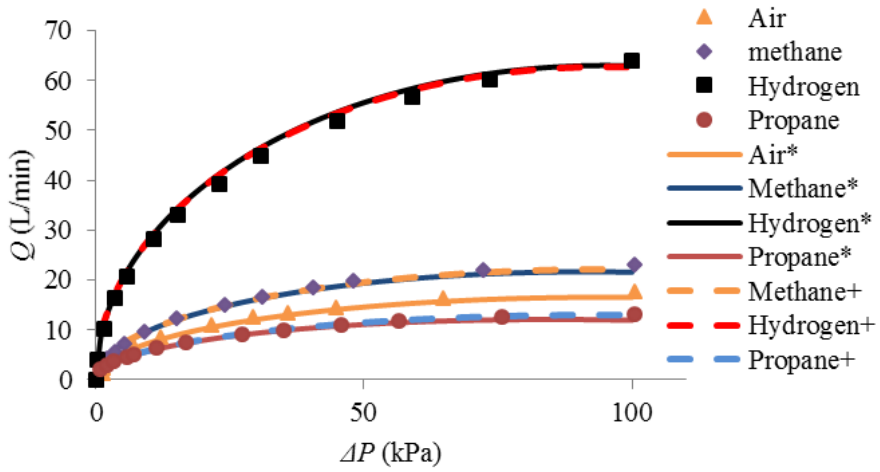

(*represents change in κ with various gases, + represents κ =1.4)

Fig.5.4 *P*-*Q* characteristic curve with various gases

downstream pressure was changed from 0.1 MPaG to atmospheric pressure through the flow rate control valve.

Figure 5.4 shows the static flow rate characteristic curve, that is, the *P*-*Q* characteristic curve with the various gases. The dashed curve represents the calculation results without considering the influence of κ, that is, κ of all gases set to 1.4. The solid curve represents the calculation results considering the different values of κ of the various gases. The two curves of the same gas were generally coinciding, and the experimental data were consistent with these calculations. Therefore, it is believed that the flow rate equation for the orifice with various gases can neglect the effect of the specific heat ratio when its value is from 1.13 to 1.4.

5.3 Pressure response in pneumatic resistance capacitance circuit

The gas flow through a valve or a pressure regulator can sometimes be seen as though a nozzle flapper. Next, the pressure response with the various properties of gases in an

isothermal chamber (ITC) was investigated. The isothermal chamber is a tank filled with copper wire, and an orifice and a nozzle flapper are used in this response experiment.

5.3.1 Calculation

The mathematical model of the ITC with an orifice and nozzle flapper is shown in Figure 5.5. The ideal gas equation for the ITC was differentiated with respect to time:

$$P_2 V_2 = m_2 R\theta \tag{5.11}$$

$$\frac{V_2 dP_2}{dt} = R\theta \frac{dm_2}{dt} + m_2 R \frac{d\theta}{dt} \tag{5.12}$$

where P_2 is the pressure in the chamber, V_2 is the volume of chamber, m_2 is the mass of air in the chamber, θ is the temperature, and R is the gas constant. Because the chamber is isothermal, $d\theta / dt = 0$ and $\theta = \theta_a$. Furthermore, $dm / dt = G$, where G is the mass flow rate. Therefore, Eq. (5.12) was changed to

$$\frac{dP_2}{dt} = \frac{R\theta_a}{V_2}(G_1 - G_2) \tag{5.13}$$

$$P_2 = \int \frac{R\theta_a (G_1 - G_2)}{V_2} dt \tag{5.14}$$

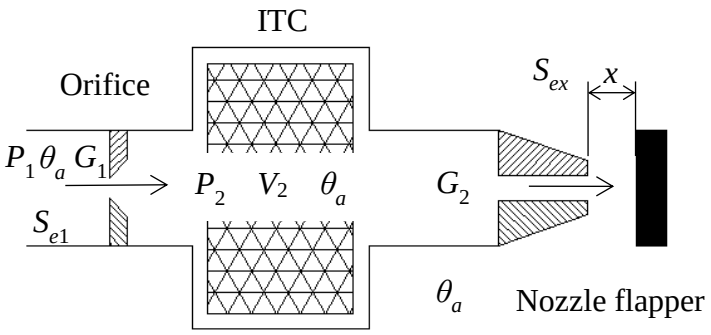

Fig.5.5 Pneumatic resistance capacitance system

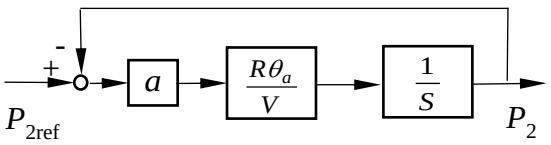

Fig.5.6 Block diagram

The flow rate through the upstream orifice G_1 and the downstream nozzle flapper G_2 are also determined by Eqs. (5.3), (5.4), and (5.5). The specific heat ratios of all gases are set to 1.4 according to the conclusion of Section 3. Using Eq. (5.6), also note:

$$G_1 = \frac{1}{\sqrt{R}}\varphi_1(S_{e1}, P_1, P_2), G_2 = \frac{1}{\sqrt{R}}\varphi_2(S_{ex}, P_2, P_a) \tag{5.15}$$

The flow rates G_1 and G_2 are linearized at the pressure balance point P_{2ref} and the flow rate gain a is defined as follows:

$$a = \frac{\Delta G_1 - \Delta G_2}{\Delta P_2} \tag{5.16}$$

The block diagram is shown in Figure 5.6.

From this block diagram, the transfer function is obtained:

$$F(s) = \frac{1}{1 + T_p s} \tag{5.17}$$

Here, T_p is the time constant [12] of the system:

$$T_p = \frac{V_2}{aR\theta_a} \tag{5.18}$$

Using Eqs. (5.15) and (5.16), we have

$$a = \frac{1}{\sqrt{R}}\left(\frac{\Delta\varphi_1(S_{e1}, P_1, P_2) - \Delta\varphi_2(S_{ex}, P_2, P_a)}{\Delta P_2}\right) \tag{5.19}$$

Defining

$$a^* = \frac{\Delta\varphi_1(S_{e1}, P_1, P_2) - \Delta\varphi_2(S_{ex}, P_2, P_a)}{\Delta P_2} \tag{5.20}$$

we get

$$a = \frac{1}{\sqrt{R}}a^*, \text{ and } T_p = \frac{1}{\sqrt{R}}\frac{V}{a^*\theta_a} \tag{5.21}$$

From Eq. (5.21), it can be seen that the time constant is inversely proportional to the square root of the gas constant of the various gases when the other experimental conditions are fixed.

5.3.2 Pressure response experiment

The pneumatic circuit of the pressure response experiment is also shown in Figure 5.3, but the flow control valve is changed to a nozzle flapper. In the discharge process, the effective area of the downstream restriction was changed from 0.15 mm^2 to 0.85 mm^2 by controlling the displacement between the nozzle and flapper with propane, while the effective area of the downstream restriction was changed from 0.1 mm^2 to 0.9 mm^2 with

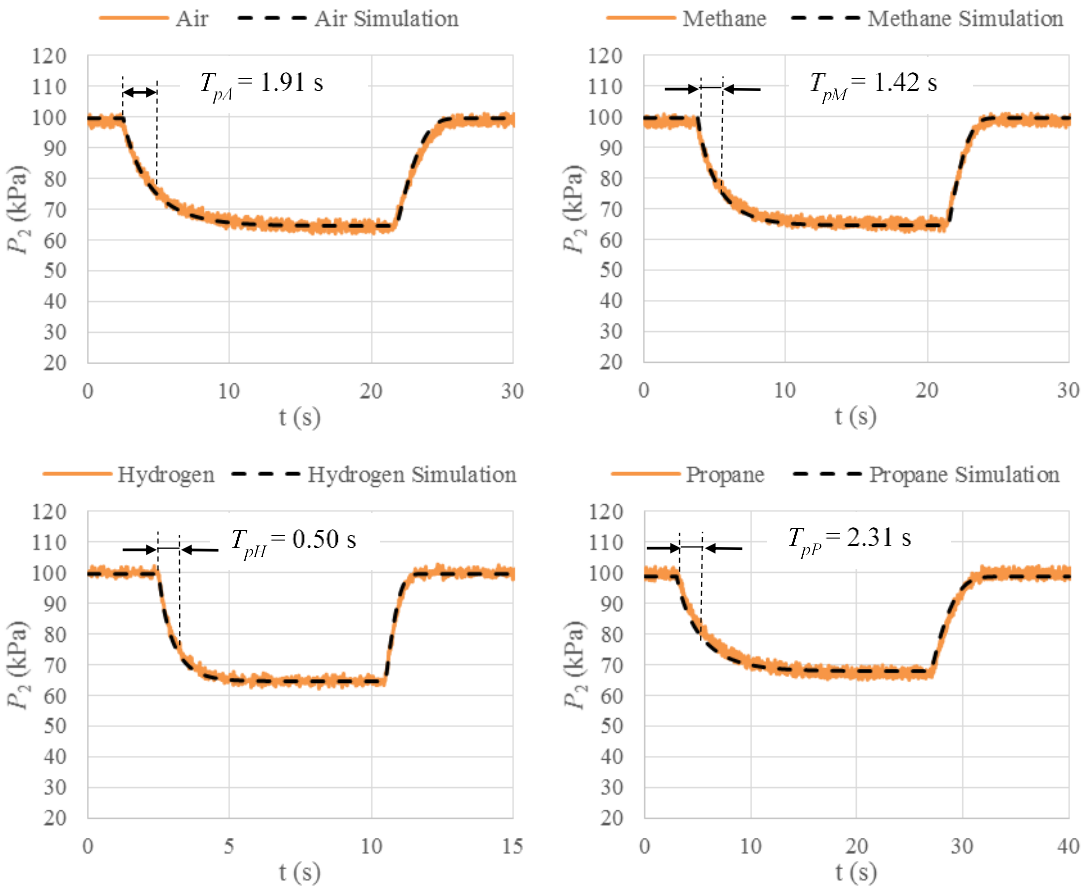

Fig.5.7 Pressure response of P_2

the other gases. Needless to say, the action is opposite in the charge process. The upstream pressure was set to 0.1 MPaG. The experimental process is illustrated as follows:

(a) Set P_1 to 0.1MPaG, and keep a little flow rate by nozzle-flapper.

(b) Turn up the flapper quickly, and wait for the response of P_2 changes to the pressure of steady state.

(c) Turn down the flapper to its original state, and record the data of pressure change.

(d) Change the gas, and repeat the actions above.

The pressure response of P_2 in the ITC is shown in Figure 5.7. The black dashed curve represents the simulation results obtained with MATLAB, and the orange curve is the experimental sampling data. The results obviously show that the pressure response speed of hydrogen is the fastest, while that of propane is the slowest. The time taken to reach an 63.2% drop in the response pressure is defined as the time constant of the various gases. Note that T_{pA}, T_{pH}, T_{pM}, and T_{pP} represent the time constant of air, hydrogen, methane, and propane, respectively. The calculation results show that T_{pA} = 1.91 s, T_{pH} = 0.50 s, T_{pM} = 1.42 s, and T_{pP} = 2.31 s. Therefore, the time constant of air is 3.82 times that of hydrogen, which is precisely equal to the reciprocal of the square root of the gas constant times. The experiment data also show agreement with the calculations, that $T_{pA}{}^{*}$= 2.12 s, $T_{pH}{}^{*}$= 0.55 s, $T_{pM}{}^{*}$ = 1.48 s, and $T_{pP}{}^{*}$= 2.61 s. Therefore, the results verify the conclusion of Eq. (5.21). As we know, the gas constant refers to the molecular weight of the gas. Thus, it is certainly believed that the high response speed of hydrogen is owing to its small molecular weight. Finally, it must be noted that the pressure control system needs a high response speed when hydrogen is used. These results can help engineers in designing gas pressure control equipment with various gases, particularly, hydrogen pressure control systems.

5.4 Pressure response in pipe

Pipe is another important constituent of pneumatic and gas pressure control systems. We performed a pressure response experiment using an 18 m pipe, and the dynamic characteristics of the pressure propagation with various gases were explicated; the pipe's inner diameter was 6 mm.

5.4.1 Experiment

Figure 5.8 shows the pneumatic circuit of the dynamic pressure response experiment. In this experiment, the upstream pressure was set to 75 kPaG, and the downstream pressure was maintained at 2.8 kPaG using a second-stage regulator KLS-5B by KATSURA Co., Ltd. The pressure in front of the pipe was measured with a pressure sensor P_f and that at the back of the pipe was recorded with P_b. The steps of the experiment are illustrated as follows:

(1) Discharge process:

a. Slowly shut the control valve 2, and hold the downstream pressure at 2.8 kPaG.

b. Shut the control valve 1.

c. Open the control valve 2 quickly and record the data until the pressure is stable.

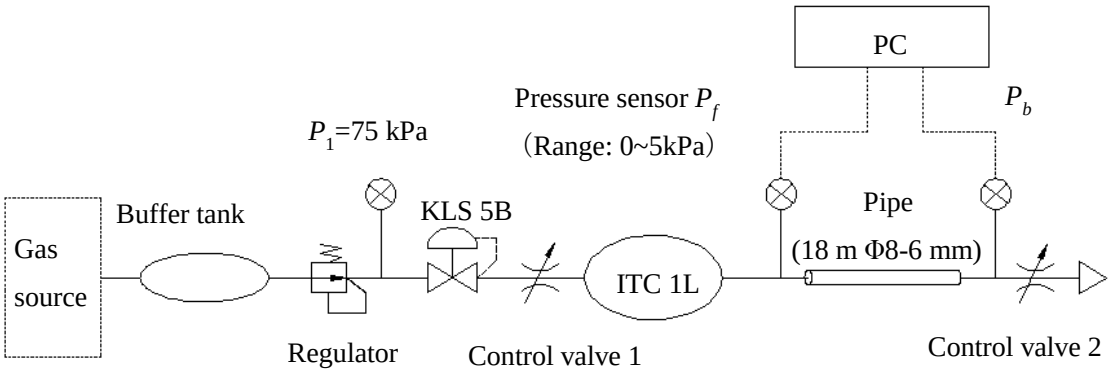

Fig.5.8 Pneumatic circuit of pressure response experiment with a pipe

(2) Charge process:

a. Shut the control valve 1, and wait till the downstream pressure decreases to the atmospheric pressure and stabilizes.

b. Shut the control valve 2.

c. Open the control valve 1 quickly and record the data until the pressure is stable.

5.4.2 Results and discussion

Figures 5.9 and 5.10 show the results of the pressure response in the discharge and charge processes, respectively, with various gases. The black curve represents the pressure response P_f in front of the pipe, and the blue curve represents the pressure response P_b at the back of the pipe.

In the discharge process, P_b drops quickly because the volume of the pipe is small, while P_f drops at the same rate as that in section 5.3.2 because it is located near the ITC. It can be observed that there is some time delay in the pressure response curve of P_f with air, methane, and propane, but the time delay with hydrogen is very small. This is assumably because the time taken for the pressure wave to travel from the back to the front of the pipe with hydrogen is way lesser than that with the other gases. The speed of sound is determined by $c = \sqrt{\kappa R\theta}$. Therefore, the speed of sound in hydrogen is way

Table 5.2 Parameters with various gases

Gas	c [m/s]	T_t [s]	T_t^* [s]	$S = \rho\sqrt{\kappa R}/\mu$ $[10^6 K^{-\frac{1}{2}} \cdot m^{-1}]$	Relative S	A_P^* [Pa]	Relative A_P^*
Air	343	0.209	0.18	1.28	1	568	1
Methane	461	0.156	0.13	1.60	1.21	645	1.14
Hydrogen	1301	0.055	0.05	0.69	0.54	294	0.52
Propane	278	0.259	0.21	3.70	2.6	1336	2.35

(* represents the experiment data)

faster than that in the other three gases because of their large gas constants. On the other hand, the large gas constant means that the molecular weight of hydrogen is very small, and that of propane is large. That is, propane is very heavy and hence it has large inertia. In Figure 5.9 (d), it seems that there is a slight vibration in P_f with propane when the pressure reaches the atmospheric pressure, while no vibration is observed with hydrogen.

The time delay phenomenon also occurs in the charge process, but the delayed pressure is P_b because of the reverse flow direction. The pressure vibration of P_b is greater than that in the discharge process because the volume at the back of the pipe without a tank is very small and a gas column vibration occurred. The period of the gas column vibration is determined by $T_t = 4L/c$. Here, L is the length of the pipe. The gas column vibration periods for air, propane, and hydrogen are 0.209 s, 0.259 s, and 0.055 s, respectively. The results in Figure 5.10 roughly accord with the calculations, and the experimental data are shown in Table 5.2.

Similar to the phenomenon of the water hammer [57], the maximum amplitude A_P of the pressure vibration at the back of the pipe is determined by

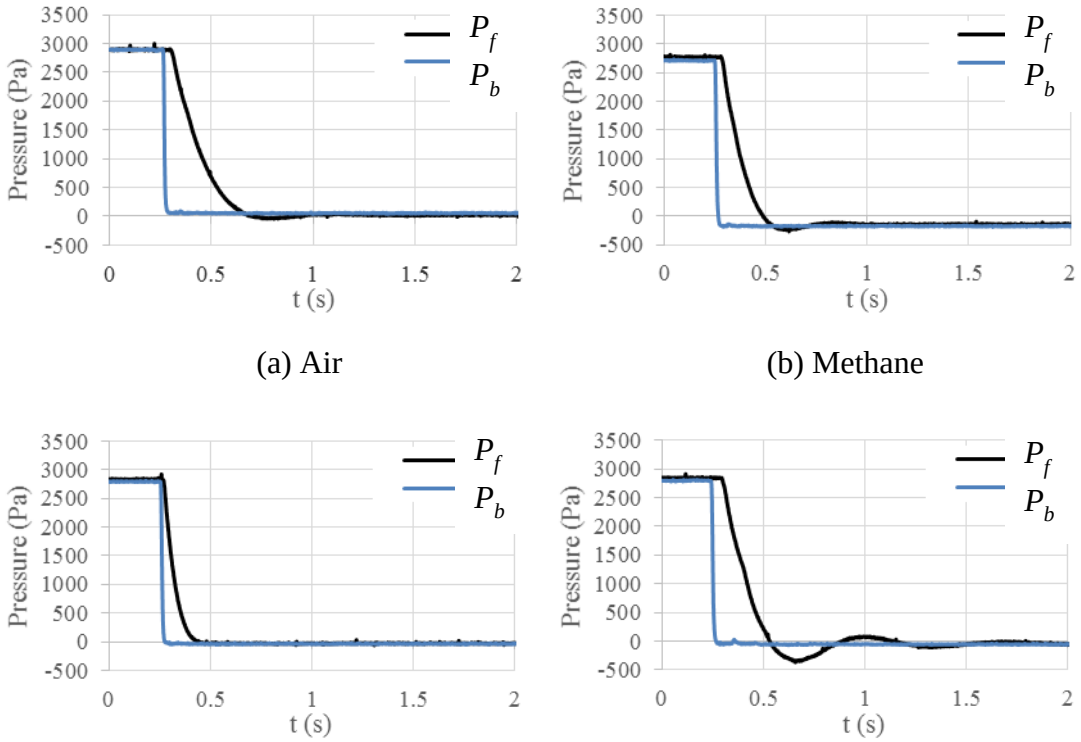

(a) Air (b) Methane

(c) Hydrogen (d) Propane

Fig.5.9 Pressure response in pipe (Discharge)

$$A_p = \rho c u \tag{5.22}$$

where u is the flow velocity. In this experiment, the pressure difference of 2.8 kPa is small and the pipe is too long so that the flow is laminar. Therefore, the flow rate equation (Eq. (2.3)) is used, and $u = Q/A$, where A is the cross-sectional area of the pipe. Using the speed of sound equation, we get

$$A_P = \rho\sqrt{\kappa R\theta}\,\frac{\pi r^4 \Delta P}{8\mu L}\,\frac{1}{A} \tag{5.23}$$

Defining a sound pressure coefficient S as $S = \dfrac{\rho\sqrt{\kappa R}}{\mu}$, Eq. (5.23) becomes

$$A_P = S \cdot \frac{\pi r^4 \Delta P\sqrt{\theta}}{8AL} \tag{5.24}$$

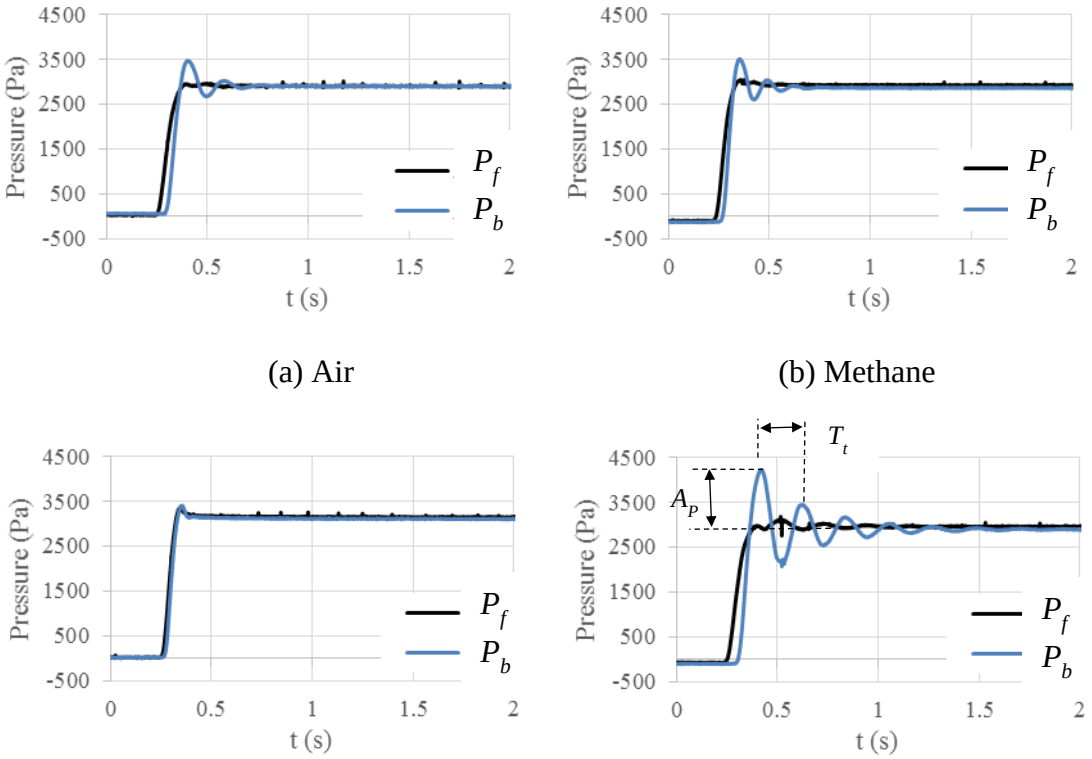

(a) Air (b) Methane

(c) Hydrogen (d) Propane

Fig.5.10 Pressure response in pipe (Charge)

From this equation, it is found that the maximum amplitude of the gas column vibration is proportional to the sound pressure coefficient S with various gases. The value of S is shown in Table 5.2. The relative sound pressure coefficient indicates that the maximum amplitude of hydrogen and propane are 0.54 times and 2.6 times that of air, respectively. The experimental results roughly agree with this calculation. Certainly, many other factors, such as friction at the pipe's inner wall and pipe shape affect the pressure response and the pressure wave propagation. Therefore, the error is inevitable, and a high-precision simulation will be performed in a future study.

From this result, we can roughly estimate the pressure response in a long pipe by using the properties of different gases. It needs to be noticed that a large pressure vibration

easily occurs in a pipe system when the gas is propane. And a rapid response pressure control system needs to be installed in a pipe system with hydrogen.

5.5 Conclusions

In this study, a static flow rate characteristic experiment using an orifice was performed with air, methane, propane, and hydrogen. The effect of the viscosity and gas constant of the gases on the flow rate measurement and *P*-*Q* characteristic curve was understood. Two dynamic pressure response experiments with a pneumatic resistance capacitance system and a pipe were performed to verify the effect of the gas constant of various gases on the pressure response speed. Finally, the following conclusions were obtained:

(1) The flow rates can be calculated by only considering the gas constant of the various gases in an orifice with a constant area under a certain pressure difference because the influence of κ is negligible when its value is from 1.13 to 1.4.

(2) The time constant of the various gases is proportional to the reciprocal of the square root of the gas constant. That is, the pressure response speed of hydrogen is 3.82 times that of air in a pneumatic resistance capacitance system.

(3) The pressure response speed in a pipe with hydrogen is much faster than that with the other three gases, and a large pressure vibration does not easily occur because of its small molecular weight. In contrast, propane has a large molecular weight. If the flows are laminar, the maximum amplitudes of the vibration are proportional to their sound pressure coefficients.

(4) The research findings can be applied in the design and manufacture of different gas systems and equipment, particularly in the application of the hydrogen.

Chapter 6 Summary and future work

6.1 Summary

The industrial compressible fluid, especially the flammable gases has been paid more and more attention in the energy source supply system in the past twenty years. For example, methane or so-called natural gas, propane, and hydrogen are all cleaner than the conventional fuel. The self-actuated pressure control system without the electrical components such as the gas governor unit is widely used in the city gas supply system for anti-explosion. There are many pressure control problems in this equipment because the system lacks the electrical controlled circuit.

In this thesis, in order to solve the nonlinear problems caused by the square characteristics flow resistance of orifice in the pressure control system, a method using porous material whose flow rate characteristics is linear was proposed to improve the characteristics of the pressure control system and pilot valve system in chapters 2 and 3. On the other hand, a simulation model of the parallel pilot valve system was proposed to analyze the dynamic characteristics of the gas governor unit in chapter 4. Finally, for the application of the hydrogen pressure control system, the differences of the pressure response with various gas properties were investigated in chapter 5. The contents of each chapter are summarized as follows.

In chapter 1, four common industrial gases, air, methane, propane, and hydrogen, and some pressure control technologies of them are introduced. Then, we introduced the gas governor unit which is an important pressure control equipment in the city gas supply system, and the pilot valve system. In the pilot valve system, there are many pressure problems, such as the pressure vibration in the downstream pipeline and the worse

dynamic pressure response at the starting of the system. In terms of these pressure problems, the characteristics of flow resistance are important. And we showed the disadvantages of the square characteristics of the flow resistance (e.g. orifice). Therefore, we proposed two methods to solve these problems, that is to say, the application of porous materials and parallel pilot valve system. At the last of this chapter, the purposes and structure of this thesis are illustrated.

In chapter 2, a method by using porous materials and an isothermal chamber is proposed for improving the characteristics of a gas pressure control system called pneumatic RC circuit. A static characteristics experiment with a porous material is performed to confirm their *P*–*Q* characteristics. Then, the mathematical model of the pneumatic RC circuit is established, and the simulation is carried out by MATLAB. A frequency response experiment is also performed to estimate their dynamic responses. The experimental results are in close agreement with the simulation results. Here, the following conclusions are drawn from this chapter: (1) The *P*–*Q* characteristics of porous materials are linear, but those of the orifice are nonlinear. The flow rate increases rapidly when the differential pressure in the orifice is small, and it gradually reduces with increasing differential pressure. However, for the porous material, the increasing rate remains invariable. (2) In the case of a pneumatic RC circuit with a porous restriction, the curves of the pressure gain and phase difference in the frequency response experiment are invariable with respect to changes in the amplitude of the input pressure. However, they are variable in the case of a pneumatic RC circuit with an orifice, because of the nonlinear flow rate characteristics of the orifice. (3) The pressure gain in the chamber with porous materials is lower than that with an orifice when the amplitude of the input pressure is small. Using porous materials instead of orifices helps to reduce the pressure

oscillation in a pneumatic chamber when the input pressure vibration is small. (4) It indicates that the pressure control system can be linearized by using the porous material easily.

In chapter 3, the new method employing porous materials is examined for improving the characteristics of the pilot valve system in the gas governor unit. An experiment is performed to confirm the static *P–Q* characteristics of a new size porous material. A test pilot valve is manufactured, and a frequency response experiment is performed in this test system to estimate its dynamic response with porous material and orifice. A mathematic model of the test pilot valve system is developed in MATLAB. The experimental results are in close agreement with the simulation results. We obtain the following conclusions: (1) The static flow characteristics of the new size porous materials are also linear, but those of orifices are nonlinear. (2) In the frequency response experiment, the gain and phase difference of the diaphragm chamber pressure P_d remain constant with changes in the amplitude of the input vibration because of the linear flow characteristics of the porous material. As a result, the control pressure is not affected by the changes in the amplitude of the input vibration. However, the control pressure changes in the case of the orifice because of its nonlinear characteristics. (3) The motion of the valve diaphragm will slightly affect the results of the dynamic response. (4) Therefore, porous materials can be used in the pilot valve system instead of an orifice to improve its dynamic characteristics by making it to be a linear system easily. And the invariable flow resistance will help engineers to choose the restrictions more easily in designing the pilot valve system.

In chapter 4, a simulation model of the parallel pilot valve system was proposed to analyze the dynamic characteristics of the gas governor unit. The mathematical models of the main pilot valve and the sub pilot valve are established. A static experiment is

carried out to confirm the static characteristics of the pilot valve and to find the relationship of the downstream pressure and the pressure inside the pilot valve. A simulation by MATLAB is implemented to investigate the dynamic characteristics of the parallel pilot valve system. Conclusions are summarized as follows: (1) The simulation model of the regulator with an air room chamber and a bleed hole, can reflect the dynamic characteristics of two type pilot valves. The sub pilot valve B has a quick response, and the main pilot valve A has a slow response because its bleed hole is restricted, adequately. The sub pilot valve B is more sensitive to the pressure than the main pilot valve A. (2) The simulation results indicate that the parallel pilot valve system owns a composite dynamic characteristics of these two pilot valves. It will possess the stability of the main pilot valve and the quick response of the sub pilot valve, simultaneously. (3) The proposed simulation model can be helpful to analyze and design the parallel pilot valve system for quick and stable pressure control.

In chapter 5, in the application of the hydrogen station and the design of the pressure control system with different gases, the properties of gas need to be carefully considered. A static flow rate characteristic experiment using an orifice is performed with various gases. The effect of the viscosity and gas constant of the gases on the flow rate measurement and *P*-*Q* characteristic curve is confirmed. Two dynamic pressure response experiments with a pneumatic resistance capacitance system and a pipe are performed to verify the effect of the gas constant of various gases on the pressure response speed. The following conclusions are obtained: (1) The flow rates can be calculated by only considering the gas constant of the various gases in an orifice with a constant area under a certain pressure difference because the influence of κ is negligible when its value is from 1.13 to 1.4. (2) The time constant of the various gases is equal to the reciprocal of

the square root of the gas constant. That is, the pressure response speed of hydrogen is 3.82 times that of air in a pneumatic resistance capacitance system. (3) The pressure response speed in a pipe with hydrogen is much faster than that with the other three gases, and a large pressure vibration does not easily occur because of its small molecular weight. In contrast, propane has a large molecular weight. If the flows are laminar, the maximum amplitudes of the vibration are proportional to their sound pressure coefficients. (4) The research findings can be applied in the design and manufacture of different gas systems and equipment, particularly in the application of the hydrogen.

6.2 Future work

The gas governor unit is an enormous and complicated system that is difficult to establish in our laboratory. Therefore, there are several tasks associated with the pilot valve system that are hoped to be done in the future:

(1) Although the effects of the porous materials in the pneumatic RC circuit and the test pilot valve system are confirmed and the dynamic characteristics of the parallel pilot valve system is verified in the simulation, the actual effects of these method are unknown up to now. Therefore, the dynamic experiment by using the porous material and parallel pilot valve system in the gas governor unit is worth being implemented in the future.

(2) Because the pressure control system can be linearized by using the porous materials, we could develop a method to judge the stability of the pilot valve system with the nonlinear and linear flow resistances base on the describing function.

Although some pressure response experiments were carried out in the pipe with various gases, but the accurate solution of the pressure propagation in the pipe is still ambiguous.

(3) Therefore, we need to find an accurate numerical solution of the pressure propagation in a pipe with various gases.

Finally, considering the application of the hydrogen in the future,

(4) We hope to develop a rapid response speed valve for hydrogen.

References

[1] Initiation: pump up the volume, http://asiaresearch.daiwacm.com/eg/cgi-bin/files/Airtac_International_Group_140415.pdf

[2] Arno De Klerk and Vinay Prasad. Methane for transportation fuel and chemical production. *In*: Trevor M. Letcher, Janet L. Scott (Eds.). Materials for a Sustainable Future. 2012, RSC Publishing, pp.327-329.

[3] Zuttel, A., Remhof, A., Borgschulte, A., Friedrichs, O., 2010. Hydrogen: the future energy carrier. *Philosophical Transactions of the Royal Society A*, **368**: 3329–3342. [http://dx.doi.org/10.1098/rsta.2010.0113]

[4] Kler, A.M., Tyurina, E.A., Potanina, Y.M., Mednikov, A.S., 2015. Estimation of efficiency of using hydrogen and aluminum as environmentally-friendly energy carriers. *International Journal of Hydrogen Energy*, **40**(43): 14775-14783. [http://dx.doi.org/10.1016/j.ijhydene.2015.09.041]

[5] Suman Dutta, 2014. A review on production, storage of hydrogen and its utilization as an energy resource. *Journal of Industrial and Engineering Chemistry*, **20**(4): 1148–1156.

[6] Hwang, Y.G., 2016. Technical trends of hydrogen manufacture, storage and transportation system for fuel cell vehicle. *Journal of The Korean Institute of Resources Recycling*, **25**(1): 48-59. [http://dx.doi.org/10.7844/kirr.2016.25.1.48]

[7] Mizuno, T., Youn, C., Nakamura, Y., Kagawa T., 2013. A sim-ulation study of radial slits pressure regulator for hydro-gen gas. 13th International Conference on Systems Simu-lation. *In*: Tan, G., Yeo, G.K., Turner, S.J., Teo, Y.M. (Eds.), AsiaSim 2013: 13th International Conference on Systems Simulation. Singapore, p.288-297. [http://dx.doi.org/10.1007/978-3-642-45037-2_27]

[8] Zhang, L.C., Liu, L.P., Xu, J.D., 2014. Research on experiment test system of mechanism of fame propagation for gas and coal dust explosion. *In*: Progress in Mine Safety Science and Engineering II, 837-842.

[9] Mohsen Saadat, Farzad A. Shirazi, Perry Y. Li, 2015. Modeling and Control of an Open Accumulator Compressed Air Energy Storage (CAES) System for Wind Turbines. *Applied Energy*, **137**, 603–616.

[10] Kato, T., Kawashima, K., Funaki, T., Kagawa, T., 2007. Active Control of a

Pneumatic Vibration Isolation Table using a Newly Developed Precise and High Response Pressure Regulator. 2007 IEEE International Conference on Control Applications, Singapore, 497-502.

[11] Kagawa, T., Shimizu, M., 1988. Nondimensional pressure responses of pneumatic RC circuits considering heat transfer. *Hydraulics & Pneumatics*, **19**(4): 308-311. [http://dx.doi.org/10.5739/jfps1970.19.308]

[12] Kagawa, T., 1982. Transient pressure response of pneumatic nozzle flapper. *Transactions of the Society of Instrument and Control Engineers*, **18**(6): 617-621. [http://dx.doi.org/10.9746/sicetr1965.18.617]

[13] Kagawa, T., Kitagawa, A., Takenaka, T., 1984. An analysis of transient response of a pneumatic transmission line terminated by volume using characteristics method. *Transactions of the Society of Instrument and Control Engineers*, **20**(11): 1014-1018. [http://dx.doi.org/10.9746/sicetr1965.20.1014]

[14] Li, G., Baggett, C., and Rosario, R. (2009) Air/Vacuum Valve Breakage Caused by Pressure Surges — Analysis and Solution. World Environmental and Water Resources Congress 2009: pp. 1-10

[15] Mohsen Shiee, K. Arman Sharifi, Morteza Fathi, Farid Najafi. Air pressure control via sliding mode approach using an on/off solenoid valve. 20th Iranian Conference on Electrical Engineering (ICEE2012), 15-17 May 2012, Tehran, Iran, pp. 857 – 861.

[16] Lilia Badykova, Dmitry Stadnick, Kirill Afanasev, Alexander Igolkin and Victor Sverbilov. Study on Dynamics of Air Pressure Reducing Valve With Focus on the Noise Attenuation Problem. 8th FPNI Ph.D Symposium on Fluid Power. Lappeenranta, Finland, June 11–13, 2014. pp. V001T01A013.

[17] Takeuchi, T., Kagawa, T., 2013. Applicability of frequency response test for stability evaluation of gas pressure regulator. *Transactions of the Society of Instrument and Control Engineers*, **49**(8): 747-754.

[18] Techakasem, Chalermrat. A study on a pressure regulator for compressible fluid systems with flow rate feedback. Doctor thesis, Tokyo Institute of Technology, 2012.

[19] Louis Schlapbach, Andreas Züttel, 2001. Hydrogen-storage materials for mobile applications. *Nature*, 414, pp.353-358. doi:10.1038/35104634

[20] Wong, J., Gambone, L., 2006. 70 MPa fueling station for hydrogen vehicles. 16th

World Hydrogen Energy Conference, Lyon, France.

[21] Nakano, A., Maeda, T., Ito, H., Masuda, M., Kawakami, Y., Tange, M., Takahashi, T., Nishida, K., 2012. Study on absorption/desorption characteristics of a metal hydride tank for boil-off gas from liquid hydrogen. International Journal of Hydrogen Energy, **37**(6): 5056-5062.

[22] Berry, S. (2003) Fundamental Principles of Pilot-operated Regulators. 78th International School of Hydrocarbon Measurement, Oklahoma, 20-22 May 2003, 588-591.

[23] Johnson D. (1974) Axial flow valve. US Patent No. US3836113 A

[24] Li, S. X., Xu, X. G., Hou, Y. Z., Li, Q., 2013. Numerical Analysis of Flow Field and Performance Optimization of Axial-Flow Pressure Reducing Valve. 3rd International Conference on Frontiers of Manufacturing and Design Science, Hong Kong, Frontiers of Manufacturing and Design Science III, PTS 1 And 2, 1362-1365.

[25] Yu, J. P., Yu, S. R., 2015. Numerical and experimental research of flow and sound fields in an axial-flow check valve and its optimization. *Advances In Mechanical Engineering*, **7**(11): 1-8.

[26] Clarence W. de Silva, Modeling and Control of Engineering Systems, CRC Press, Taylor & Francis Group, 2010, pp.286-287.

[27] Techakasem, C., Youn, C., Kagawa, T., 2013. A Pneumatic Pressure Regulator with Flow Feedback, *Transactions Of The Japan Fluid Power System Society*, 44, 87-93.

[28] Peter Vasilyev, Leonid Fromzel. Analytical Study of Piping Flow-Induced Vibration. Example of Implementation. 17th International Conference on Structural Mechanics in Reactor Technology, Prague, Czech Republic, 2003.

[29] Martinez, M. E., Tallavo, F., Ewins, D. J., 1998. Vibration Test and Analysis of Gas Pipelines to Validate Operation Beyond Their Design Levels. Proc. SPIE Vol. 3243, Proceedings of the 16th International Modal Analysis Conference, 878-883.

[30] Kong, K. K., Khoo, S. Y., Ong, Z. C., Eng, H. C., et al., 2014. Failure analysis of flow-induced vibration problem of in-serviced duplex stainless steel piping system in oil and gas industry. *Materials Research Innovations,* **18**: 417-422.

[31] Waxman, M., Davis, H.A., Horowitz, M. and Everhart, B. (1984) Automated Pressure Regulator. *Review of Scientific Instruments*, **55**: 1467-1470.

[32] Nakano, M., Tajima, K. and Outa, E. (1983) Aerodynamic Study on Noise and Vibration Generated in High Pressure Gas Valves. *Bulletin of the JSME*, **26**: 372-379. http://dx.doi.org/10.1299/jsme1958.26.372

[33] Earney, W.H. (2011) Causes and Cures of Regulator Instability. 86th International School of Hydrocarbon Measurement, Oklahoma, 10-12 May 2011, 739-743.

[34] Chalermrat, T., Kim, I., Youn, C. and Kagawa, T. (2011) Gas Governor Pilot Valve with Integral and Feed-forward Structure. SICE Annual Conference 2011, Tokyo, 13-18 September 2011, 1463-1467.

[35] Zafer, N. and Luecke, G.R. (2008) Stability of Gas Pressure Regulators. *Applied Mathematical Modelling*, **32**: 61-82. http://dx.doi.org/10.1016/j.apm.2006.11.003

[36] Ng, K.W. (1994) Control Valve Noise. *ISA Transactions*, **33**: 275-286. http://dx.doi.org/10.1016/0019-0578(94)90098-1

[37] El Golli Rami, Bezian Jean-Jacques, Delenne Bruno, Menu François, 2007. Modelling of a pressure regulator. *International Journal of Pressure Vessels and Piping*. **84**(4): 234–243.

[38] Lipták, B.G. (1995) Instrument Engineers' Handbook, (Volume 2) Third Edition: Process Control. Butterworth-Heinemann.

[39] Ray, W.A. (1972) Pilot Regulator Operated Main Valve. US Patent No. 3666173.

[40] Katchka, J.R. (1967) Pressure Regulator for Diaphragm Gas Valves. US Patent No. 3360198.

[41] Hamilton, J.K. (1952) Pilot Controlled Gas Pressure Regulator. US Patent No. 2593557.

[42] Kagawa, T. and Kodaira, K. (1984) Effect of Non-linear Flow Rate Characteristics on the Frequency Response of a Pneumatic RC Circuit. *Hydraulics & Pneumatics*, **15**: 473-479.

[43] Kagawa, T. (1981) The Effect of Heat Transfer on the Dynamics of Pneumatic RC Circuits. *Hydraulics & Pneumatics*, **12**: 209-212.

[44] J. Krope, D. Dobersek and D. Goricanec, Flow Pressure Analysis of Pipe Networks with Linear Theory Method. Proceedings of WSEAS/IASME International Conference on Fluid Mechanics, Miami, Florida, 18-20 January 2006, 59-62.

[45] Dong, D. and Li, X.N., 2015. Development of a Novel Parallel-spool Pilot Operated High-pressure Solenoid Valve with High Flow Rate and High Speed. *Chinese Journal of Mechanical Engineering*, **28**(2): 369-378.

[46] Kubota Atsushi and Sadayasu Takashi, Gas Pressure Regulator. JP Patent No. 53-078637, U(1978).

[47] Yokota, S. and Nakano, K. (1982) Pressure Flow Frequency Characteristics of a Cylindrical Choke. *Hydraulics & Pneumatics*, **13**: 199-205.

[48] Oertel, H. (2004) Prandtl's Essentials of Fluid Mechanics, 2nd ed., Springer, New York, 190-193.

[49] Andrade, J.S., Costa, U.M.S., Almeida, M.P., Makse, H.A., Stanley, H.E., 1999. Inertial effects on fluid flow through disordered porous media. *Physical Review Letters*, **82**(26): 5249–5252.

[50] Antohe, B.V., Lage, J.L., Price, D.C., Weber, R.M., 1997. Experimental determination of permeability and inertia coefficients of mechanically compressed aluminum porous matrices. *Journal of Fluids Engineering*, **119**: 404–412.

[51] Beavers, G.S., Sparrow, E.M., 1969. Non-Darcy flow through fibrous porous media. *Journal of Applied Mechanics*, **36**(4), 711–714.

[52] Beavers, G.S., Sparrow, E.M., 1971. Compressible gas flow through a porous material. *International Journal of Heat and Mass Transfer*, **14**(11): 1855-1859.

[53] Jin, L.W., Kai, C.L., 2008. Pressure drop and friction factor of steady and oscillating flows in open-cell porous media. *Transport in Porous Media*, **72**: 37–52.

[54] Zhong, W., Li, X., Liu, F., Tao, G., Lu, B., Kagawa, T., 2014. Measurement and Correlation of Pressure Drop Characteristics for Air Flow through Sintered Metal Porous Media. *Transport in Porous Media*, **101**(1): 53-67.

[55] Kagawa Toshiharu, Nishimura Riki, and Youn Chongho, Development of High Speed Response Laminar Flow Meter for Air Conditioning. 10th International Conference on Fluid Control, Measurements, and Visualization, Moscow, Russia, August, 2009.

[56] Kawashima, K., Fujita, T., Kagawa, T., 1998. Unsteady Flow Generator of Air Using Isothermal Chamber. *Transactions of the Society of Instrument and Control Engineers*, **34**(12): 1773-1778.

[57] David E. Olson. Pipe Vibration Testing and Analysis. *In*: (editor) K. R. Rao. Companion Guide to the ASME Boiler & Pressure Vessel Code, Volume 2, Second Edition, Chapter 37, 2006.

Acknowledgements

I here express my special gratitude to my academic supervisor, Professor Toshiharu KAGAWA and Associate professor Kotaro TADANO, for their encouragement and valuable advice during the past three years of my study at Tokyo Institute of Technology. The support they provided me in my studies and life in Japan was fundamental for this work.

I would also like to my express special gratitude to Professor Kazuhiro YOSHIDA, and Assistant professor Chongho YOUN for their professional instruction and orientations in my research and life during these three years.

I would like to gratefully acknowledge

Associate professor Hayato YOSHIOKA

Associate professor Shigeki MATSUMURA

Associate professor Toshio TAKAYAMA

For the attention and the constructive feedback on the elaboration of this work.

I am thankful to Dr. Jun Li for her friendship, and helpful discussions in the course of this study. My sincere thanks are due to Dr. Daisuke Sakamoto, Dr. Nobuhiro Tsuchiya, Ms. Lai Lai Oo, Mr. Shengzhi Chen, Mr. Kousuke Mitsuhashi, Mr. Izumi Saito, and Mr. Katsuya Nagai, for their friendship and enthusiasm while I was working on my thesis.

I gratefully acknowledge the generous support from the China Scholarship Council that provided me the scholarship along the doctoral course at Tokyo Institute of Technology.

Finally, I wish to dedicate this work to my parents, for their lifelong support.

Jiehong PENG

August 1, 2016